

Visualizing CREB family transcription factor activation in living cells

Dissertation zur Erlangung des Doktorgrades der Naturwissenschaften

An der Fakultät für Biologie der
Ludwig-Maximilians-Universität
München

Vorgelegt von
Michael Friedrich

München, Juli 2007

Erstgutachter: Prof. Dr. Alexander Borst

Zweitgutachter: Prof. Dr. Rainer Uhl

Tag der mündlichen Prüfung: 02.07.07

1. Abstract

Many transcription factors integrate a variety of cellular stimuli to produce a transcriptional response. There is increasing evidence that the timing and kinetics of activation are crucial in determining specificity and strength of gene expression, however so far only few tools are available to address these questions in live cells and these have severe drawbacks, like very low signal strength, complicated handling, irreversibility and lack of good targeting properties. The Ca^{2+} - and cyclic adenosine monophosphate responsive element-binding protein (CREB) and the related ATF-1 and CREM are stimulus inducible transcription factors that link certain forms of cellular activity to changes in gene expression and are involved in differentiation, cancer, survival and neuronal plasticity. Using fluorescence resonance energy transfer (FRET) we here develop genetically encoded indicators that enable imaging activation of CREB family transcription factors due to phosphorylation of the critical serine 133 and subsequent recruitment of a coactivator in single live cells. The indicator for CREB activation due to phosphorylation (ICAP) consists of the kinase inducible domain (KID) of CREB fused together with the KIX of CREB binding protein (CBP) via a flexible linker, sandwiched between a cyan and a yellow variant of the green fluorescent protein. The specificity and reliability of ICAP as a measure for CREB activation was demonstrated first in the cuvette and then in the nucleus and mitochondria of HeLa cells. After that, we analyzed the properties of ICAP in primary hippocampal neurons, where we characterize different signaling pathways with distinct kinetics that lead to CREB activation. Furthermore, combining the imaging of CREB activation with calcium imaging we see a summation of CREB activation in neurons that can be achieved by appropriately timed depolarizing stimuli and occurs even when individual stimulations are separated by hours. Finally, sensors for the activation of ATF-1, CREM and the recruitment of P300, were introduced and preliminarily characterized. On the whole, these array of biosensors complement the toolbox for the investigation of the activation of the CREB family of transcription factors in living cells and organisms.

Table of contents

Table of contents	V
Abbreviations	VII
1. Abstract	1
2. Introduction	3
2.1 The CREB family of transcription factors.....	3
2.2 Phosphorylation dependent activation of CREB family members.....	7
2.3 Signal transduction via CREB.....	9
2.4 Tools to visualize CREB activation.....	13
2.5 Green fluorescent proteins, fluorescence and the basics of FRET.....	14
2.6 Genetically encoded fluorescent biosensors.....	18
3. Materials and Methods	21
3.1 Molecular cloning.....	21
3.1.1 PC and web assisted DNA sequence analysis.....	21
3.1.2 Gene amplification.....	21
3.1.3 Spectrometric determination of DNA concentration.....	22
3.1.4 Restriction of DNA.....	23
3.1.5 Ligation of DNA fragments.....	23
3.1.6 Agarose gel electrophoresis.....	24
3.1.7 Preparation and transformation of competent E.coli.....	24
3.1.8 Site-directed mutagenesis by PCR.....	26
3.2 Working with proteins.....	27
3.2.1 Recombinant protein expression in bacteria.....	27
3.2.2 Protein purification.....	27
3.2.3 SDS-Polyacrylamide-gel-electrophoresis.....	28
3.2.4 Western blot.....	29
3.2.5 Fluorescence spectroscopy.....	30
3.3 Cell culture.....	30
3.3.1 Propagation and transfection of HeLa cells.....	31
3.3.2 Preparation and transfection of primary hippocampal neurons.....	32
3.3.3 Quantification of gene expression using a luciferase assay.....	33
3.4 Fluorescence microscopy.....	33

3.4.1 Measuring CREB activation and calcium.....	34
3.5 Materials.....	35
3.5.1 Instruments.....	35
3.5.2 Consumables.....	35
3.5.3 Buffers, Solutions and Media.....	35
3.5.4 Chemicals and Products.....	38
3.5.5 DNA Plasmids and E. coli strains.....	40
4. Results.....	41
4.1 Construction and characterization of fluorescent biosensors for CREB family transcription factor activation.....	41
4.2 Measuring ICAP activation in HeLa cells.....	43
4.3 Neuronal CREB activation visualized with ICAP.....	48
4.3.1 Visualizing calcium dependent summation of CREB activation in neurons.....	59
4.4 Visualizing ATF-1, CREM and P300 activation.....	70
5. Discussion.....	77
5.1 The specificity and reliability of ICAP.....	77
5.2 Studying CREB activation in mitochondria.....	78
5.3 Reliable and reversible imaging of CREB activation in primary hippocampal neurons.....	79
5.3.1 CREB activation after GABAergic stimulation.....	80
5.3.2 Simultaneous measurement of calcium and CREB activation in microiontophoretically stimulated neurons.....	82
5.3.3 Investigating the interrelationship of calcium and CREB activation in neurons.....	83
5.3.4 Visualizing CREB family transcription factors in living neurons.....	85
5.4 Further outlook.....	87
6. References.....	91
Thanks and Acknowledgements.....	103
Curriculum vitae.....	105

ABBREVIATIONS

ACTH	Adrenocorticotropic hormone
AM	acetoxymethyl
AMPA	α -amino-3-hydroxy-5-methyl-4-isoxazole propionic acid
APV	2-amino-5-phosphonovalerate
ATF-1	Activating transcription factor 1
BAPTA	1,2-bis-[2-aminophenoxy]ethane-N,N,N',N'-tetraacetic acid
BBS	BES-buffered saline
BES	N,N-bis[2-hydroxyethyl]-2-aminoethanesulfonic acid
BFP	blue mutant of GFP
C	cytosine
CCD	charge-coupled device
CFP	cyan fluorescent protein
CMV	cytomegalovirus
CNS	central nervous system
CREB	Calcium and cAMP responsive element binding protein
CREM	cAMP responsive element modulator
CPA	Cyclopiazonic acid
DMSO	dimethyl sulfoxide
DNA	desoxyribonucleic acid
DsRed	red fluorescent protein from <i>Discosoma</i> sp.
EDTA	ethylenediamine tetraacetic acid
EGFP	"enhanced" version of GFP
EGTA	ethylene glycol-bis[β -amino-ethyl ether] N,N,N',N'-tetraacetic acid
ER	endoplasmatic reticulum
F	fluorescence light intensity
FAD	flavin adenine dinucleotide
FCS	fetal calf serum
FRET	fluorescence resonance energy transfer
G	guanine
GABA	Gamma amino butyric acid

GFP	green fluorescent protein
HBSS	Hanks' balanced salt solution
HeLa	Henrietta Lacks
HEK	human embryonic kidney
HEPES	N-(2-hydroxyethyl)piperazine-N'-(2-ethanesulfonic acid)
ICER	Inducible cAMP early repressor
IP₃	inositol-1,4,5-trisphosphate
IPTG	isopropyl- β -D-thiogalactopyranoside
kD	kilodalton
Kd	dissociation constant
KN-62	1-[N,O-Bis-(5-isoquinolinesulfonyl)-N-methyl-L-tyrosyl]-4-phenylpiperazine
M	marker protein
MAPKAP-K2/3	Mitogen activated protein kinase-activated protein kinase 2/3
MSK-1	Mitogen- and Stress activated protein kinase 1
NADH	nicotinamide adenine dinucleotide (reduced form)
NMDA	N-methyl-D-aspartate
NTA	nitriloacetic acid
OD	optical density
P	postnatal day
PBS	phosphate-buffered saline
PBT	phosphate-buffered saline with Triton X-100
PCR	polymerase chain reaction
PFA	polyformaldehyde
PIPES	piperazine-1,4-bis(2-ethanesulfonic acid)
PMSF	phenylmethylsulfonylfluoride
Pp90RSK	90 kD ribosomal S-6 kinase
R	ratio; fluorescence intensity of acceptor emission over donor emission
R_{max}	ratio R at highest ligand concentration
R_{min}	ratio R in ligand-free conditions
SDS	sodium dodecyl sulfate
T	thymine

TAE	tris-acetate-EDTA electrophoresis buffer
TE	tris-EDTA buffer
U0126	1,4-Diamino-2,3-dicyano-1,4-bis(2-aminophenylthio)-butadiene
WT	wildtype
YFP	yellow fluorescent protein
$\Delta F/F$	fractional change in fluorescent light intensity
ΔR	difference of ratio R under Ca-saturated and Ca-free conditions

2.Introduction

Many of the most striking and also alarming features of cellular function depend on long term adaptive changes. Among these are e.g. memory formation, immune system function, development of various sensory and motor processes, but also serious diseases like cancer and disorders of the nervous system. Long term adaptive responses of cells during cell-cell communication often require changes in the expression levels of certain genes. In contrast to the constitutive expression of house keeping genes, these activity dependent genes are induced in a stimulus dependent manner. The mechanism of this activity dependency of genes involves the activation of certain transcription factors that can be induced by appropriate stimuli. Examples of transcription factors that work this way are the calcium response factor (CaRF), the downstream response element-antagonist modulator (DREAM), the nuclear factor of activated T-cells (NFAT), nuclear factor- κ B (NF- κ B) and the cAMP and calcium responsive element-binding protein (CREB) (West et al., 2002). The work at hand concentrates on CREB and aims at the construction, characterization and application of genetically encodable fluorescent biosensors for the activation of CREB family of transcription factors in live cells, tissues and transgenic animals.

In the first part of the introduction a brief overview of CREB function and regulation will be given.

2.1 The CREB family of transcription factors

The CREB protein is probably the best characterized stimulus-inducible transcription factor (Shaywitz and Greenberg., 1999; Mayr and Montminy 2001; Conkright and Montminy, 2005; Carlezon et al., 2005). It was discovered during studies of the cAMP inducibility of the somatostatin gene as a protein that binds to a 8 –bp cAMP-responsive element (CRE) in the somatostatin promoter, 5'-TGACGTCA-3' (Hoeffler et al., 1988; Gonzalez et al., 1989). But CREB is not the only protein that is able to bind to CREs and activate transcription. Further screenings unearthed the activating transcription factor 1 (ATF-1) (Hai et al., 1989) and the cAMP-responsive element

modulator (CREM) (Foulkes et al., 1991a,b) that share extensive sequence homologies with CREB but also show certain differences, especially in the kinase inducible domain (KID), that will be explained below. These DNA binding and transcription initiating proteins have several structural features in common and thus belong to the vast superfamily of the bZIP transcription factors together with c-Fos, c-Jun, c-Myc etc (Shaywitz and Greenberg., 1999; Mayr and Montminy 2001) . The representative features of the bZIP proteins are a leucine rich domain at the C-terminus necessary for the dimerization of the transcription factors and N-terminal adjacent a basic region containing many lysines and arginines that mediate DNA binding. Subsequent to activation, these proteins first dimerize, then bind to their particular DNA sequence before interacting via specific glutamine rich domains with general transcription factors and the RNA-polymerase machinery. Among the bZIP factors, CREB, ATF-1 and CREM constitute a subgroup that share extensive homology within the bZIP region. This homology enables these factors to form also heterodimers in addition to homodimers. Further in this text this subgroup will be referred to as the CREB family of transcription factors (Fig. 1) (Shaywitz and Greenberg., 1999; Mayr and Montminy 2001). Members of this family can undergo alternative splicing and thereby create isoforms that differ in their function. For example ICER is a splice variant of CREM and is a repressor of CRE – dependent transcription. For these factors to be stimulus inducible they need the kinase inducible domain (KID) as shown in figure 1 and especially in figure 2. This domain contains several important sites for posttranslational modification particularly phosphorylation, e.g. serin 133. Phosphorylation of the serine 133, e.g., initiates the events, that finally lead to the CRE-dependent building of mRNA. In addition to the serine 133, several other residues within the KID can be posttranslationally modified, among them serin 129, serin 142/143 etc. The CREB family transcription factors are phosphorylated by a variety of serin/threonine kinases, e.g. protein kinase A (PKA), protein kinase C (PKC), calcium calmodulin kinase II, IV (CaMK II, CaMK IV), casein kinase II (CK II), pp90 ribosomal S6 kinase (pp90 RSK) etc., all of them recognize different amino acid sequences (table 1). The many different kinases with their variform consensus recognition sequences (table 1) and the endogenous differences in the KIDs of the CREB family members (Fig.2) are very likely among the factors that determine signal discrimination and finally the transcriptional output (see Shaywitz and Greenberg., 1999; Mayr and Montminy 2001 for extensive review).

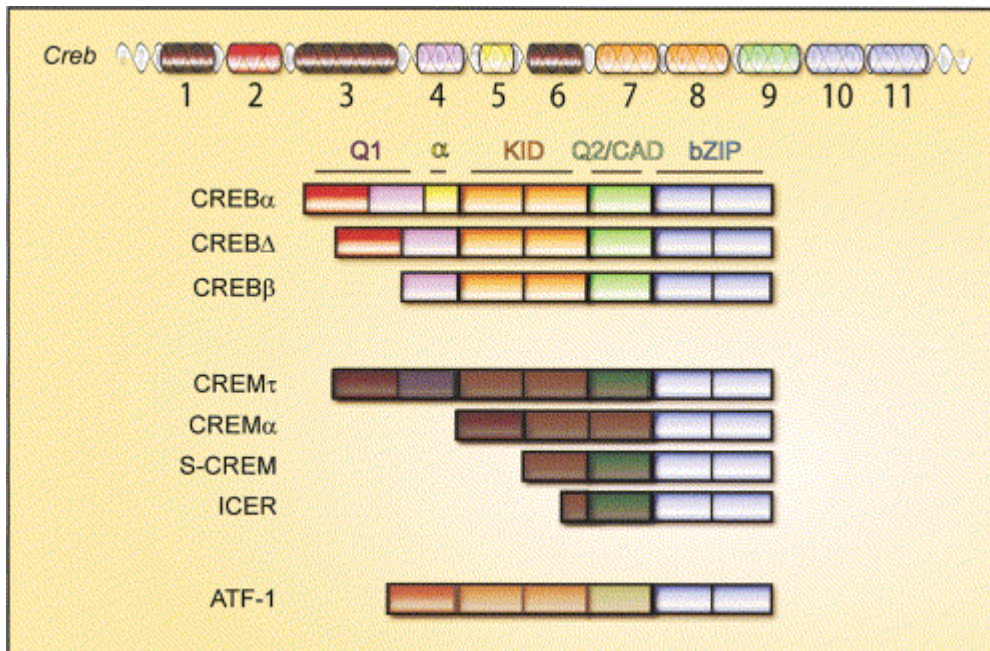


Figure 1: The CREB family of transcription factors. Depicted is the gene structure and the domain structure of CREB family transcription factors. Alternative splice variants of the *CREB* and *CREM* genes are shown. S-CREM and ICER are repressors of transcription (Lonze and Ginty, 2002).

The mechanistic background of signal discrimination is still a mystery. With respect to the endogenous differences within the KID, one possibility is, how close the kinase recognition sequences are related to the consensus sequences. Changes in just a few amino acids could result in an altered affinity of the kinase to the substrate and thus affect CREB dependent gene transcription strongly. Other possibilities are that the differences in the KIDs of the CREB family members influences the pretethering of the protein in discrete signaling domains or the binding of adapter proteins, e.g. repressors. This could strongly enhance or weaken the transcriptional activity of the proteins. Other possibilities that could allow CREB proteins to discriminate between qualitatively and quantitatively different signals are discussed below.

It has been shown that CREM and ATF-1, while sharing extensive homology with CREB, differ significantly in their ability to activate transcription in response to certain stimuli (Shaywitz and Greenberg, 1999).

				133		142				
CREBα	120	DSQKR	REILS	RRPSY	RKILN	DLSSD	APGVP	RIEEE	KSEEE	159
		*				*	*	*		
CREMτ	104	DSHKR	REILS	RRPSY	RKILN	ELS [*] SD	VPGIP	KIEEE	KSEEE	143
					*	*				
ATF-1	50	SSQKA	HGILA	RRPSY	RKILK	DL [*] S [*] SE	DTRGR	KGDGE	NSGVS	89

Figure 2: Comparison of the KID regions of CREB, CREM and ATF-1. Amino residues 120- 159 of the KID of CREB are shown in comparison with the homologous regions of CREM (104- 143) and ATF-1 (50- 89). The yellow box emphasizes the high degree of identity between the three proteins in the region corresponding to amino acids 130- 145 of CREB. The gray box shows the homology between CREB and CREM in the region corresponding to amino acids 120- 159 of CREB. Asterisks indicate nonidentical residues. (From Shaywitz and Greenberg, 1999).

This argues against a mere compensatory function of CREM and ATF-1. Moreover, a tissue specific expression pattern of some of the CREB family members, CREM in testis (Foulkes et al., 1992 a,b), truncated CREM isoforms in the neuroendocrine axis e.g., supports the notion of a distinct function of the family members. Nevertheless the expression of CREB and ATF-1 overlaps widely (Shaywitz and Greenberg, 1999) and it will be interesting to elucidate the mechanism of their differential regulation, which could be reflected in their activation time or the on and off kinetics of their activation (Wu et al., 2001a; Lee et al.,2005).

PKA	...RRPS...
CaMK IV	...hydrophobic-xRxxS...
GSK-3	...SxxxS-P...
CK-II	...SxxE/D...
PKC	...SQKRR...
pp90 RSK	...RxxS...

Table 1: Konsensus recognition sequences for some CREB kinases. R : arginine, P: proline, S: serine, S-P: phosphorylated serine, E: glutamic acid, D: aspartic acid, Q: glutamine, x: any amino acid.

2.2 Phosphorylation dependent activation of CREB family members

As already mentioned above activation of CREB family transcription factors require phosphorylation of certain amino acid residues in the kinase inducible domain of the protein. From more than 20 years of research on CREB we can conclude that one amino acid plays a pivotal role in CREB activation: the serine 133 (Gonzalez et al., 1989). Serine 133 phosphorylation is absolutely necessary but not always sufficient for CREB dependent gene expression (Lonze and Ginty, 2002). This issue will be discussed in more detail below when the other phosphorylation sites are considered. First we shall have a closer look at the actual mechanism of CREB activation. The domain that is most important for CREB activation is the KID, which contains the serine 133 residue. In its unphosphorylated state, the KID has a random coil formation. After being phosphorylated at serine 133 the KID undergoes a folding transition from a random coil to a helical conformation (Radhakrishnan et al., 1997). This folding transition and the consequent unclenching is like the opening of a venus fly trap (Fig. 3). In the early days of CREB research there has been a debate whether this phosphorylation enhances the stability of the protein, or whether it regulates its subcellular localization, or if it regulates the dimerization and DNA binding (Shaywitz and Greenberg, 1999). Later experiments showed that the phosphorylation affects neither of these processes but rather leads to the recruitment of a transcriptional coactivator, CREB binding protein (CBP) (Chrivia et al., 1993). The 3D structure of this interaction is depicted in figure 3. And now it also becomes obvious what the reason for this venustrap- like opening of the KID is: the folding transition of the KID creates a binding interface for the three intricately folded helices of the KID interaction domain (KIX) of CBP and thereby facilitates binding of CREB to CBP. The recruitment of the transcriptional coactivator CBP has at least two consequences that are essential for the initiation of transcription: First, CBP has an intrinsic histone acetyltransferase activity, that enables the CREB-CBP complex to modify inactive chromatin to chromatin that is readily accessible for transcription. Second, the modular domain structure of CBP, which is similar to CREB, contains interaction motifs for the basal transcription machinery, including TF IID, TF IIB, TAF 130, TBP and RNA polymerase II (Chrivia et al., 1993). Thus, the binding of CBP to CREB facilitates the

assembly of the RNA- polymerase complex on active chromatin and therefore is the crucial step in initiating CREB dependent transcription. Serine 133 phosphorylation, CBP binding and subsequent gene transcription is certainly the backbone of the understanding of CREB function but other factors, like additional phosphorylation sites on CREB and CBP, other coactivators and promoter elements, various types of posttranslational modifications and tissue specific differences add multiple layers of complexity to the unraveling of CREB dependent gene expression. Discussing all these events would definitely go beyond the scope of this work, thus I will focus on additional phosphorylation sites. The most thoroughly investigated additional phosphorylation sites within the KID are serines 142/143 (Lonze and Ginty, 2002). It has, for example, been shown that phosphorylation of serine 142 is necessary in the entrainment of the circadian clock in mice (Gau et al., 2002). In this study, serine 142 participates positively in CREB mediated gene expression. Interestingly, structural studies revealed that phosphorylation of serine 142 blocks the interaction of the KID with the KIX (Radhakrishnan et al., 1997) . Inactivation of serine 142, under these experimental conditions, enhanced the ability of calcium to activate CREB, arguing for an inhibitory role of the serine 142. Surely, the extent and physiological consequence of serine 142 phosphorylation is dependent on the type of cell and tissue. In this context it is intriguing to speculate that different patterns of phosphorylation on the various serines and threonines, but also other posttranslational modifications, could be responsible for distinct modes of activity. Multiphosphorylation passwords could open different lines to specific coactivator or inhibitor interactions and thereby intricately discriminate between incoming signals (Deisseroth and Tsien, 2002). Additional layers of complexity are added by the fact that CBP itself is phosphorylated on many residues.

In the light of all the possible cell and tissue dependent modifications, the kinetic component of these modifications and the multiple protein-protein interactions this molecule can be involved in, it becomes obvious that we are merely at the beginning of the understanding of CREB function.

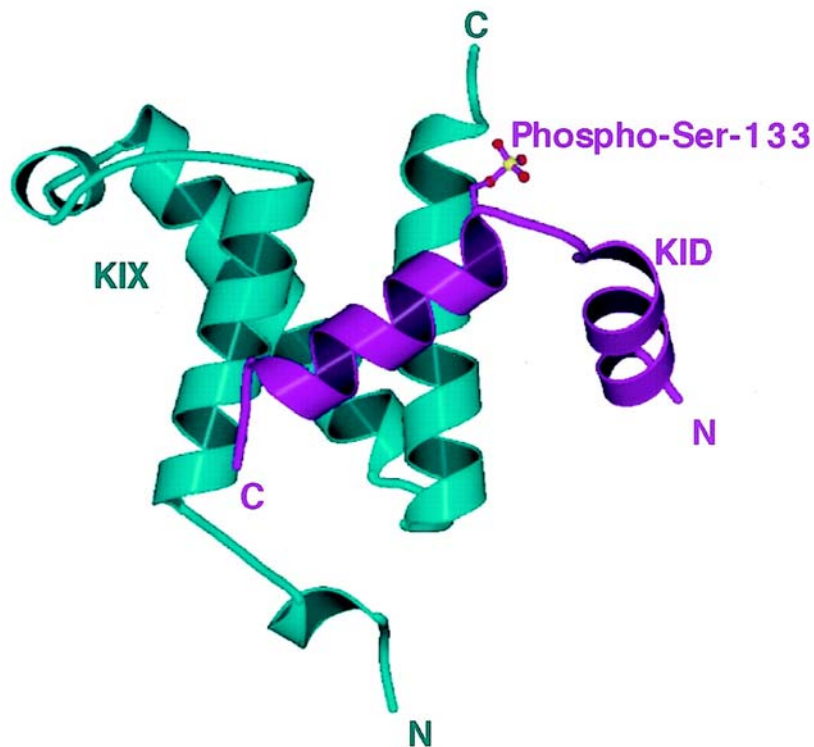


Figure 3: Ribbon diagram of the KID-KIX interaction. The structure is deduced from NMR. In turquoise are shown the 3 helices of the KIX and in pink the phosphorylated helical KID. The phosphoserine residue is depicted in a ball-and-stick representation. After the phosphorylation induced folding transition of the KID, the C-terminal helix of the KID binds to a hydrophobic surface formed by helices α -1 and α -3 of KIX (Radhakrishnan et al., 1997).

2.3 Signal transduction via CREB

As already mentioned above CREB is phosphorylated by a variety of kinases. In this chapter I would like to embed these kinases in the context of their signal transduction cascades and thereby describe the cell biological relevance of CREB. CREB is ubiquitously expressed throughout the body and therefore is involved in different kinds of activity dependent regulations of gene expression in all cell types, but the tissue in which it is best characterized is the nervous system (Marie et al., 2005; Wu et al., 2001b). There it responds to growth factors (Shaywitz and Greenberg, 1999; Finkbeiner, 2000), hormones (Richards, 2001), membrane depolarization and neurotransmitters (Deisseroth et al., 2003; Fields et al., 2005) (Fig. 4). Despite the heterogeneity of the initial signal, most of them have in common, that they elicit an

intracellular second messenger cascade. Two such messengers are especially important in this respect, cAMP and calcium, and I will discuss them both in the following text, beginning with signals that elevate cAMP. Many hormones and neurotransmitters, like adrenaline, adenosine or ACTH, act by binding to their cognate receptors, often seven-transmembrane domain class receptors. This binding event leads to the activation of coupled trimeric membrane bound G-proteins, which in turn, depending on the type of G-protein, activate different effector molecules. One type of effector molecule is the adenylyl cyclase, an enzyme that catalyses the production of cAMP. cAMP can serve many purposes in the cell, but its primary target is the cAMP-dependent protein kinase (PKA). Binding of cAMP to the regulatory subunit of the PKA results in the dissociation of the regulatory from the catalytical subunit, which in turn translocates into the nucleus of the cell and there phosphorylates certain substrates, among them CREB. The hormone-cAMP-PKA-CREB pathway is essential in many metabolic processes, like pulse frequency, water resorption, glucose and calcium metabolism (Richards, 2001).

Similar to cAMP, calcium is a versatile second messenger in many cellular actions. Calcium can on the one hand enter the cytoplasm from the outside of the cell, via calcium channels that can be voltage gated channels, e.g. L- or N- type calcium channels, or ligand gated channels, e.g. AMPA receptors or NMDA receptors. In the nervous system membrane depolarization, which leads to calcium influx through voltage gated calcium channels is the most prominent cause for the intracellular elevation of calcium and thus also CREB activation. On the other hand a cytosolic increase of the calcium concentration can come from internal stores, via IP₃ – receptors or ryanodine receptors. Once in the cytoplasm calcium is immediately bound by high affinity calcium binding proteins that come in all flavours. Examples are calmodulin, calbindin, calpain, calcineurin to mention just a few. Importantly, in terms of CREB activation, calcium bound calmodulin can activate effector kinases like the calcium/calmodulin dependent kinases (CaMK) (Shaywitz and Greenberg, 1999; West et al., 2001). They come in four types I, II, III, and IV, most important of them being II and IV. CaMK IV is located in the nucleus and is activated directly by the nuclear calcium pool. CaMK II expression is confined to certain parts of the brain and is a cytosolic protein that can enter the nucleus. All CaMK can phosphorylate CREB on the serine 133 residue and CaMK II can also phosphorylate serine 142, as mentioned above (for review see Hook and Means, 2001). But the CaMK are not the

only kinases that are able to activate CREB. Ribosomal s6 kinases 1-3, protein kinase C and also protein kinase A can phosphorylate CREB in response to calcium influx.

Moreover, other pathways exist, that do not need cAMP or calcium to phosphorylate CREB. These signaling cascades are initiated, above else, by growth factors, e.g. nerve growth factor (NGF) (Riccio et al., 1999), brain derived neurotrophic factor (BDNF) or epidermal growth factor (EGF) (Finkbeiner, 2000). Growth factor receptors are intrinsic receptor tyrosine kinases. Binding of the cognate ligand results in dimerization or even multimerization of the receptor and to an autophosphorylation of certain tyrosine residues within the cytosolic domain of the receptor. These phosphorylated tyrosines are recognized by proteins that harbour certain specified domains, e.g. Sh-2 domains. Thus, specific phosphorylation and specific recognition of phosphorylated amino acids is used to propagate the signal to kinases that activate effector molecules, like CREB and other transcription factors. Involved in the transduction of growth factor mediated signals are the MAPKAP-K2/3, the pp90 RSK 1-3 and the MSK1, that are all able to phosphorylate CREB on the crucial serine 133. Growth factor signaling to CREB is heavily involved in developmental processes, but also in synaptic plasticity and learning and memory.

The signaling cascades that I described above do not work separated from each other, offering manifold possibilities for interplay (Fig. 4). For example for calcium/calmodulin plenty interaction partners exist in the cell, all being part of another signaling pathway that culminates in CREB phosphorylation.

This interplay makes the tedious struggle to understand CREB function even harder.

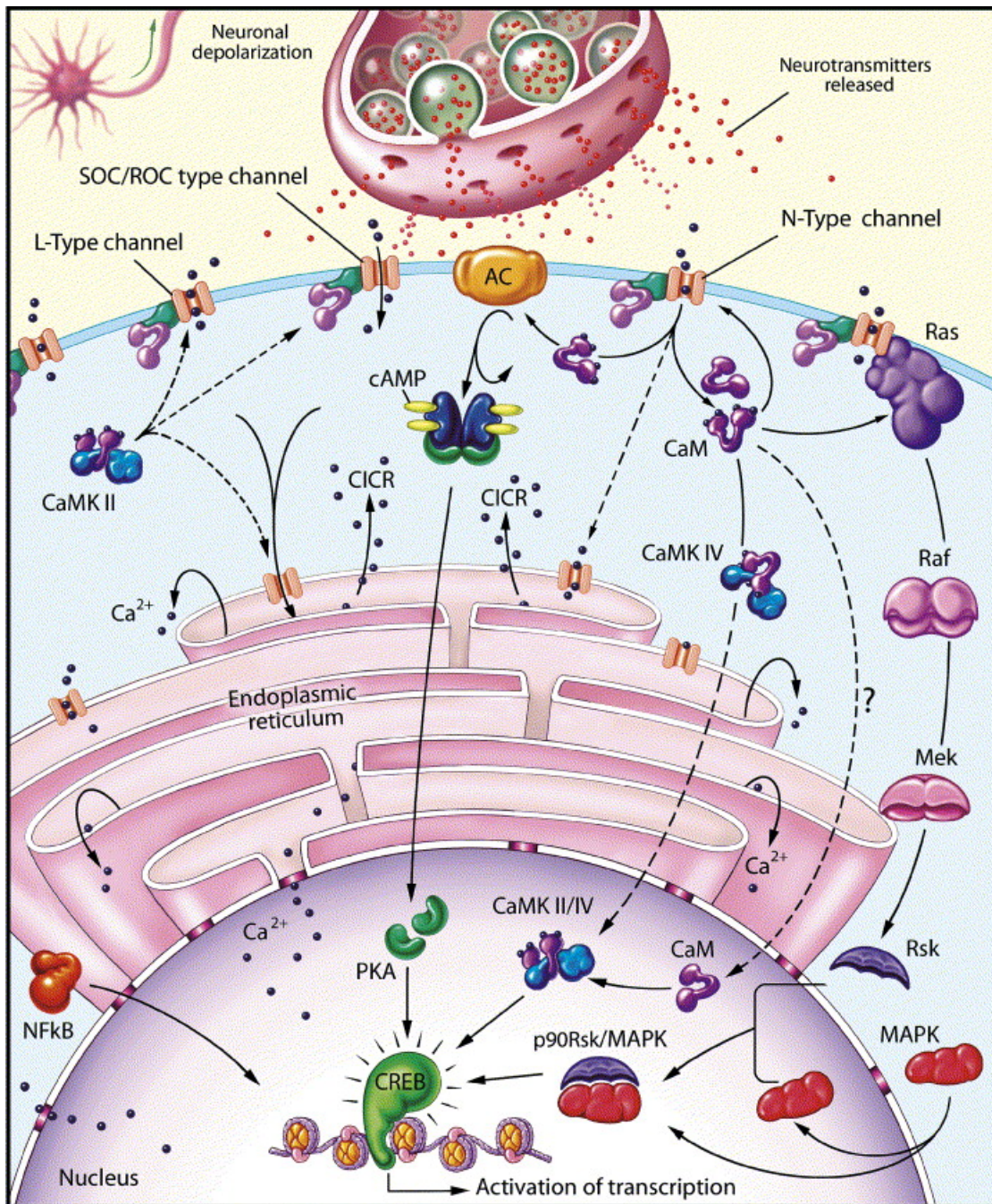


Figure 4: Signaling and CREB. Many different signaling cascades converge on CREB to finally activate transcription in the nucleus. Amongst them are the MAPK pathways, involving Ras, Raf, Mek, Rsk and the p90Rsk/MAPK, the adenyly cyclase-cAMP-PKA-CREB pathway and the CaMK IV pathway. Also shown are actions of CaMK II on calcium channels and calcium release from internal stores. These processes play a role in modulation of the above mentioned pathways. Please note the interplay between the three signaling cascades, e.g. on the level of calcium/calmodulin, that activates the AC, various calcium channel, the CaMKinases and also Ras (For abbreviations please see list) (Fields et al., 2005).

2.4 Tools to visualize CREB activation

The most widely used tool to investigate CREB activation in cells and tissue is definitely the phospho-specific antibody against p-serine-133 (Shaywitz and Greenberg, 1999). This method is easy to apply and gives strong signals in western blot analysis and also immunocytochemical stainings. Nevertheless, the range of application of this technique is limited, because death of the cell, that is analysed, is obligatory, allowing only for snapshots at given time points. Furthermore immunostainings are difficult to quantify and often require averaging over many different cells in a tissue is necessary (Liu and Graybiel, 1996 and 1998; Wu et al., 2001a). Moreover, a thorough analysis of CREB activation in living tissue or even transgenic animals under physiologically more appropriate conditions with a satisfactory spatial and temporal resolution is not feasible. This brings us to the question, how could an optimal tool for the visualization of CREB activation look like. First of all, getting the tool into the preferred tissue should be a non-invasive process, that does as few harm to the cell as possible. Then, it would be desirable to have a means to specifically label certain structures in the cell, e.g. the nucleus or mitochondria, where CREB phosphorylation occurs. Of course, easy handling and read-out would also be on the wishing list of such a tool. Ideally, it should allow for real-time measurements in living cells and tissue under physiological conditions, accounting also for the spatial and temporal heterogeneity of the process of CREB activation. To reach these criteria two attempts have been made. One approach used a split enzyme complementation assay, that employed the phosphorylation dependent interaction of the KID and the KIX (Spotts et al., 2002). The binding of the KID to the KIX brought together the two halves of a split beta-lactamase enzyme, forming a functional enzyme that could convert a substrate that changes its fluorescence spectrum. This tool could be used in living neurons. Unfortunately, this tool did not allow for reversible imaging of CREB activation, and the authors did not show targeting of the sensor to subcellular localizations, or stimulate with physiologically relevant stimuli. Another approach used two GFP variants, cyan fluorescent protein (CFP) and yellow fluorescent protein (YFP), and fused the CFP to the KID and the YFP to the KIX, building a bimolecular CREB sensor (Mayr et al., 2001). Interaction of KID and KIX changed the distance and/or the angle of the two

fluorophores thereby altering the efficiency of fluorescence resonance energy transfer (FRET) between the two fluorophores. This sensor reported CREB activation and CBP recruitment in the nucleus of HEK293 cells. Unfortunately, the sensor is not easy to handle due to the fact that two separate constructs have to be transfected into cells in equal concentrations to exclude measuring artefacts. The signal read-out of the sensor is quite small and averaging is necessary to get clear signals.

Despite these efforts to create a tool for imaging the activation of CREB, still an easy-to-handle, reversible sensor with reasonable signal strength and the possibility to target it to the nucleus and mitochondria, is desperately needed. Genetically encodable fluorescent biosensors are at the moment the method of choice for studying signaling processes in live cells. They consist of variants of the green fluorescent proteins and, between them, certain molecules that undergo a conformational change upon binding of a ligand or after phosphorylation. The basic principles of the function of such indicators will be described in the next chapter.

2.5 Green fluorescent proteins, fluorescence and the basics of FRET

The green fluorescent protein (GFP) was discovered already 1962 by Shimomura et al., but it took 30 more years for the *gfp* gene to be cloned and thus for GFP to become one of the most versatile and useful tools in molecular biology. In 1992 different groups showed that expression of the *gfp* gene in other organisms creates fluorescence, which was the milestone discovery that led to the widespread use of GFP in today's labs (for extensive review see Tsien 1998). The structural properties of GFP (Fig. 5) make it particularly resistant against environmental stresses and provide the background for its fluorescence characteristics. It consists of 238 amino acids which form a β -barrel with a diameter of 30 Å and a length of 40 Å. The barrel is made of eleven tightly-fitted staves of β -sheets that protect an α -helix that runs up the axis of the GFP (Fig. 5). The helix within the barrel of the GFP holds, like a scaffolding, the chromophore of the GFP. This central position of the chromophore protects it against photochemical damage and diffusible ligands from outside. The chromophore of wild type GFP is a para-hydroxybenzylideneimidazolinone formed by the tripeptide Serine – Tyrosine – Glycine, which are the amino acids 65, 66, 67. The

specific chemical structure of this tripeptide, with its double bonds and phenol/phenolate forms, gives the GFP its characteristic excitation maxima at 395 nm and 475 nm and emission at 508 nm and 503 nm, respectively. Directed mutagenesis and the resulting change of amino acids in the chromophore or near the chromophore lead to the great variety of different colours of GFPs. For example, the mutations: S65T, S72A and T203F, result in a shift of the emission to longer wavelengths giving rise to yellow fluorescent proteins. Changing Y66W, N146I, M153T and V163A gives cyan fluorescent proteins, where the emission peak is shifted towards shorter wavelengths. Via site-directed change of amino acids it is not only possible to vary the colour of the GFP, but also the brightness, the maturation time, the expression efficiency in different systems and the sensitivity of the GFP to environmental factors like the pH or chloride concentration (Griesbeck et al., 2001; Zapata-Hommer and Griesbeck, 2003; Rizzo et al., 2004).

The two GFP variants used in this work are ECFP with the mutations F64L, S65T, Y66W, N146I, M153T and V163A (Heim and Tsien, 1996), and Citrine with the mutations S65G, V68L, Q69M, S72A, T203Y and V163A (Griesbeck et al., 2001). In recent years fluorescent proteins were purified from many other organisms besides *Aequoria victoria* (Shagin et al., 2004). It is interesting to note that from an evolutionary point of view the expression of fluorescent proteins seem to be an ancestral state in the metazoa since both lines, the bilateria and the cnidaria, at this very early arborisation, have closely related GFP-like fluorescent proteins. In the cnidaria phylum fluorescent proteins appear in many groups within the hydrozoa and the anthozoa (Shagin et al., 2004). They come in various colors ranging from cyan over green, yellow, red to even colorless variants.

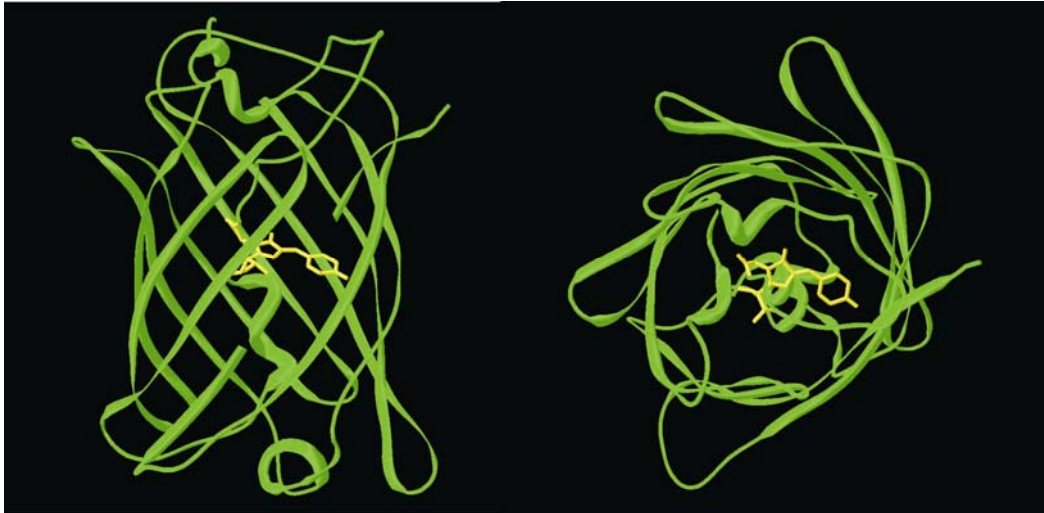


Figure 5: The structure of the GFP. In green is shown the β -barrel with the protecting β -sheets surrounding the Ser-Tyr-Gly chromophore (yellow) on the α -helix in the middle. On the left is a side view and on the right is a top view of the protein. (Jain and Ranganathan, 2004)

For application in molecular and cellular biology especially important are the red shifted variants from *discosoma* species, that have been heavily worked on in the last years foremostly by Roger Tsien's group (Shaner et al., 2004). Now there exist several color variants from yellow to red that can be used for all kinds of applications. The problems with many new GFPs are, that they are not monomeric, which results in certain applications in a unintentional aggregation of the molecule. Furthermore, the maturation time is in many cases up to several days and strongly dependent on low temperature which makes these fluorescent proteins difficult to use in mammalian systems. Nevertheless, the work on these proteins continues because of the desparate need of many different color variants for multicolor staining of cells and several other applications in cellular biology.

Among these applications is the use of GFPs for fluorescence resonance energy transfer (FRET), where the changes of the emission intensities of the respective GFPs are measured under FRET and no FRET conditions (for background on fluorescence and FRET see Lakowicz, 1999). FRET is the radiationless transfer of excited state energy from a donor protein to an acceptor protein (Fig. 6). FRET efficiency is strongly depending on three variables: First, the emission of the donor has to overlap significantly with the excitation of the acceptor. Optimally, the excitation wavelength of the donor is far enough away from the excitation of the acceptor, so that no bleed through between the channels occurs. The ideal excitation

and emission can be fine tuned by the use of appropriate filters. Second, the orientation of the fluorophores to one another is extremely important because the efficiency of the formation of the transition dipoles of the chromophores increases the more parallel the chromophores are aligned (Fig. 6). Last but not least the distance is of utmost importance, since FRET efficiency is related to distance with the inverse sixth power (Fig. 6). Thus FRET can be used in molecular and cellular biology to investigate processes that lead to changes in distance or orientation of molecules, for example protein interactions or colocalization of proteins. FRET has been successfully employed in genetically encoded fluorescent biosensors (GEFB), where two spectral variants of GFPs sandwich a linker molecule (Guerrero and Isacoff, 2001; Zhang et al., 2002; Miyawaki 2003 a,b; Griesbeck 2004). The choice of the linker molecule depends on the process one wants to investigate. The prerequisite is that the linker molecule has to undergo a conformational change that alters the distance or the orientation of the fluorophores and thus FRET efficiency. The different types of linker molecules that have already been successfully employed in GEFBs will be described in the next chapter.

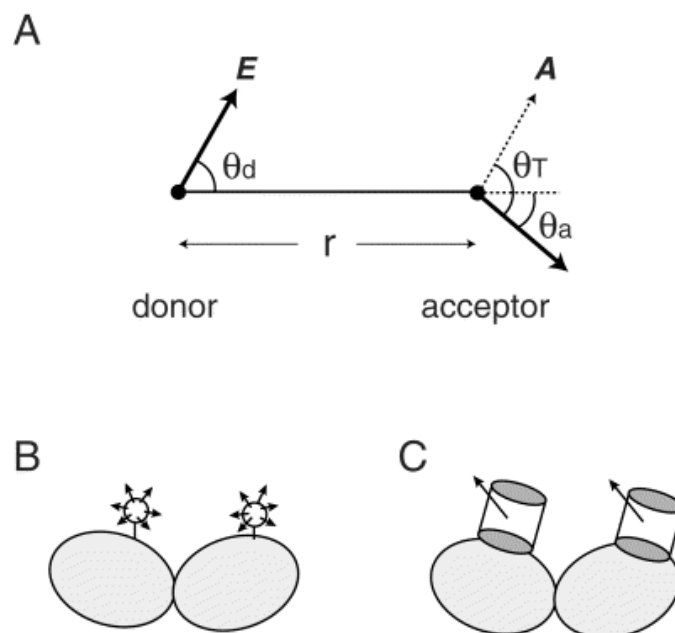


Figure 6: FRET depends on distance and angle of the fluorophores. In (A) E shows the direction of the emission transition dipole of the donor and A shows the direction of the absorption dipole of the acceptor. The orientation factor κ^2 is given by:

$\kappa^2 = (\cos\theta_T - 3 \cos\theta_d \cos\theta_a)^2$; The rate of FRET is dependent on κ^2 and r^{-6} . r is the distance between the donor and the acceptor. In (B) the relative orientation is variable due to free rotational freedom of the fluorophores. κ^2 is assumed to be 2/3. In (C) two spectral variants of GFPs are fused. Here the orientation is fixed. (Miyawaki, A. 2003)

2.6 Genetically encoded fluorescent biosensors

For designing and constructing GEFB some things have to be considered concerning the overall structure of the sensor (Zhang et al., 2002). It is possible to build a single or a double chromophore sensor, and if you choose the double chromophore version you can choose between intermolecular FRET or intramolecular FRET. I already discussed the drawbacks of an intermolecular FRET sensor in chapter 1.4, so I will focus on single chromophore and intramolecular FRET sensors (Fig. 7). Single chromophore sensors often consist of a fluorescent protein that is engineered to be sensitive to the molecule of interest, e.g. via insertion of a conformationally responsive domain or via fusing such a domain to the carboxyl and amino termini of the fluorescent protein. In such way very useful reporters for cellular calcium were constructed, e.g. G-Camps (Nakai et al., 2001), pericams (Nagai et al., 2001) and camgaroos (Griesbeck et al., 2001).

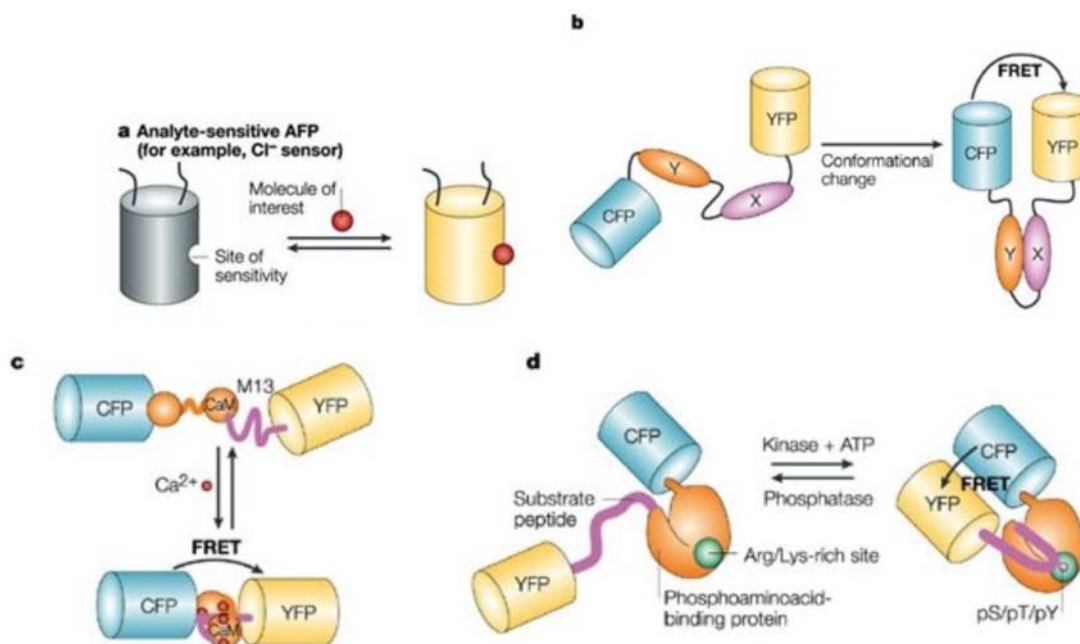


Figure 7: Genetically encoded fluorescent biosensors. In (a) is shown a single chromophore sensor where the fluorescent protein was engineered to be sensitive to a molecule of interest. (b) shows an intramolecular FRET sensor that is responsive to an interaction of the two proteins x and y. (c) depicts the famous cameleon calcium indicator that uses calmodulin and the M13 peptide which both wrap around each other when calcium is present. In (d) a phosphorylation sensitive sensor is shown that employs a substrate peptide and a phosphoaminoacid binding domain. (modified from Zhang et al. 2002).

Double chromophore indicators that make use of intramolecular FRET by the time exist in many forms and have also been applied in cell culture systems, slice culture systems and transgenically in worms, flies, zebra fish and mice (Griesbeck 2004). The fact that this approach is very useful is impressively demonstrated by the number of different sensors. There are sensor for all kinds of ions like calcium (Miyawaki et al., 1997; Heim and Griesbeck, 2004), and chloride (Kuner and Augustine, 2000; Duebel et al., 2006), or sensors for metabolites like glucose or maltose (Fehr et al., 2002; Stitt 2002). For use in the nervous sytem there are sensors for synaptic activity (Miesenbock et al., 1998), for glutamate (Okumoto et al., 2005), for calcium/calmodulin dependent kinase II (Takao et al., 2005), for membrane voltage (Siegel and Isacoff, 1997; Sakai et al., 2001; Baker et al., 2006), cAMP (Nikolaev et al., 2004) and cGMP (Honda et al., 2001; Nikolaev et al., 2006). For cellular signaling in general there exist sensors for protein kinases A (Zhang et al., 2001), B (Sasaki et al., 2003; Kunkel et al., 2004), C (Violin et al., 2003; Gallegos et al., 2006), for the small GTPases rho (Pertz et al., 2004 and 2006), ran (Kalab et al., 2002 and 2006), rac/cdc 42 (Itoh et al., 2002), ras and rap1 (Mochizuki et al., 2001) and G-protein coupled receptors (Vilardaga et al., 2003), for phosphoinositides (Ananthanarayanan et al., 2005), phosphotyrosine kinases (Ting et al., 2001; Kurokawa et al., 2001) and src (Wang et al., 2005). Due to the simplicity of the approach almost every signaling process in the cell that involves somehow, directly or indirectly, a conformational change can be monitored by such an indicator. These sensors can be used in different experimental settings, for example in pharmacological screenings for drug discovery, but also for basic research in transgenic animals. Recently, mainly different versions of the calcium indicators yellow cameleon and G-Camp were used to monitor cellular calcium in *C.elegans*, *drosophila*, zebrafish and to a certain extend in mice (Griesbeck, O. 2004). Unfortunately, the cameleons suffered massive loss of applicability in transgenic mice, probably due to interactions of calmodulin with

endogenous calmodulin binding proteins. This was overcome by the new generation calcium sensor TN-L15 (Heim and Griesbeck, 2004; Heim et al., 2007).

On the whole GEFB offer tremendous possibilities to assess cellular processes in real time in living cells and therefore their properties are further improved and tuned and novel types of sensors are designed and constructed. In this work I present genetically encoded fluorescent biosensors for the visualization of CREB family transcription factors and the application in live cells.

3. Materials and Methods

3.1 Molecular cloning

3.1.1 PC and web assisted DNA sequence analysis

A prerequisite for the handling and modification of recombinant DNA is a detailed knowledge of the base pair composition of the DNA fragment to analyse. All constructs in this work are sequenced and the data is stored on a accompanying cd-rom. These sequences provide necessary information, e.g. on restriction enzyme cutting sites, putative primer sequences and the succes of mutation experiments. The tools for this analysis are freely available on the web. For sequence alignments the blast tool from the ncbi homepage was used

<http://www.ncbi.nlm.nih.gov/blast/bl2seq/wblast2.cgi>.

To get the reverse complement, e.g. when analysing the data of a reverse primed DNA sequence, the tool on :

http://www.bioinformatics.vg/bioinformatics_tools/JVT.shtml was used.

Concerning the analysis of restriction enzyme cutting sites the NEBcutter V2.0 was used <http://tools.neb.com/NEBcutter2/index.php> .

For the translation of DNA sequences into protein sequences a tool from the ExPASy homepage was used: <http://www.expasy.org/tools/dna.html>.

3.1.2 Gene amplification by PCR

For polymerase chain reaction (PCR) either a Vent polymerase (NEB, Beverly, USA) or a Pfu polymerase (Stratagene, La Holla, USA) in their respective reaction buffer were used according to the instructions of the manufacturer. Different primer annealing temperatures were used dependent on the length and GC content of the primer. The primer are from MWG- Biotech, Munich, Germany.

PCR reaction mix (volume: 50 µl):

50 -60 ng plasmid DNA as reaction template
1 µl dNTP solution (12.5 mM)
2 µl primer No. 1 (50 µM)
2 µl primer No. 2 (50 µM)
5 µl polymerase buffer
33 µl H₂O
5 µl Dimethylsulfoxid (Sigma, St. Louis, USA)
1 µl (2 U) polymerase.

Reaction cycles:

5 min heating to 95 °C;
30 amplification cycles:
30 sec 95 °C: melting of double-stranded DNA
30 sec annealing of primers; temperatures varying from 52-62 °C
2 min 72 °C: DNA synthesis;
After cycle completion: 3 min 72 °C; reaction termination by cooling to 15 °C.

The choice of the primer is essential for a PCR to work. It should be at least 20 bases long and have more G/C bases than A/T. The base composition defines the melting temperature and the annealing temperature, which is calculated by the formula: T_m (in °C) = 2 (A+T) + 4 (G+C). A melting temperature of at least 78 °C is desirable.

3.1.3 Spectrometric determination of DNA concentration

For successful cloning it is essential to know the concentration of the DNA. Double-stranded DNA has an absorption maximum at 260 nm; by measuring the absorption of DNA in an aqueous solution in a 1 cm quartz cuvette, the DNA concentration of the sample could be calculated using the following formula:

$$\text{DNA conc. } [\mu\text{g/ml}] = \text{OD}_{260} * 50 * \text{dilution factor}$$

3.1.4 Restriction of DNA

After PCR, the amplified gene has to be purified from the PCR reaction conditions to be ready for the restriction enzyme conditions. For this we used the QIAquick PCR purification kit (Quiagen, Hilden, Germany). Restriction digestion of DNA fragments was employed to generate sticky ends for directed cloning of vectors and inserts. Insert and vector were cut with either one or two restriction enzymes at a time, depending on the salt concentration of the buffers of the enzymes. All enzymes and buffers were from NEB (Beverly, USA) and used according to the instructions of the manufacturer. 0.5 – 1 µg DNA for analytical purposes and up to 10 µg DNA for larger preparations were cut with 1-5 U restriction enzyme per µg DNA. To avoid unspecific cutting, the concentration of restriction enzymes was always kept below 10 % of the total volume. Incubation times were between 1 hour (for analytical purposes) and 3 hours for larger amounts of DNA and quantitative preparation at a temperature suitable for the respective enzyme. The efficiency was controlled by running a 1% agarose gel. A straight forward method to get digested DNA fragments for further processing is to extract the preferred band from the gel. For the extraction and purification of DNA from agarose gels the QIAquick gel extraction kit (Quiagen, Hilden, Germany) was used.

3.1.5 Ligation of DNA fragments

To get recombinant plasmid DNA containing the desired fragments it is necessary to ligate the respective DNA fragments. In ligation reactions the ratio of insert to vector varied from 3:1 to 5:1. DNA concentrations were estimated on agarose gels via comparison to standard DNA ladders (NEB, Beverly, USA). The ligation reaction mix was either incubated at 16 °C overnight or between 0.5 and 1.0 hours at room temperature. For later transformation in bacteria between 1 µl and 15 µl were used.

Ligation assay

- 1.5 µl ligase buffer (10x, provided by manufacturer)
- 1.0 µl vector
- 4.0 µl insert
- 1.0 µl (400 U) T4 DNA ligase (NEB, Beverly, USA)

7.5 µl H₂O

3.1.6 Agarose gel electrophoresis

To quickly and easily assess the success of molecular cloning experiments DNA can be visualized on agarose gels. Agarose (Biomol, Hamburg, Germany) is a polysaccharide from D- and L- Galactose which polymerases to a matrix, building pores that vary in size and thus form a molecular sieve. Through this sieve DNA fragments are filtered and wander with a speed that is proportional to their size allowing for separation of DNA fragments of different length. The pore size of the sieve can be modified by changing the concentration of agarose. In this study 1%-gels were used. To make the DNA visible an intercalating agent like ethidium bromide is used that emits orange-red light upon UV-excitation. For this purpose 0.5 g of Agarose were solved in 50 ml of TAE-buffer (for buffer ingredients please see the materials part in chapter 3.5.3) and supplemented with 2.5 µg/ml ethidium bromide. DNA was mixed with orange-G loading buffer. The separation was achieved with 5-10 V/cm electrode distance.

3.1.7 Preparation and transformation of competent *E. coli*

4 ml LB medium were inoculated with the desired strain of *E.coli* DH 5α and grown at 37 °C overnight. The following morning, the culture was transferred into 300 ml LB medium and grown to an OD 600 of 0.55, the flask placed on ice for 20 minutes, and the cells harvested by centrifugation at 2500 g and 4 °C for 20 minutes. The medium was completely poured off and remaining drops of medium were removed by putting the open bottles on paper towels for a short time. The cells were resuspended in about 60-80 ml of refrigerated Inoue transformation buffer and harvested by centrifugation at 2500 g and 4 °C for 15 min. The medium was once again poured off, the cell pellet resuspended in about 20 ml of refrigerated Inoue transformation buffer, and 1.5 ml DMSO added to the suspension. After 10 minutes incubation on ice, the cells were transferred in small aliquots of 50 µl into pre-cooled tubes, frozen in liquid nitrogen, and stored at -80 °C until usage.

To amplify the cloned constructs as whole plasmids the ability of bacteria to take up double stranded DNA from medium is used. Once the bacteria ingested the plasmid it will be amplified by the bacterial machinery and by the multiplication of the bacteria. For specificity the cloned plasmids contained an ampicillin resistance gene which renders the bacteria resistant against ampicillin in the medium.

Transformation protocol (Inoue method)

1. Add 25 ng DNA to 50 μ l bacterial culture and incubate on ice for 30 min
2. Incubate at 42 °C for 90 sec
3. Cool for 1-2 min on ice
4. Add 200 μ l LB medium and plate on ampicillin containing agar plate
5. Incubate over night at 37 °C.

Transformation protocol (Electroporation)

1. 0.2-0.3 μ g/ μ l DNA in 50 μ l electrocompetent *E. coli*
2. Put bacteria in pre-cooled cuvette
3. In electroporator: 2500 V
4. Put bacteria in 0.5 ml SOC medium
5. Incubate at 37 °C, shaking (220 rpm) for 1 hour
6. plate on ampicillin agar plate

The grown colonies should contain the desired plasmid and can be used to inoculate a 2 ml ampicillin LB medium culture. From this culture the plasmid was purified using either the QIAprep Spin miniprep kit (Quiagen, Hilden, Germany) or the Pure Yield Plasmid Midiprep system (Promega, Madison, USA) depending on the further application of the amplified plasmids and the requirements for high or low DNA concentration.

3.1.8 Site-directed mutagenesis by PCR

In order to achieve a single amino acid exchange in a protein, oligonucleotide primers were designed that introduce a point mutation in the desired DNA codon. A mutagenic primer pair contains the same DNA sequence in opposite directions, while

the mutated base is located in the middle with about 10-15 additional bases of the original DNA sequence on both sides. The primer length was chosen so as to reach a melting temperature of about 78 °C after the following formula: $T_m = 2(A+T) + 4(G+C)$. Care was taken that the primers' GC content amounted to at least 40% and that both primer ends contained GC bases when possible. In the PCR reaction, primer extension times were set to 2 minutes per 1000 base pairs of template DNA.

PCR reaction mix

5-50 ng plasmid DNA as reaction template
0.8 µl dNTP solution (12.5 mM)
2.5 µl primer 1 (10 pM)
2.5 µl primer 2 (10 pM)
5 µl Pfu polymerase buffer (10x, provided by manufacturer)
32.5 µl H₂O
1 µl (2.5 U) Pfu polymerase
5 µl DMSO

Reaction cycles

30 sec heating to 95 °C;
16 amplification cycles:
30 sec 95 °C (melting of double-stranded DNA)
1 min 55 °C (annealing of primers)
2 min per 1 kb template at 68 °C (DNA extension)
Reaction termination by cooling to 15 °C.

In order to get rid of unmutated template DNA, 20 µl of the reaction mix were incubated at 37 °C for 2 hours with 1 µl (20 U) Dpn I restriction enzyme (NEB, Beverly, USA) which cuts the unwanted methylated plasmid DNA. 2 µl of this restriction assay were used for transformation of bacteria.

3.2 Working with proteins

3.2.1 Recombinant protein expression in bacteria

Proteins can be expressed in bacterial strains that are suitable for this purpose. For amplification of plasmids DH 5 α were used and for protein expression BL 21 are the strain of choice. But not only the bacterial strain is important, also the expression vector is of high relevance. We used pRSET B (Invitrogen, Carlsbad, USA), which is a bacterial expression vector with the promoter of the bacteriophage T7 and contains an inframe polyhistidin stretch at the 5'-region necessary for purification. The addition of Isopropyl- β -D-Thiogalactosid (IPTG) induces the T7 RNA polymerase in the genome of the BL 21 and this polymerase can now transcribe the gene of interest, in our case the genetically encoded biosensor. Most efficient expression levels were achieved when bacteria of the BL 21 strain were transformed as described above and directly transferred afterwards into a 15 ml tube containing 4 ml LB medium with the appropriate selective antibiotic, here ampicillin (50 μ g/ml). The starter culture was grown overnight at 37 °C and 225 rpm shaking and used to inoculate a larger (usually 400 ml) culture the next day. Cells were grown at 37 °C until they reached an optical density of 0.8 to 1.0, usually after 5-6 hours, and protein expression was then induced by adding a final concentration of 0.5 to 1 μ M IPTG as well as an extra dose of antibiotic. Expression was allowed to run overnight at room temperature and 180 rpm shaking, and the bacteria containing the protein finally harvested by centrifugation at 6000 g for 15 min.

3.2.2 Protein purification

The bacterial pellet is then resuspended in 10 ml protein resuspension buffer. To avoid proteolysis three protease inhibitors are added to the resuspension buffer: PMSF (1 μ M), Pepstatin (5 μ g/ml) and Leupeptin (1 μ g/ml). Then the resuspended protein solution is frozen at -80 °C and thawed 10 later to facilitate cell lysis by destroying cell membranes due to the formation of water crystals. Further attacking

the bacterial cell membrane 1 mg lysozyme was added to the lysate and the mixture was then incubated on ice for 30 min. Next, 0.1% Triton-X-100, 5 µg/ml DNase I and 5 µg/ml RNase were added and the cell suspension the lysed 20 minutes in an ultrasound bath containing ice water. After that the lysate was centrifuged for 30 minutes at 13000 rpm, the supernatant containing the recombinant protein decanted, and 300- 500 µl of Ni-NTA agarose slurry added to the supernatant. The solution was gently shaken 2 hours or overnight at 4 °C, which allows the polyhistidin stretch of the recombinant protein to bind to the nickel ions in the Ni-NTA resin. Following the binding the resin is decanted into a polypropylen column (Quiagen, Hilden, Germany) and washed with 20 column volumes of protein resuspension buffer containing 10 mM imidazole. Imidazole is a competitor for the nickel ions and thus, when increasing the concentration of imidazole to 150 mM in the resuspension buffer, this buffer can be used to elute the washed protein from the resin. Subsequently, the protein is dialysed in a dialysis hose (Roth, Karlsruhe, Germany) for at least 6 hours in PBS. The concentration of the purified protein was determined according to the law of Lambert-Beer: Absorption (at 280 nm) = $c * d * \epsilon$, c being the concentration, d the thickness of the cuvette (1cm) and ϵ the molar extinction coefficient. The extinction coefficient was determined on the website: www.expasy.org/tools/protparam.html using the primary aminoacid sequence of the protein. The protein was denatured in Guanidiniumhydrochloride (6 M)/ phosphate buffer (0.02 M, pH= 6.5).

3.2.3 SDS-Polyacrylamide-gel-electrophoresis

In order to separate proteins of different length and estimate their size they are analyzed in a SDS-PAGE. The sodiumdodecylsulfate (SDS) denaturates the proteins and thus they are separated in an electric field through the molecular sieve effect of the gel. The molecular weight of the protein equals the logarithm of the distance the protein traveled on the gel.

Ingredients of an 8% resolving gel:

4.64 ml H₂O

2.5 ml Tris-HCl buffer 1.5 M, pH 8.8

100 µl 10% SDS

2.66 ml Acrylamide

80 µl 10% Ammoniumpersulfate
10 µl Tetramethylethyldiamin (TEMED)

Ingredients of an 3% stacking gel:

3.8 ml H₂O
1.5 ml Tris-HCl buffer 0.5 M. pH 6.8
60 µl 10% SDS
0.6 ml Acrylamide
40 µl Ammoniumpersulfate
10 µl TEMED

The polymerisation takes 20-30 minutes. The samples are mixed with SDS loading buffer and cooked for 10 minutes at 95 °C. The gel is then run with 25 mA for 2-3 hours. Finally the gel is stained with coomassie brilliant blue.

3.2.4 Western blot

In this study we used the semi-dry western blotting procedure. The samples were separated on a SDS-Page and then the gel was sandwiched in the blotting chamber between six whatman papers and a nitrocellulose membrane. The transfer of the protein from the gel to the nitrocellulose membrane was accomplished with a voltage of 1 mA/m² for one hour. To check if the blot was successful a ponceau staining of the protein on the nitrocellulose membrane was done. After that the membrane was washed with a mixture of PBS and 0.1% Tween 25 (PBST). Blocking of the membrane to avoid unspecific binding of the primary antibody was done using 1% milk in PBST for one hour at room temperature. Now, after two five minutes wash steps with PBST, the primary antibody in a 1:3000 dilution in PBST was added and incubated overnight at 4 °C with gentle shaking. The next day, unbound antibody was removed by three five minutes wash steps with PBST. Afterwards the secondary antibody, diluted in PBST with 0.5% milk, was added and incubated 45 min at room temperature. Finally, after five five minutes wash steps the membrane was bathed in luminescence solution (Roth, Karlsruhe, Germany) for one minute and photographed on an X-ray film (Amersham, UK).

3.2.5 Fluorescence spectroscopy

The properties concerning the phosphorylation dependency of the fluorescence emission intensities of the purified proteins were investigated in a fluorescence spectrometer. The excitation wavelength used was 432 nm and emission was measured between 440 and 600 nm. The thickness of the cuvette was 1 cm. Emission intensities were measured at 475 nm (CFP) and at 525 nm (YFP) with a scan rate of 120 nm/min and a PMT detector voltage of 670 V. The excitation and emission slit was 5 nm. Purified protein kinase A (NEB, Beverly, USA) and calcium/calmodulin dependent kinase IV (Upstate, Charlottesville, USA) were used.

Phosphorylation assay:

869 μ l H₂O

100 μ l kinase reaction buffer (10x, provided by manufacturer)

20 μ l indicator construct (800 nM)

10 μ l ATP (200 μ M – 1 mM)

1 μ l purified kinase (2.5 U)

3.3 Cell culture

In this study two cell lines, HEK and HeLa cells, and primary hippocampal neurons were used for fluorescence imaging and western blot analysis. All cells were kept at 37 °C with a CO₂ concentration of 6.0%.

3.3.1 Propagation and transfection of HeLa cells

HeLa cells were grown on sterile plastic cell culture dishes (5 cm) and split every 2-3 days depending on the confluency (approx. 500 000 cells per dish).

Splitting protocol:

1. Remove old medium
2. Wash with PBS

3. Incubate with trypsin for 2-5 min and triturate with pipette
4. Put fresh medium into new dishes
5. Add 2-4 drops of the trypsin digested cell containing medium into new dishes

For fluorescence imaging cells are plated on 35 mm glass bottom dishes that were coated with poly-lysine over night and contain DMEM/10% FCS. Cells can be transfected immediately after splitting, which is usually more efficient, or the day after splitting. Two transfection methods were used for HeLa cells, one using Lipofectin (Invitrogen, Carlsbad, USA) and the other employing calcium phosphate precipitation of DNA. Using Lipofectin the transfection mix was prepared by diluting 2-3 µg plasmid DNA per dish in 100 µl FCS-free DMEM, and separately 6 µl Lipofectin reagent per dish in another 100 µl FCS-free DMEM. After 30 - 45 minutes incubation time, the two solutions were combined and kept at room temperature for another 15 – 20 minutes. Each dish received 200 µl transfection mix, was incubated for 24 hours, and the medium replaced with fresh DMEM/ 10% FCS. Imaging was performed 1-3 days post transfection. The calcium phosphate transfection method, which was almost exclusively employed for transfection of primary neurons will be explained in the next chapter. For western blot experiments or imaging the cells were serum starved for 6-12 hours. After that cells were washed with PBS several times and then lysed with a SDS containing lysis buffer on the shaker for 12 minutes. Then cells were centrifuged and the supernatant was used for experiments.

3.3.2 Preparation and transfection of primary hippocampal neurons

17-19-day pregnant Wistar rats were killed with CO₂ and the uterus containing the embryos removed and put in a petri dish with PBS. In a sterile environment, the embryos were dissected out of their sacs and transferred in another petri dish containing PBS. Under a dissection microscope, each embryos' skull was opened using a sharp forceps, the skullcap pulled away from the cortex, and the brain tissue dissected free. Excised brains were immediately placed into cold HBSS, the meninges removed with a pair of sharp fine-tipped forceps, and the desired brain region dissected free. For dissociating the tissue, the preparations were incubated for

20 minutes at 37°C in a solution of 1mg/ml dispase in HBSS. The dispase solution was removed after incubation and replaced with the same amount of DMEM/10% FCS. After this, the cells were dissociated by trituration with a flame-polished glass pipette. Glass-bottom cell culture dishes (35 mm) were pre-incubated for about two hours in Poly-L-Lysine solution, then rinsed with PBS and filled with 2 ml DMEM/10% FCS. The cell density of the triturated neurons was checked and the neurons plated onto the dishes and incubated overnight in DMEM/10% FCS at 37°C and 5% CO₂. The medium was changed after 8-24 hours to Neurobasal/B27 medium in which the neurons were kept for up to 6 weeks or longer.

For transfection of one 35 mm dish containing about 2 ml medium, 100 µl of CaCl₂ solution for phosphate transfections were mixed thoroughly with 10 µg DNA, then 100 µl 2x BBS solution added, mixed carefully again, and incubated for 20 minutes. Shortly before transfection, some of the old, conditioned medium (~ 0.5 ml) was removed from the dish and stored at 4°C. All 200 µl of the transfection mix were put in small droplets onto the cell layers and the dishes were incubated at 37°C for 1-4 hours. In order to remove as much of the CaPO₄ precipitate as possible, the dishes were carefully rinsed 2-3 times with pre-warmed Neurobasal medium, and afterwards supplied with 1.5 ml fresh Neurobasal medium together with the 0.5 ml conditioned medium taken out before the transfection. Depending on the promotor efficiency, protein expression could be detected 24-48 hours after transfection and normally lasted for several days. Prior to experiments the cells were kept at room temperature for 10 – 30 minutes.

3.3.3 Quantification of gene expression using a luciferase assay

To investigate CRE – dependent gene expression after high potassium stimulation in hippocampal neurons we used the pXP2 luciferase vector containing the promoter region of the “even – skipped homeo box homolog 1” from drosophila (a generous gift from M. Montminy, La Jolla, USA). Quantification was achieved with the Dual-luciferase reporter assay system from Promega, which was used according to the technical specifications of the manufacturer. We used a Cary eclipse fluorescence spectrophotometer for the analysis.

3.4 Fluorescence microscopy

Once the cells are fluorescently labeled they are ready for imaging under an appropriate fluorescent microscope. We used a Zeiss Axiovert 35M onto which a CCD camera was attached. A xenon lamp provided the light which was guided through a filter wheel with filters for CFP, YFP and fura-2. A liquid light guide leads the light into the microscope where it is reflected by a 455 DCLP dichroic mirror and directed to the sample. From the sample the light traverses the dichroic mirror and passes through another filter wheel, for emission filtering, before it reaches the camera. The whole system is operated by Metafluor 4.6 software. Exposure time of the sample varied from 200 – 800 msec. This also depended on if a neutral density filter was used. For ICAP imaging we used a neutral density filter 1.0 and an exposure time of 400 msec. For fura-2 imaging the exposure time was 800 msec. A binning of 2 was used. Acquisition time was every 10-30 sec for ICAP and every 10 sec for fura-2.

3.4.1 Measuring CREB activation and calcium

Different cellular assays were performed to characterise ICAP in living cells. The activation kinetics of ICAP were characterised by various pharmacological reagents. Forskolin (final concentration: 50 μ M) activates the adenylyl cyclase and thus elevates cAMP levels, histamine (50 -100 μ M) recruits calcium from internal stores, potassium chloride (50 mM) depolarizes the neuronal cell membrane and activates several internal signaling pathways, glutamate and NMDA mobilize calcium from external medium and internal stores and also activate cell death pathways and BDNF (100 ng/ml) binds to trkB and activates mainly the mitogen/extracellular signal related kinase (MAPK) pathway. The reagents were bath applied and not washed out unless indicated differently in the text. KCl, glutamate and NMDA were also iontophoretically (holding current: 20 nA; ejection current: 1 μ A) applied. To specifically assess the contributions of the different pathways pharmacological inhibitors of certain components of cellular signaling process were used. KN-62 (10 μ M) inhibits calcium/calmodulin dependent kinases, U0126 (10 μ M) inhibits the MAPK pathway

and H-89 (25 μ M) inhibits the cAMP/PKA pathway. The specific blockers were applied prior to experiment and incubated between 10-30 min before the experiment was done.

To simultaneously measure calcium events in the same cell fura-2 as an acetoxy-methylester was loaded into the cell. For this the cells were incubated with fura-2 (5 μ M) solved in pluronic acid for one hour, then washed and used for experiments. For fura-2 imaging 350 nm and 380 nm excitation filters were used and a 500/20 emission filter.

Confocal imaging of ICAP and mitotracker was done using a Leica DM IRE2 microscope with a TCS Sp2 confocal head.

3.5 Materials

3.5.1 Instruments

Autoflow CO ₂ Water-Jacketed Incubator	NuAire, Plymouth (USA)
Cary 100 Scan UV-Visible Spectrophotometer	Varian, Mulgrave (Australia)
Cary Eclipse fluorescence spectrophotometer	Varian, Mulgrave (Australia)
CCD-Camera Cool Snap HQ	Roper Scientific, Tucson (USA)
Dissecting Microscope	Leitz, Stuttgart (Germany)
Dual Current Generator 260	World Precision Instruments, Sarasota (USA)
Dyad DNA Engine Peltier Thermal Cycler	MJ Research Inc., Waltham (USA)
Metafluor 4.6 imaging software	Universal Imaging, Downingtown (USA)
Microscope Axiovert 35M	Zeiss, Oberkochen (Germany)
Shutter Lambda 10-2	Sutter Instruments, Novato (USA)

3.5.2 Consumables

Elutip-D Minicolumns	Schleicher & Schüll, Keene (USA)
Falcon Tissue Culture Plate, 12 Well	Becton Dickinson, Franklin Lakes (USA)
Glass Bottom Culture Dishes 35mm, Nr. P35G-0-14-C	MatTek Corp., Ashland (USA)
Polypropylene Columns	Qiagen, Hilden (Germany)
QIAquick Gel Extraction Kit	Qiagen, Hilden (Germany)

QIAquick PCR Purification Kit	Qiagen, Hilden (Germany)
Thermo-Fast 48 Well Plates for PCR	AB-Gene, Epsom (UK)

3.5.3 Buffers, Solutions, and Media

Name	Recipe
BBS (2x)	50 mM BES (acid), pH 6.96 280 mM NaCl 1.5 mM Na ₂ HPO ₄
Blocking buffer	5% Milk in PBST
CaCl ₂ solution for phosphate transfections	250 mM CaCl ₂ in H ₂ O
Coomassie staining solution	0.25 g coomassie brilliant blue BR-250, 45 ml methanol, 45 ml H ₂ O, 10 ml glacial acetic acid
Coomassie destaining solution	500 ml methanol, 400 ml water, 100 ml glacial acetic acid
DMEM/10% FCS	500 ml DMEM 50 ml FCS, heat-inactivated
DNA Gel Loading Buffer (10x)	100 mM Tris/HCl, pH 7.5 10 mM EDTA 50% Glycerol 1% Orange G
DNA Purification Buffer: High Salt	20 mM Tris/HCl, pH 7.4 1 M NaCl 1 mM EDTA
DNA Purification Buffer: Low Salt	20 mM Tris/HCl, pH 7.4 200 mM NaCl 1 mM EDTA
HBSS for imaging	25 mM HEPES pH 7.4 140 mM NaCl 5 mM KCl 1 mM CaCl ₂ 1 mM MgCl ₂

Name	Recipe
	1 mM Glucose 0.25% BSA
HBSS with high KCl for imaging	25 mM HEPES, pH 7.4 40 mM NaCl 100 mM KCl 1 mM CaCl ₂ 1 mM MgCl ₂ 1 mM Glucose 0.25% BSA
Inoue Transformation Buffer for competent cells	10 mM PIPES, pH 6.7 250 mM KCl 15 mM CaCl ₂ 55 mM MnCl ₂
MOPS Buffer for fluorescence spectroscopy	10 mM MOPS, pH 7.0 100 mM KCl
Neurobasal/B27	500 ml Neurobasal medium 10 ml B27 supplement
PBS (10x)	100 mM Na ₂ HPO ₄ , pH 7.4 20 mM KH ₂ PO ₄ 1.37 M NaCl 27 mM KCl
PBT (1x)	0.05% Triton X-100 in 1x PBS
Poly-L-Lysine	0.01% (w/v) Poly-L-Lysine Hydrobromide in H ₂ O
Protein Kinase A reaction buffer	50 mM Tris-HCl, 10 mM MgCl, pH 7.5
Protein running buffer	25 mM Tris base, 250 mM glycine, 0.1% SDS; pH 8.3
Proteinsample loading buffer	62.5 mM Tris-HCl (pH 6.8), 2% SDS, 10% Glycerol, 50 mM dithiothreitol, 0.1% bromphenolblue
Protein Resuspension Buffer	20 mM NaPO ₄ , pH 7.8

Name	Recipe
	300 mM NaCl
TAE (10x)	48.4 g Tris base 11.4 ml glacial acetic acid 20 ml of 0.5 M EDTA, pH 8.0 add H ₂ O to 1 liter
TAE (1x)	40 mM Tris-acetate 1 mM EDTA
Transfer Buffer	25 mM Tris base, 0,2 M Glycin, 20% Methanol (pH 8.5)
TE (1x)	10 mM Tris/HCl, pH 8.4 1 mM EDTA

3.5.4 Chemicals and Products

Name	Supplier
Agar	Sigma, St. Louis (USA)
Ampicillin, sodium salt	Roth, Karlsruhe (Germany)
AP5 (D-AP5)	Tocris Cookson, Bristol (UK)
AP5 (DL-AP5)	Tocris Cookson, Bristol (UK)
BAPTA, AM-ester	Molecular Probes, Eugene (USA)
BAPTA, tetrapotassium salt	Molecular Probes, Eugene (USA)
BES	Roth, Karlsruhe (Germany)
Bovine Serum Albumin (BSA)	Sigma, St. Louis (USA)
Calcium Chloride, dihydrate	Sigma, St. Louis (USA)
Carbachol	Sigma, St. Louis (USA)
Deoxyribonuclease	Sigma, St. Louis (USA)
Dispase	Gibco, Grand Island (USA)
Dithiothreitol	Sigma, St. Louis (USA)
DMSO (Dimethylsulfoxide)	Sigma, St. Louis (USA)
Dulbecco's modified Eagle's medium (DMEM) w/o Sodium Pyruvate; w/ 4500 mg/ml Glucose; w/ Pyridoxine-HCl	Invitrogen, Carlsbad (USA)

Name	Supplier
Dulbecco's modified Eagle's medium /F12	Invitrogen, Carlsbad (USA)
EGTA (Ethylene glycol bis(beta-amino ethyl ether tetra-acetic acid)	Sigma, St. Louis (USA)
Foetal Bovine Serum	Gibco, Grand Island (USA)
Forskolin	Sigma, St. Louis, (USA)
Gel/Mount mounting medium	Biomed, Foster City (USA)
Glucose (D-+)-Glucose anhydrous, min 99%)	Sigma, St. Louis (USA)
Glycine	Merck, Darmstadt (Germany)
H-89	Sigma, St. Louis (USA)
HEPES free acid	Sigma, St. Louis (USA)
Histamine	Sigma, St. Louis (USA)
Imidazole	Merck, Darmstadt (Germany)
Ionomycin, calcium salt	Sigma, St. Louis (USA)
KN-62, 1-[N,O-bis(5-isoquinolinesulfonyl)-N-methyl-L-tyrosyl]-4-phenylpiperazine	Sigma, St. Louis (USA)
Leupeptin hydrochloride	Sigma, St. Louis (USA)
L-Glutamic acid	Roth, Karlsruhe (Germany)
Lipofectin	Invitrogen, Carlsbad (USA)
Lysozyme	Sigma, St. Louis (USA)
Magnesium chloride hexahydrate	Merck, Darmstadt (Germany)
MES monohydrate	Sigma, St. Louis (USA)
MOPS	Merck, Darmstadt (Germany)
NeuroBasal medium	Gibco, Grand Island (USA)
Ni-NTA Agarose	Qiagen, Hilden (Germany)
NMDA (N-Methyl-D-Aspartic Acid)	Sigma, St. Louis (USA)
Penicillin-Streptomycin	Gibco, Grand Island (USA)
Pepstatin A	Sigma, St. Louis (USA)
Pfu polymerase	Stratagene, La Jolla (USA)
Phenylmethylsulfonylfluoride (PMSF)	Sigma, St. Louis (USA)
PIPES	Sigma, St. Louis (USA)
Pluronic F-127 in DMSO	Molecular Probes, Eugene (USA)

Name	Supplier
Poly-L-lysine hydrobromide	Sigma, St. Louis (USA)
Potassium chloride	Merck, Darmstadt (Germany)
Ribonuclease A	Sigma, St. Louis (USA)
Saccharose	Merck, Darmstadt (Germany)
Sodium bicarbonate	Sigma, St. Louis (USA)
Sodium chloride	Sigma, St. Louis (USA)
Sodium phosphate monobasic, anhydrous	Sigma, St. Louis (USA)
T4-Ligase	New England Biolabs, Beverly (USA)
Tissue-Tek	Sakura, Tokyo (Japan)
Triton-X-100	Sigma, St. Louis (USA)
Trizma Base	Sigma, St. Louis (USA)
Trypsin	Sigma, St. Louis (USA)
Trypsin-EDTA	Gibco, Grand Island (USA)
U0126	Sigma, St. Louis (USA)
Vent polymerase	New England Biolabs, Beverly (USA)

3.5.5 DNA Plasmids and E. coli Strains

Plasmid name	Supplier
pCDNA3	Invitrogen, Carlsbad (USA)
pRSETB	Invitrogen, Carlsbad (USA)
Strain name	Supplier
BL21(DE3)	Invitrogen, Carlsbad (USA)
DH5 α	Invitrogen, Carlsbad (USA)

4. Results

4.1 Construction and characterization of fluorescent biosensors for CREB family transcription factor activation

The aim of this study was to construct and characterize genetically encoded fluorescent indicators for the activation of CREB family transcription factors for the application in live cells and tissues. As a starting point we decided to employ the kinase inducible domain (KID) of CREB and the corresponding interaction domain (KIX) of the CREB binding protein. The idea was to fuse the two domains together via a flexible linker and sandwich the fusion protein between a cyan and a yellow fluorescent protein. Thus, the first construct contained the full length KID and the full length KIX linked by the short peptide GGSGGT. The tuning of the sensor by varying the length and the structure of the KID, KIX and linker region and thereby optimizing FRET efficiency was described in a previous study (Friedrich, M. Diplomarbeit 2004). This work focuses on the characterization of the CREB family sensors in live cells, tissues and transgenic model organisms.

The optimized indicator constructs used in this work are shown in figure 8. The indicator for CREB activation due to phosphorylation was termed ICAP and is the prototype for all other constructs. ICAP contains the amino acids 121-160 of the KID and the amino acids 586-662 of KIX fused with the linker peptide GGSGGT, sandwiched between CFP and citrine (Griesbeck et al, 2001). This *bauplan* was the backbone for all other sensor constructs used in this study. The modifications, as indicated in figure 8, were the exchange of citrine for the circular permuted variant citrine cp174 (Mank et al., 2006), the fusion of nuclear (NLS) and mitochondrial (mt) localization sequences, the exchange of the KID for the KIDs of ATF-1 and CREM and the exchange of the KIX of CBP for the KIX of P300. The ATF-1, CREM and P300 sensors, as well as the NLS-ICAP and mt-ICAP, will be referred to in later chapters. Before the characterization in living cells, ICAP's properties were tested in a fluorescence spectrometer. Therefore ICAP was expressed in *E.coli*, purified and then an emission spectrum was taken exciting the fusion construct at 432 nm (Fig. 9 A). The spectrum showed the characteristic emission maxima of CFP at 475 nm and

of YFP at 528 nm. In its unphosphorylated state, high basal FRET occurred between CFP and YFP (Fig. 9 A). Adding purified catalytic subunit of protein kinase A (PKA) to the reaction resulted in a increase of the CFP emission intensity at 475 nm and a concomitant decrease of the YFP intensity at 528 nm. Exchanging the citrine with the circular permuted variant cp 174 caused the ratio change after PKA addition observed with ICAP to revert, i.e. the CFP intensity decreased and the YFP intensity increased, from a significantly lower basal FRET between the two fluorophores (Fig. 9 B).

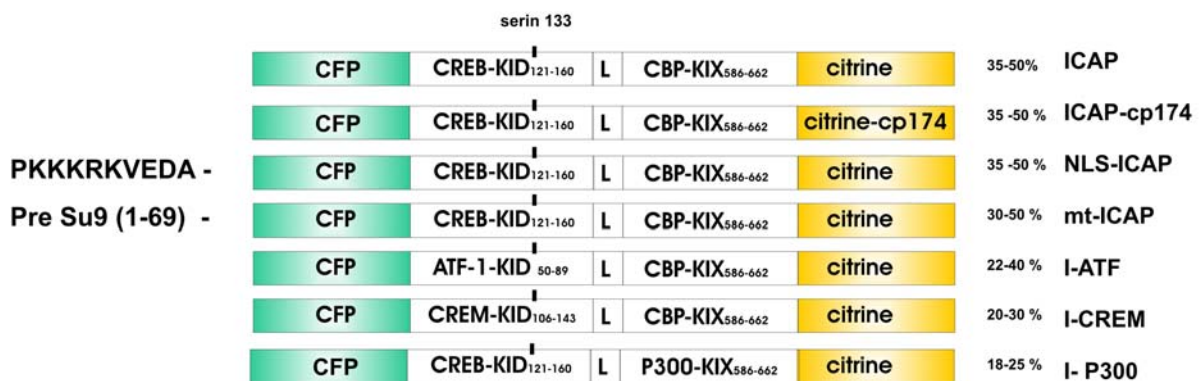


Figure 8: Schematic drawing of the different indicator constructs. The linker between the two fluorophores CFP and citrine consists of the kinase inducible domain (KID) of CREB, ATF-1 and CREM, and the KID interaction domain (KIX) von CBP or P300. In ICAP cp174 citrine was exchanged for citrine cp 174. For nuclear localization (NLS) and mitochondrial localization (mt) the respective targeting peptides are shown. The serine 133 within the KID is emphasized. On the right side you can see the range of the maximal ratio change. L is the linker GGSGGT.

From these experiments we hypothesized the working principle of the sensor as depicted in figure 9 C. In the unphosphorylated state the random coil conformation of the KID fused to the KIX facilitates FRET between the fluorophores. Phosphorylation of the serine 133 stabilizes a helical conformation of the KID and the binding of KIX to the helical KID separates the fluorophores and thus disrupts FRET. To verify the specificity of the hypothesized reaction we performed control experiments, which are shown in figure 9 D and E. In these experiments we could show that excluding one of the crucial components, ATP and PKA, of the assay, or mutating serine 133 to the non-phosphorylatable alanine, abolished the time dependent change in the emission ratio of CFP divided by YFP completely. The ability to elicit a change in the emission ratio over time was not limited to PKA. CaMK

IV treatment of the purified sensor construct also lead to a change in the CFP/YFP ratio, albeit with a smaller maximal change after 60 minutes.

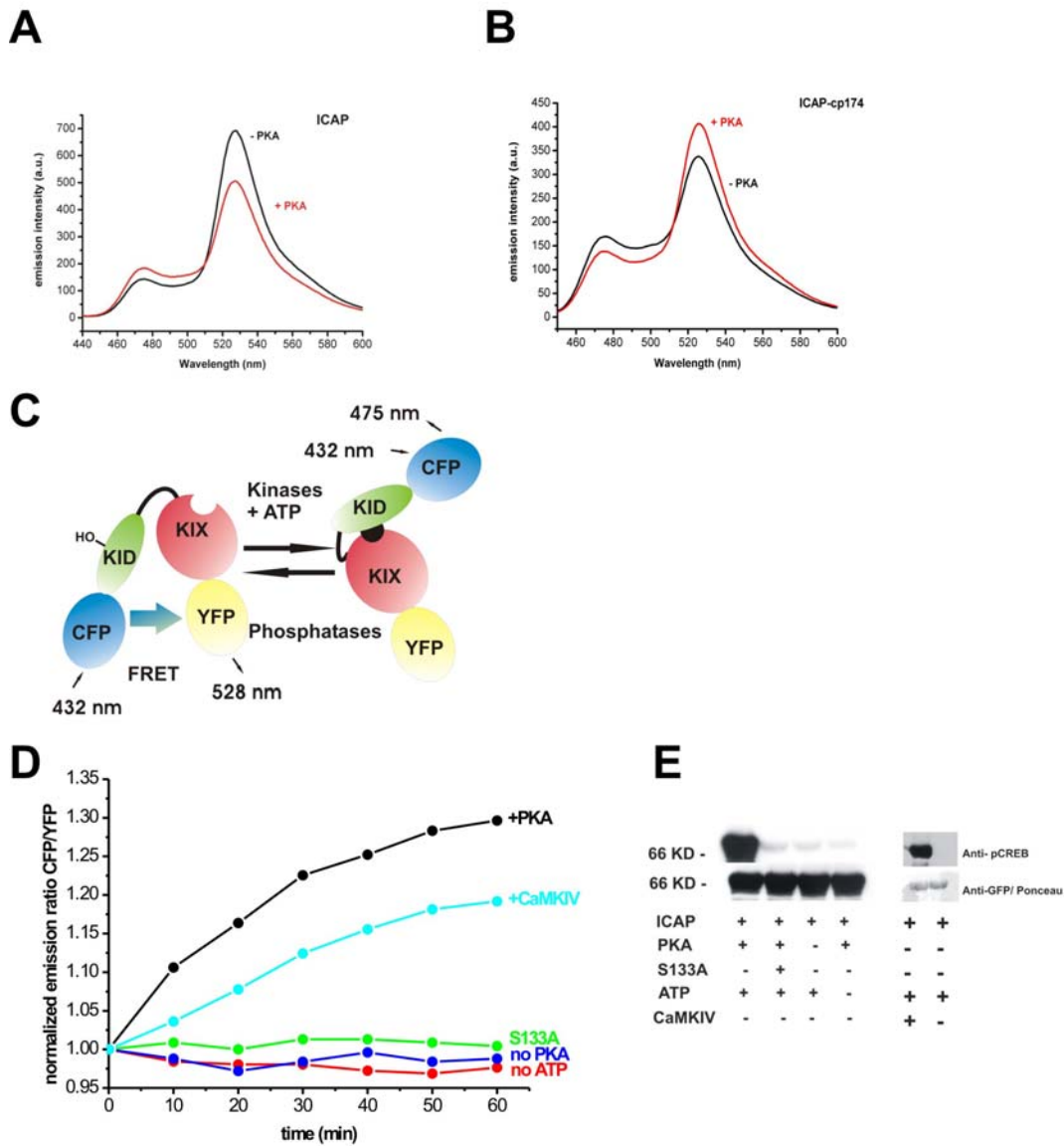


Figure 9: In vitro characterization of ICAP. Emission spectra of ICAP (A) and ICAP-cp174 (B) excited at 432 nm before (black line) and 60 minutes after phosphorylation (red line) of the sensor using Protein Kinase A. Note that ICAP-cp174 is reverted in its response behaviour to phosphorylation. (C) ICAP shows high FRET under resting conditions. Upon phosphorylation of the critical serine 133 (indicated as OH) within the KID domain, KID interacts with the KIX domain thereby reducing FRET from CFP to Citrine. (D) In vitro time course of ratio change in ICAP after phosphorylation with recombinant Protein Kinase A or CaMK IV. A ratio change was absent when either PKA or ATP was omitted from the assay or when the critical serine 133 was mutated to alanine.

(E) Western Blot analysis of recombinant ICAP using antibodies specific for phosphorylated serine 133-KID (anti-pCREB) or GFP after various treatments.

Western blot analysis using a specific antibody that recognizes phosphorylated serine 133 demonstrated that the serine 133 of the indicator was indeed phosphorylated under kinase assay conditions in contrast to control conditions, where no phosphorylation at serine 133 was detected (Fig. 9 E). The same was true for phosphorylation after CaMK IV treatment.

4.2 Measuring ICAP activation in HeLa cells

CREB is ubiquitously expressed in all cells of the body and there it is localized in the nucleus and the mitochondria. It seems to be, in great part, constitutively bound to promoter elements in the nuclear and mitochondrial genome, waiting for incoming signals to initiate gene transcription. Therefore we fused small signaling peptides to the N-terminus of ICAP (Fig. 8) to target it to the nucleus and the mitochondria. In the first part of this chapter we will focus on ICAP activation in the nucleus. In figure 10 A HeLa cells transfected with NLS-ICAP are shown. ICAP is almost exclusively expressed in the nucleus and only a faint residual expression can be seen in the cytoplasm. Bath application of histamine resulted in a change of the emission ratio CFP/YFP in a time dependent manner, which, in figure 10 A, is color coded. After 50 minutes the maximal ratio change was between 20 and 30 %. The next set of experiments was to assess the specificity of NLS-ICAP activation in HeLa cells. We stimulated HeLa cells that were transfected with NLS-ICAP with histamine and forskolin to investigate the kinetics of ICAP activation in living cells. The onset of the activation was already clearly visible 2 minutes after application of histamine or forskolin. The maximal ratio change was reached approximately 30-40 minutes after stimulus application. Mutation of serine 133 to alanine in NLS-ICAP abolished the stimulus dependent FRET change and thus demonstrates the specificity of the reaction. To further prove the reliability of the CREB biosensor we incubated the cells with the pharmacological inhibitor H-89 to block PKA activation in cells. This treatment prevented the observed ratio change after forskolin application (Fig. 10 C), and even lowered the CFP/YFP emission ratio below baseline

levels, indicating a relatively high endogenous basal PKA activity. Application of the solvent DMSO (Fig. 10 C) and 50 mM KCl (data not shown) resulted in a significantly lower maximal ratio change than the positive controls with forskolin and histamine.

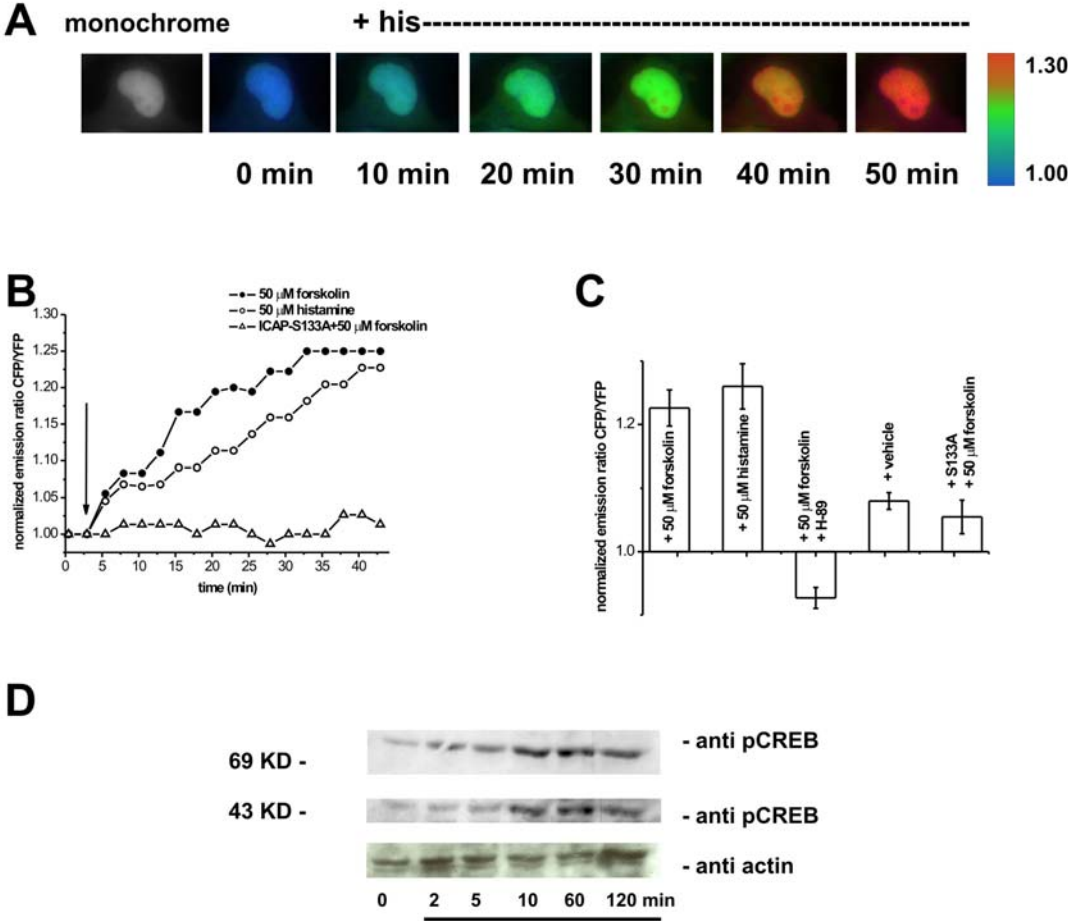


Figure 10: Characterization of ICAP in HeLa cells. (A) Ratio image time lapse of a HeLa cell transfected with NLS-ICAP and stimulated with histamine at the indicated time point (+his). (B) CREB activation in HeLa cells stimulated with forskolin (50 μM) or histamine (50 μM). Cells transfected with NLS-ICAP S133A in which the critical serine residue 133 is mutated to alanine did not show any ratio changes after stimulation with forskolin, demonstrating the in vivo specificity of ICAP. (C) Quantification of the results from (B). Additionally, results from experiments with H-89 and a vehicle control are shown. All emission ratios were taken after an experimental time of 50 minutes. Error bars represent the standard error of the mean from at least three independent experiments. (D) Comparison of ICAP phosphorylation (band at 66 kD) and phosphorylation of endogenous CREB (band at 43 kD) by Western Blot in HeLa cells transfected with NLS-ICAP and stimulated with 50 μM forskolin.

An essential prove for the applicability and reliability of the CREB sensor is to compare the phosphorylation time course and the extent of the overall phosphorylation of the artificial sensor with that of endogenous CREB. For this purpose we performed western blot analysis of HeLa cells transfected with NLS-ICAP, using the specific antibody for serine 133 phosphorylation. Due to their different molecular weight, endogenous CREB, with a molecular weight of approximately 43 KD, and the biosensor with round about 67 KD, could be compared on the same western blot. In figure 10 D the western blot against phosphorylated serine 133 is shown. The onset of phosphorylation is in both cases very fast and clearly visible after 2 min. Both reactions saturate at 60 min, and after 120 min the extent of dephosphorylation is comparable both at 43 KD and at 66 KD. On the whole the kinetics and overall extent of phosphorylation of the sensor and of endogenous CREB resemble each other rather closely.

It has been shown in several studies (Bevilaqua, L.R.M. et al., 1999; Schuh, R.A. et al., 2005; Ryu, H.et al., 2005; Lee, J. et al., 2005) that CREB is localized in the mitochondrial matrix and there binds to CRE-elements and initiates mitochondrial gene transcription. Therefore we fused a mitochondrial localization peptide to the N-terminus of the sensor and expressed the construct in HeLa cells (Fig. 8, 11 A). The putative mitochondrial localization was confirmed by co-loading of mitotracker, which is a commercially available dye that accumulates in the mitochondrial matrix (Fig. 11 B). An overlay of the YFP channel and the mitotracker channel verifies the co-localization of the indicator construct and the mitotracker (Fig. 11 C), which lead us to conclude, that mt-ICAP is exclusively expressed in the mitochondrial matrix. To investigate the activation properties of the sensor in the mitochondria we used histamine and forskolin, testing calcium and cAMP dependent CREB activation. Interestingly, the activation kinetics were markedly different when we directly compared ICAP activation after histamine and forskolin application (Fig. 11 D). Similar to the forskolin induced ICAP activation in the nucleus, the activation kinetics of mt-ICAP after forskolin application was rather slow saturating after 30 min (Fig. 11 D). Contrarily, application of histamine (Fig. 11 D) and also coffeine (data not shown) resulted in a fast and massive activation of mt-ICAP, saturating already within 15 minutes after the stimulus was applied. This prompted us to further investigate the putative calcium dependent activation of mt-ICAP (Fig. 11 E, F). We assessed the

contribution of calcium by chelating free calcium with the acetoxymethylester of BAPTA. BAPTA reduced the activation of mt-ICAP significantly. Residual activation is probably due to the simultaneous activation the cAMP pathway. To find out about the source of calcium we pretreated the cells with CPA to empty internal calcium stores and we found that mt-ICAP activation was significantly reduced. Inhibition of CaMK IV with KN-62 likewise reduced the activation of mt-ICAP (Fig. 11 E, F).

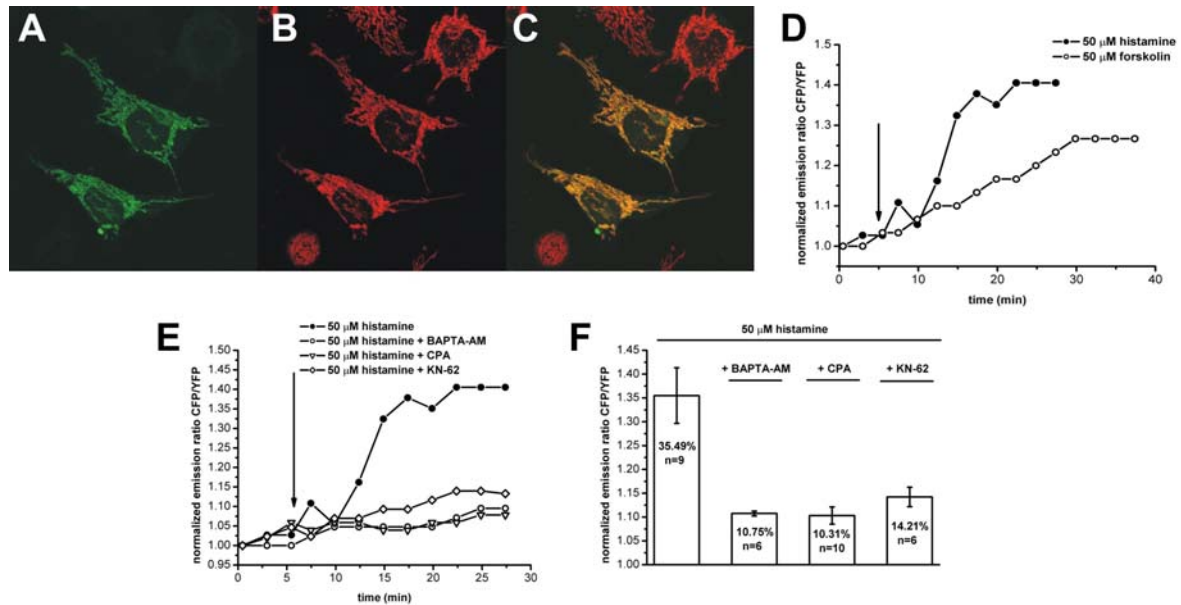


Figure 11: Characterization of mt-ICAP. (A) HeLa cells transfected with mt-ICAP and loaded with mitotracker excited at 488 nm (B) The same HeLa cells excited at 578 nm. (C) Overlay of the pictures in (A) and (B). (D) Time courses of the activation of mt-ICAP after histamine (filled circles) and forskolin (open circles) stimulation. The arrow indicates the time point of the application. (E) Comparison of the time course of mt-ICAP activation after histamine application (filled circles) with time courses of mt-ICAP activation in the presence of the indicated pharmacological inhibitors. (F) Quantification of the results in (E).

Application of KN-62 did not lead to a complete abrogation of the mt-ICAP activation. This, together with the results after BAPTA and CPA application, also shows that calcium is not the only second messenger activated after histamine application. The heterogeneity of the calcium dependent mt-ICAP activation reflected in the relatively broad error bars in Figure 11 F and previous research on calcium dynamics in mitochondria (for review see Alonso, T., et al. 2006) lead us to hypothesize microdomains of CREB activation in mitochondria. To test this hypothesis we investigated mt-ICAP activation in subsets of mitochondria after histamine stimulation

(Fig. 12). Unstimulated HeLa cells showed a homogenous ground state, meaning unphosphorylated state, ratio of CFP/YFP (Fig. 12, upper panel, far left). This is noteworthy because it means that all sensor molecules started from the same baseline. Stimulation of these cells with histamine activated mt-ICAP with very heterogenous characteristics, meaning that different mitochondrial regions in the cell responded differently to the stimulus (Fig. 12 upper panel). A higher magnification of a subset of mitochondria revealed locally restricted mt-ICAP activation “hot spots” after 10 minutes of stimulation with histamine (Fig. 12, lower panel).

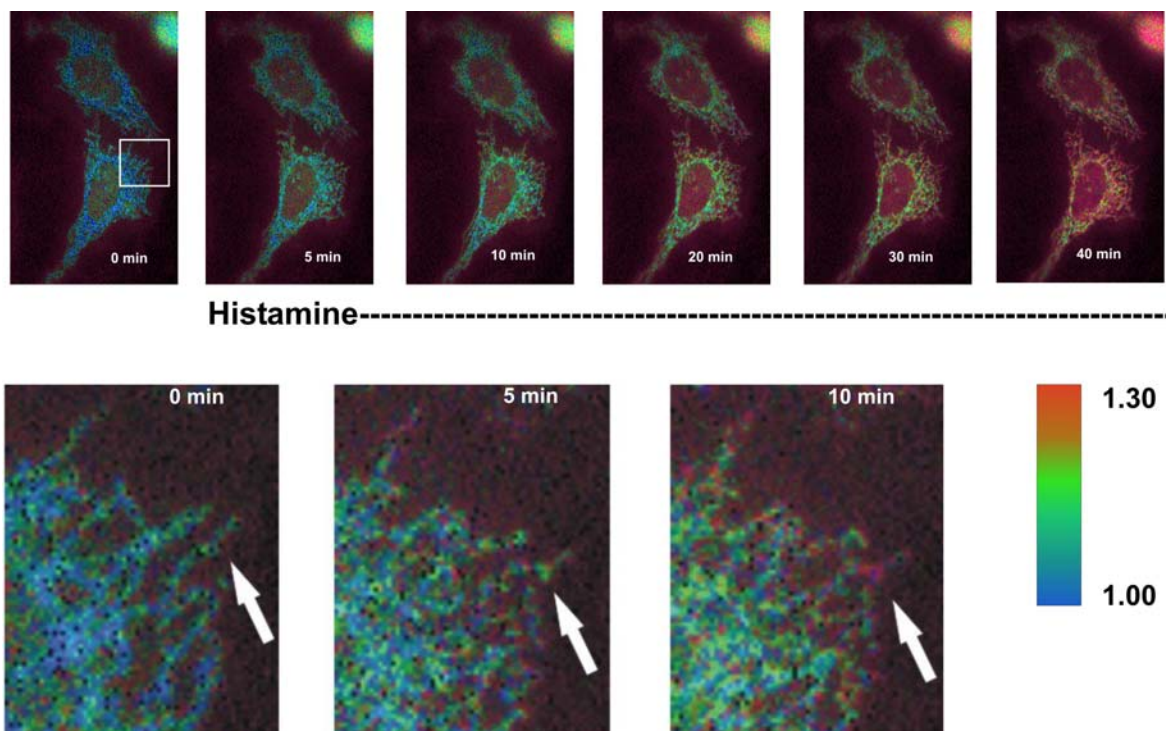


Figure 12: Mt-ICAP activation in subsets of mitochondria. HeLa cells transfected with mt-ICAP and stimulated with histamine for the indicated time. The CFP/YFP ratio is color coded blue meaning no activation, the sensor is in its ground state, and red meaning maximal activation. The white box in the upper left picture marks an area that is magnified in the lower panel. The white arrow hints at subsets of mitochondria where the activation is faster than in the surrounding mitochondria.

In these “hot spots” mt-ICAP activation seems to happen faster than in the surrounding subsets of mitochondria, where the activation kinetics was slower. In addition, it is also worth considering, that the “hot spots” lie more to the periphery of the cell, whereas in the mitochondrial regions closer to the nucleus the activation was, in general, slower and more homogenous (Fig. 12, white arrow in lower panel).

4.3 Neuronal CREB activation visualized with ICAP

Despite its ubiquitous expression, most research on the transcription factor CREB has focused on its function and regulation in the nervous system. This is not astonishing because of its prominent role in neuronal survival, synaptic plasticity and memory formation. Therefore, in this part of the study, we changed the experimental setting from HeLa cells to primary hippocampal neurons to investigate CREB activation in real time in living neurons. The logic of the experimental course was to first characterize the response properties of ICAP in living hippocampal neurons, in a sense that we wanted to compare the characteristics of the activation of our sensor with the published characteristics of the activation of endogenous CREB. Additionally, we set out to analyze CREB activation in developing hippocampal neurons after GABA_A – and GABA_B – receptor stimulation. Secondly, we sought to explore the interrelationship between dynamic calcium signals, as calcium is one of the most important second messengers that activate CREB in neurons, and CREB activation in single living cells. In the last part we examined the activation of other members of the CREB family namely ATF-1 and CREM, and the recruitment of P300, a CBP homologue.

The physiology of HeLa cells and primary hippocampal neurons is fundamentally different not the least because HeLa cells are an immortal cell line derived from a cervical cancer and thus do not necessarily display “normal” traits of a cell. Hence, it is of importance to again assess the behaviour and the response properties of the sensor in primary neurons. For this purpose we transfected primary hippocampal neurons with NLS-ICAP and checked whether the sensor localized to the nucleus of the cell. Fluorescence could almost exclusively be found in the nucleus of the transfected neuron (Fig. 13 A). Residual fluorescence in the cytoplasm is most probably due to the fact that the sensor is continually translated at ribosomes in the cytoplasm before being transported to the nucleus. It has been shown that various stimuli activate signaling pathways culminating in CREB phosphorylation. To test if our sensor detects signals that activate CREB, i.e. if there occurs a significant ratio change upon stimulation of the neurons we applied neurobiologically relevant stimuli to the cell and measured the emission intensities of the fluorophores and calculated

the emission ratio of CFP/YFP (Fig. 13 B). First, to have a direct comparison to ICAP activation in HeLa cells and in the cuvette, we applied forskolin to activate the adenylyl cyclase and thereby stimulate PKA activity. Stimulating ICAP transfected neurons with forskolin resulted in a change of the CFP/YFP ratio in a time dependent manner. Activation started immediately within 2 minutes after bath application of forskolin and began to saturate after 40-50 minutes. The activation time constant was $47,0 \pm 0.28$ min (n=3). The onset of the activation and the time point for saturation correspond well to published material on CREB activation in neurons (Shaywitz and Greenberg, 1999).

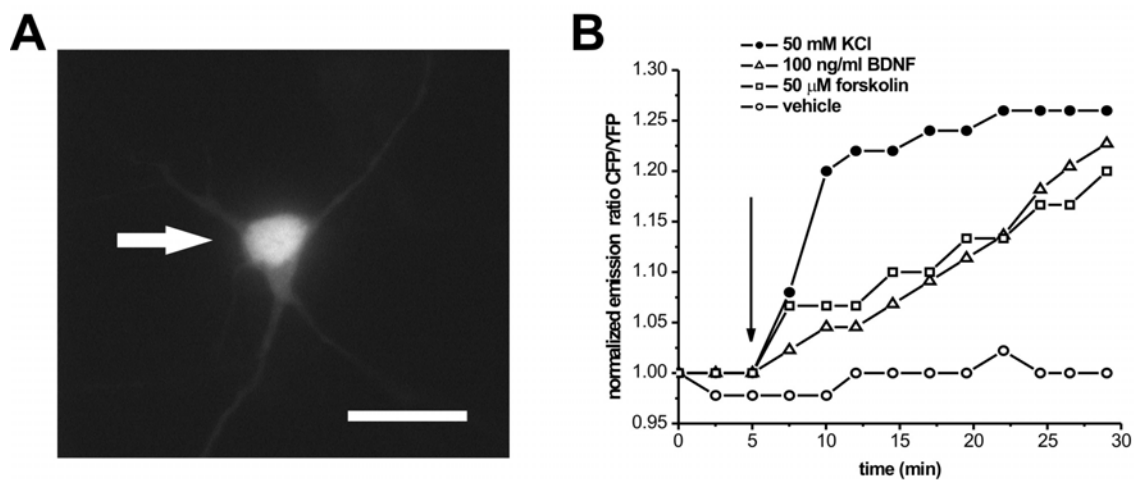


Figure 13: Test of functionality with ICAP in primary hippocampal neurons. (A) Neuron transfected with NLS-ICAP. White arrow marks the nucleus of the cell. White bar represents 20 μ m. (B) Time courses of ICAP activation after several stimuli. Three pathways with different temporal features converge on CREB in hippocampal neurons. A fast high potassium-mediated CREB activation can be differentiated from slower activations by forskolin (50 μ M) or the neurotrophin BDNF. Black arrow marks the time point of bath application of the agent.

The most prominent and maybe the best characterized pathway to CREB phosphorylation in neurons is after membrane depolarization by increasing the extracellular potassium concentration. It has been shown, that high potassium stimulation of neurons clamps the membrane potential of the neuron to 0 mV which according to current knowledge provides maximal activation of voltage-gated sources of calcium influx (Wu et al., 2001a). When we stimulated transfected neurons

this way we found that CREB was activated very strong and very fast compared to the forskolin stimulus. The activation occurred immediately and saturated after 5-10 minutes. The activation time constant was 2.2 ± 0.42 min (n=12), which is almost 20 times faster than the forskolin mediated activation. These data is well in accordance to published data about CREB activation after calcium influx inside the cell (Wu et al., 2001). Calcium and cAMP are, nonetheless, not the only signaling pathways to activate CREB. Among several others is the mitogen- extra cellular signal activated protein kinase (MAPK) pathway the most important. This pathway transfers signals elicited by neurotrophic factors and thus is essential in the development and the modulation of the nervous system. The neurotrophic factor BDNF has been shown to activate CREB in neurons and thus we tested whether we could measure the BDNF mediated CREB phosphorylation. Bath application of 100 ng/ml BDNF resulted in a change of the emission ratio of CFP/YFP in a time dependent manner. The reaction started immediately within 2 minutes of the stimulation and saturated after approximately 50 minutes. The activation time constant was 52.5 min \pm 0.43 min (n=3).

So far we only tested whether NLS-ICAP could be activated by certain stimuli and hypothesized the corresponding pathways. In the following set of experiments we dissected out the different signaling pathways that contribute to the respective activation characteristics using pharmacological inhibitors. First, we analyzed the fast high potassium mediated ICAP response. In a publication of Wu et al., from 2001, it has been found that two pathways contribute to the high potassium mediated activation of endogenous CREB: A fast calcium/calmodulin dependent kinase IV (CaMK IV) pathway and slower mitogen activated protein kinase (MAPK) pathway. If our sensor activation really corresponds to endogenous CREB activation, as we proposed in Fig. 10 D, we should be able to differentiate between the fast CaMK IV pathway and the slow MAPK pathway and visualize them with our sensor in living neurons. When we stimulated neurons that were transfected with NLS-ICAP with high potassium in the presence of KN-62, which is a blocker of CaMKinases, we observed an activation of ICAP that was slower (time constant: 32.21 ± 0.32 min, n=3) in comparison to the control without KN-62 and also reduced in amplitude (Fig. 14 A, D). To check if this slow activation is mediated by the MAPK pathway we applied U0126, a potent inhibitor of the MAPK, together with KN-62 (Fig. 14 A, D). Having both blockers present in the medium completely abolished ICAP activation

during the observed time period (Fig. 14 A,D). Interestingly, application of U0126 alone, without KN-62, before stimulation with KCl, did not affect ICAP activation in any respect (data not shown).

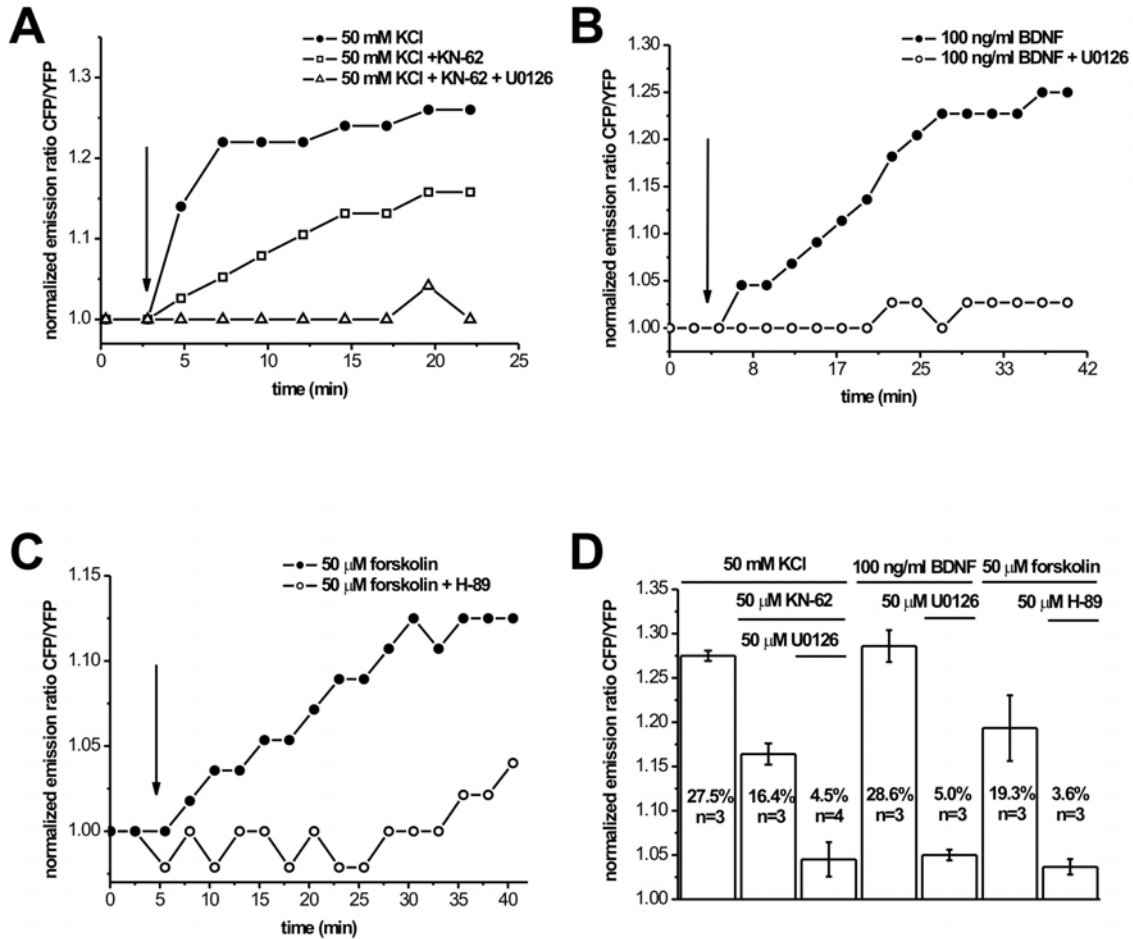


Figure 14: Characterization of ICAP activation in primary hippocampal neurons. (A) Time courses of ICAP activation after high potassium stimulation under different inhibitor regimes. The high potassium-mediated activation is dissected into a fast calcium/calmodulin kinase-dependent pathway that is blocked by KN-62 (50 μ M) and a slower component dependent on the MAP kinase pathway that is blocked by U0126 (50 μ M). (B) Time course of the activation of ICAP after bath application of BDNF (filled circles) and in the presence of U0126 (open circles). (C) Time course of ICAP activation after stimulation with forskolin in the absence (filled circles) and presence of H-89. (D) Summary of the pharmacology of ICAP activation after stimulation with high potassium, forskolin and BDNF. ICAP activation was determined 30 minutes after stimulation in the presence or absence of the various compounds.

In the next set of experiments we assessed the specificity of ICAP activation after BDNF application. It has been shown, that the main pathway that is active after

BDNF application is the MAP kinase pathway with a smaller contribution of the CaMK IV pathway (Finkbeiner, S. et al., 1997). Preincubation of the cells with U0126 before BDNF application resulted in a almost complete abolishment of the ICAP activation over time (Fig. 14 B, D). However, preincubating the cells with KN-62 (data not shown) also reduced the activation of ICAP markedly, which is in accordance with published data (Finkbeiner, S., et al., 1997). Another important pathway that leads to CREB activation that we tested and dissected here was the cAMP-PKA-pathway. Therefore we stimulated neurons with forskolin, in the absence and presence of the PKA inhibitor H-89, and measured the CFP/YFP emission ratio change over time (Fig. 14 C). With no H-89 present in the medium ICAP was activated as described above, however, when preincubating the cells with H-89 this activation was reduced after bath application of forskolin (Fig. 14 C,D).

Visualizing CREB activation in living cells is the prerequisite for a thorough analysis of the events that lead to important long term adaptive changes. However, the influence of activity dependent gene expression on cells is not only modulated by the onset timepoint and the kinetics of the activation, but also by the time point and the kinetics of the cessation of the signal. That is why it is of importance to assess if the sensor can not only visualize the activation of CREB phosphorylation, but also the deactivation. In our case it was again especially vital to distinguish between imaging an artefact, i.e. something inherent to the properties of the sensor itself, and imaging real activation of endogenous CREB. We began tackling these questions by simply washing the high potassium out of the medium after 2-3 minutes with HBSS for three times. Removing the potassium chloride this way resulted in a prompt decrease of the CFP/YFP ratio over time (Fig. 15 A). The average time constant for the rise was 5.84 ± 1.4 min (n=7). It is interesting to state that the emission ratio in almost no case went down to baseline levels, but stayed elevated at a value of 30-50 % of the maximal ratio change (Fig. 15 A, B). In an attempt to understand the reason behind this we plotted the maximal ratio change after stimulation against the percent decrease which is always in relation to the maximal ratio change (Fig. 15 B). From this plot we learned that the higher the maximal ratio change of the sensor is, the higher is the percentual decrease of the signal after wash out, and the closer to

baseline levels gets the signal after the wash out (Fig. 15 B). This phenomenon could be an artefact of the sensor in a sense that it is not possible for the sensor to completely refold to its ground state and thus revert to its initial CFP/YFP ratio. To test this possibility we applied NMDA, a stimulus that only transiently stimulates CREB phosphorylation and from that it has been demonstrated that after 15-20 minutes no phosphorylation of endogenous CREB was present any more (Lee et al., 2005). Application of NMDA lead to an immediate robust increase of the CFP/YFP emission ratio, but, within ten minutes after the maximal change, returned to baseline levels (Fig. 15 C). This total reversion of the CFP/YFP emission ratio is accompanied by an increase in YFP fluorescence and the concomitant decrease in CFP fluorescence, which was expected from the work in the cuvette (Fig. 15 D).

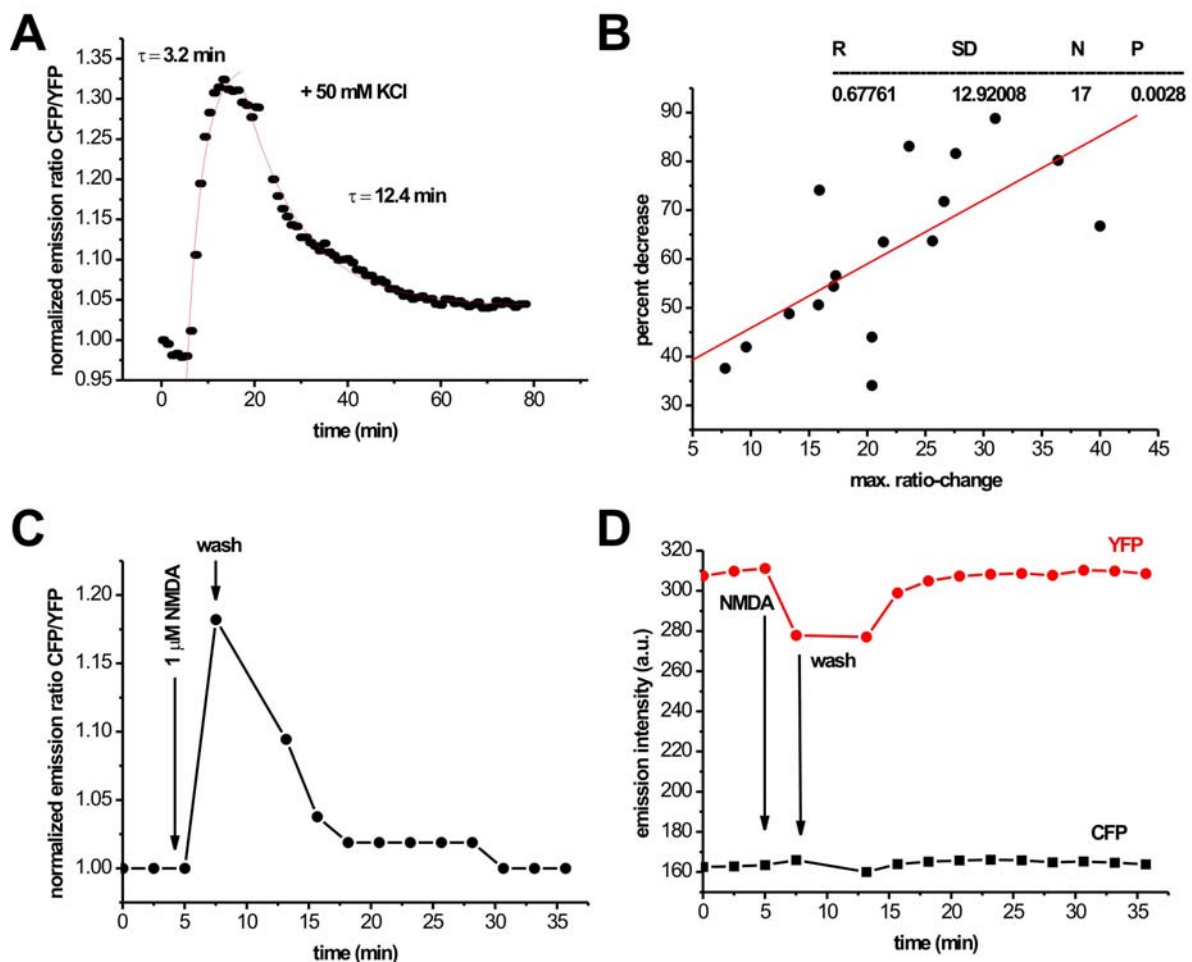


Figure 15: ICAP activation is reversible. (A) Time course of ICAP activation after application of KCl and ICAP deactivation following the wash out of KCl. The time constants were calculated by a single exponential fit of the curves. (B) Plot of the maximal ratio change after saturation of the signal against

the percentual decrease of the signal. The percent decrease was calculated by dividing the emission ratio after complete wash out of the stimulus by the maximal saturated emission ratio in the presence of the stimulus. (C) Time course of ICAP activation after application of NMDA. (D) Time courses of the two fluorophores of the sensor, CFP and YFP, from the experiment in Fig. 15 C.

In the nervous system CREB is activated by a variety of stimuli, including neurotransmitters, neuromodulators and many others. For the characterization of our CREB sensor it is crucial to test many of these stimuli to confirm the reliability and the specificity of ICAP. It has been demonstrated that during development GABA is first excitatory and, due to a developmental switch in the expression of sodium, potassium and chloride ion exchangers, shifts to inhibitory (for review: Stein, V. and Nicoll, R.A., 2003). Furthermore, CREB seems to be activated during that excitatory time window of GABA and even regulate BDNF expression (Obrietan, K., 2002). To test whether ICAP can also be phosphorylated after GABA stimulation in young neurons, and whether this activation is mediated by GABA_A-receptors or GABA_B-receptors, we bath applied GABA, the GABA_A-receptor stimulatory agent muscimol and the GABA_B-receptor stimulatory agent baclofen.

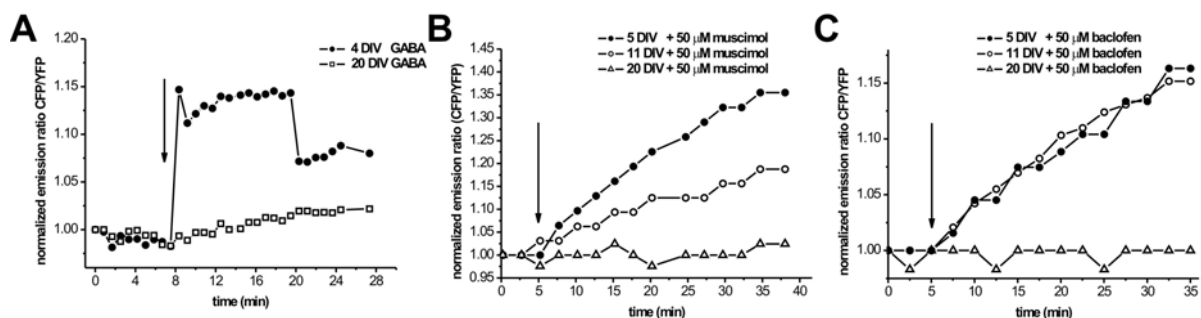


Figure 16: GABA, muscimol and baclofen stimulate CREB activation in a developmental time dependent manner. (A) CREB activation is monitored as the CFP/YFP ratio over time after the addition of 50 μM GABA in young neurons (4 days in vitro = DIV) and in older neurons (20 DIV). (B) Time courses of CREB activation after the application of muscimol in young (5 DIV), middle aged (11 DIV) and older neurons (20 DIV). (C) Time courses of CREB activation after baclofen application in young (5 DIV), middle aged (11 DIV) and older neurons (20 DIV). Black arrow marks the time point of application.

Stimulating ICAP transfected neurons, that were kept in the culture dish for 4 days, with GABA lead to an immediate and fast increase in the CFP/YFP ratio of ICAP (Fig. 16 A). The same stimulus did not result in a significant ratio change in neurons that

were kept 20 days in vitro (Fig. 16 A). GABA binds and activates both GABA_A-receptors and GABA_B-receptors. In order to discriminate between GABA_A-receptor and GABA_B-receptor activation, we chose muscimol and baclofen, respectively. Muscimol application to young (5 DIV) neurons resulted in a robust increase in the CFP/YFP emission ratio, whereas in middle aged (11 DIV) and older neurons (20 DIV) the increase in the emission ratio is moderate (11 DIV) and completely gone (20 DIV) (Fig. 16 B). Interestingly, when we stimulated young neurons (5 DIV) and middle aged neurons (11 DIV) with baclofen, a GABA_B-receptor agonist, we also find a robust increase in the CFP/YFP emission ratio (Fig. 16 C), which has not been demonstrated before. Even more astonishing is the fact, that in older neurons (20 DIV) the increase in the CFP/YFP ratio is abolished completely (Fig. 16 C).

The GABA_A-receptor is a chloride ion channel and the chloride conductance is directly influenced by the chloride potential of the cell. This chloride potential changes in dependency on the expression levels of NKCC 1 and KCC 2, which are a sodium, potassium and chloride cotransporter and a potassium, chloride cotransporter, both of which are developmentally regulated. But the GABA_B-receptor is a G-protein coupled receptor with no obvious relation to the conductance of chloride, the chloride potential or any obvious dependence on developmental effects. Thus we began to unravel the signaling events that lead to CREB activation after baclofen application and GABA_B-receptor activation and compared them to the muscimol mediated signaling events that lead to CREB activation in young 4-6 DIV neurons. From previous studies we learned that the MAPKinase pathway is involved in GABA_A-receptor mediated CREB activation (Obrietan et al., 2002). We confirmed these results by preincubating neurons with U0126 prior to stimulation. Application of muscimol (Fig. 17 A) or baclofen (Fig. 17 B) to these U0126 preincubated cells did not result in a significant CFP/YFP emission ratio change. Since the main effect of chloride in developing neurons is depolarization of the membrane and the activation of voltage gated calcium channels, we also tested for the activation of the main mediator of calcium dependent signaling in neurons: CaMKinases, by the preincubation with KN-62. Interestingly, both muscimol and baclofen dependent CREB activation was gone after preincubation with KN-62 (Fig. 17 A, B). This prompted us to test whether somehow baclofen stimulation alone could trigger calcium influx into the cell by calcium imaging. Application of muscimol to 11 DIV neurons resulted in a massive influx of calcium into the cytoplasm of the cell (Fig. 17 C),

whereas baclofen application did not result in a measurable calcium influx (Fig. 17 D). This is interesting, because in the previous experiment we clearly demonstrate an involvement of CaMKinases. So we hypothesized putative calcium microdomains after baclofen mediated GABA_B-receptor activation to be the cause for these results. In order to test this hypothesis we preincubated the neurons with the acetoxymethyl ester version of the calcium chelator BAPTA. Then we stimulated with baclofen and, fascinatingly, we could not observe a significant activation of CREB (Fig. 17 E). In addition we preincubated the neurons with CPA, a blocker of internal calcium stores, and stimulated with baclofen. Under these conditions we, too, could not detect significant CREB activation (Fig. 17 E).

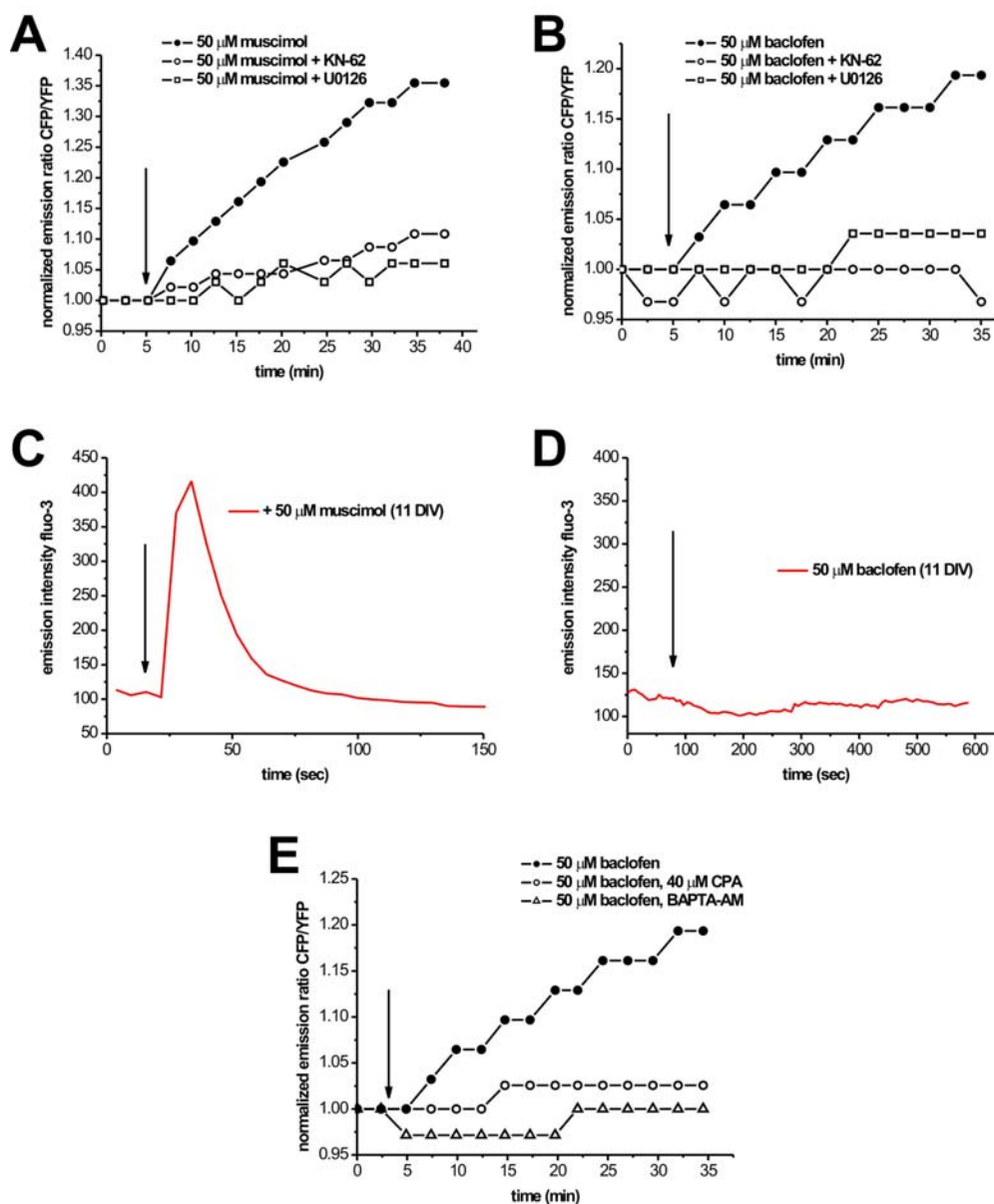


Figure 17: Analysing the signaling pathways that activate CREB after muscimol and baclofen stimulation. (A, B) Time courses of CREB activation after muscimol (A) and baclofen (B) stimulation under different reaction conditions: positive control (black dots), preincubated with KN-62 (open circles) and preincubated with U0126 (open squares). (C, D) Time courses of the emission intensities of the calcium dye fluo-3, loaded in 11 DIV neurons, stimulated with muscimol (C) and baclofen (D). (E) Time courses of CREB activation after baclofen stimulation under various stimulus regimes: positive control (black dots), preincubated with CPA (open circles) and preincubated with BAPTA-AM (open triangles). Black arrows indicate time point of stimulation.

From these sets of experiments we learned that ICAP activation reliably and reversibly monitors CREB activation in living cells. Therefore we started out to investigate the precise temporal regulation of CREB by the second messenger calcium in living cells. For this purpose we had to establish two modifications to our experimental procedures. First, we used the synthetic calcium dye fura-2 (Fig 18 B, D) , which we loaded in cells that were transfected with ICAP, to measure cellular calcium levels concurrent with CREB activation in the same living cell. This allowed us for the first time to directly correlate calcium elevations in neurons with the activation of CREB. Second, we filled electrodes with various stimuli and positioned it closely to the cell of interest. Then we iontophoretically ejected the stimulating agent. Thus we gained a far more precise control of stimulating a cell, especially in the timing of the stimulus (Fig 18 A, C).

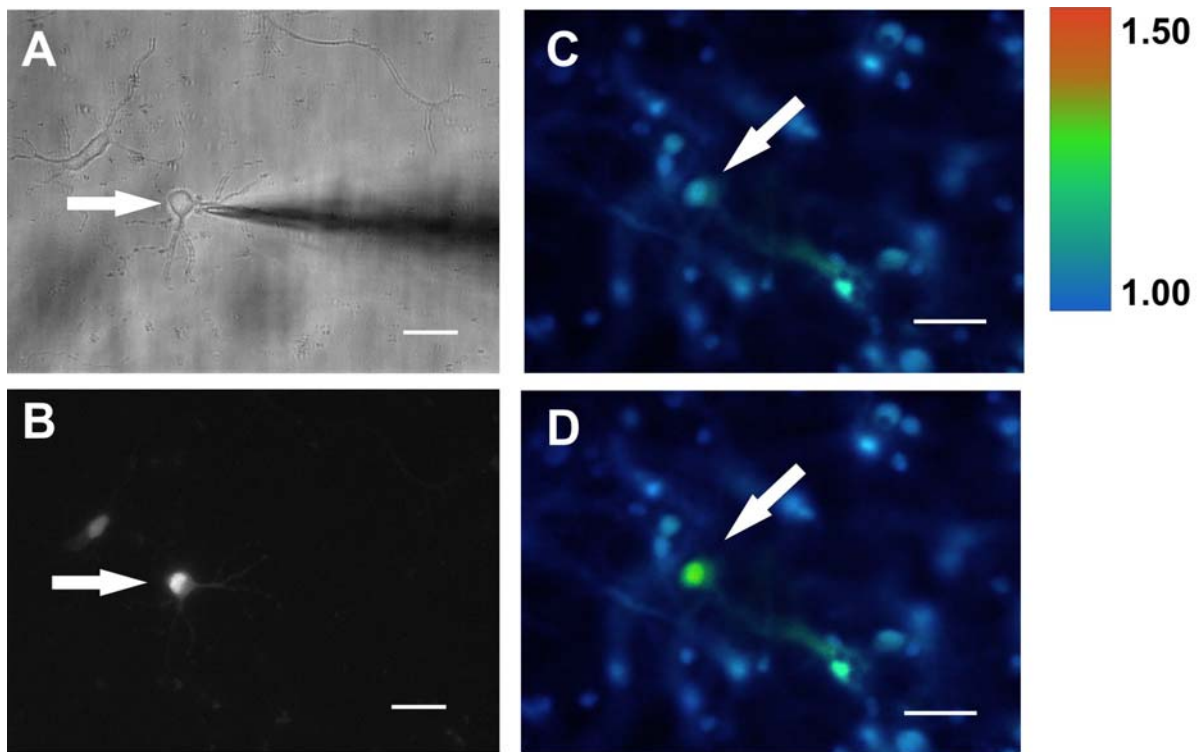


Figure 18: Microiontophoretical application of agents. (A) Hippocampal neuron in culture (white arrow) imaged by bright field microscopy and stimulated by a microiontophoresis pipette containing 50 mM KCl. White bar = 20 μ m. (B) The same cell excited with light of 432 nm and imaged with an 535/25 emission filter. (C,D) Hippocampal neurons loaded with fura-2. In the next two pictures the 350/380 nm ratio is color coded as indicated on the right. The cell indicated with the white arrow is stimulated with a microiontophoresis pipette. (D) The 350/380 nm ratio in the same neuron 10 sec after stimulation. White bar = 20 μ m.

Having established fura-2 imaging and microiontophoretic stimulation we tested next if we can measure calcium with fura-2 and CREB with ICAP simultaneously in the same living cell. We used specific filter sets for fura-2 imaging that allows good separation of fura-2 and ICAP signals. Control experiments, where we measured fura-2 and ICAP in cells that were either loaded with fura-2 or transfected with ICAP showed that no significant signal perturbation or bleed through occurred (data not shown). Then we loaded ICAP transfected neurons with fura-2 and iontophoretically applied glutamate or NMDA (Fig. 19).

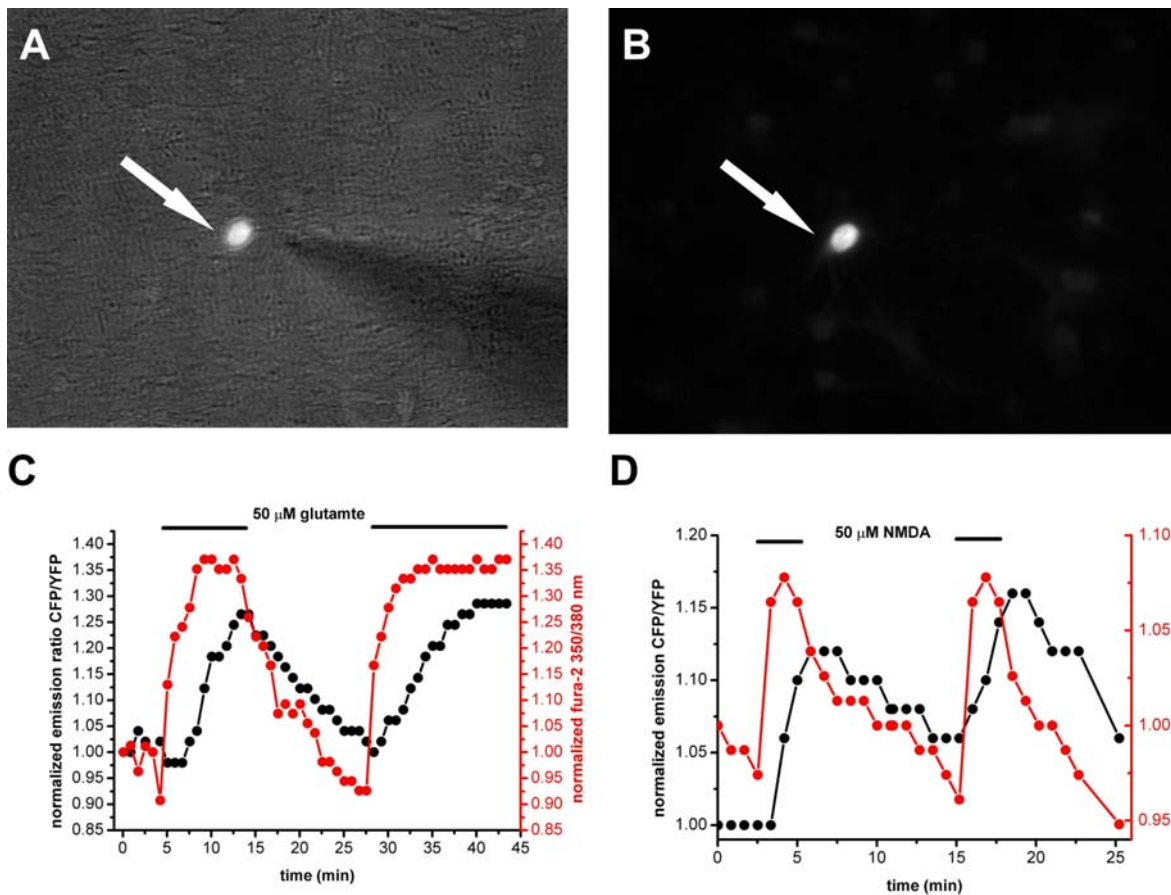


Figure 19: Imaging calcium and CREB activation after glutamate and NMDA application. (A, B) Hippocampal neuron (white arrow) excited at 432 nm, imaged with a 535/25 filter and stimulated iontophoretically with stimulation pipette filled with the respective agent. Under bright field illumination (A), without bright field light (B). (C, D) Simultaneous measurement of calcium and CREB activation by calculating the 350/380 nm ratio for fura-2 (red) and the 475/525 nm ratio for ICAP (black). Black bars represent the presence of the respective agent, glutamate (C) and NMDA (D) for the indicated time period.

In Figure 19 C we stimulated with 50 μ M glutamate and measured simultaneously the emission intensities of fura-2 at 350/380 nm and of ICAP at 475/525 nm. Interestingly, we found that applying glutamate immediately lead to an increase of the 350/380 nm ratio, marking calcium influx into the cell, but the ICAP ratio only started to rise 2.5 minutes later (Fig. 19 C). In the presence of calcium more and more ICAP got activated imaged as an increase in the CFP/YFP ratio. Stopping the glutamate ejection readily resulted in a decrease of the intracellular calcium concentration. Remarkably, CREB phosphorylation followed the calcium concentration and decreased with a delay of about 10 – 12 minutes (Fig. 19 C). This activation was

repeateable, arguing for the robustness of this activation. Similar results were obtained when instead of glutamate NMDA was used as a stimulus (Fig. 19 D).

4.3.1 Visualizing calcium dependent summation of CREB activation in living neurons

At this point we have now established the reliability and sensitivity of ICAP and we have shown that the activation of ICAP indeed corresponds well to the activation of endogenous CREB. So it is justified to speak of CREB activation when talking about the activity dependent change in the emission ratio of ICAP. We now set out to make use of the advantageous properties of ICAP and investigate the fine tuning of calcium dependent CREB activation in living cells. One of the most important types of neurotransmission in the brain uses electrical signals, so called action potentials, to propagate information. To mimick action potential mediated calcium influx we used high concentrations of potassium chloride as described above. In the first set of experiments we applied this high potassium concentrations iontophoretically to single cells and simultaneously measured the calcium concentration and CREB activation in the same cell. There are at least four possibilities for calcium signals to vary and thereby encode information: calcium transients can vary in amplitude, i.e. the amount of calcium ions that enter the cytoplasm, they can vary in duration, i.e. the amount of time the calcium ions are present in the cytoplasm, they can vary in frequency, i.e. the interval between the calcium transients and they can vary in their location where they enter the cytoplasm. In Figure 20 we assessed how the amplitude and the duration of the calcium signals influenced CREB activation. The resting concentration in our neurons was around 80 nM (Fig. 20 A), which is in good agreement with previous studies.

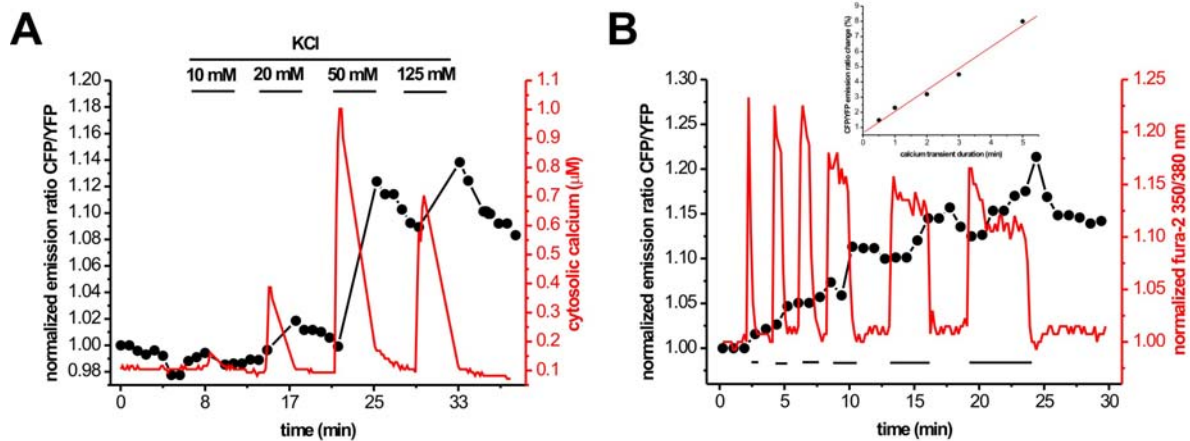


Figure 20: The amplitude and duration of calcium signals and CREB activation. (A) Application of different concentrations of KCl to hippocampal neurons. CREB activation (black dots) was calculated as the emission ratio of CFP/YFP, calcium concentration was calculated from fura-2 emission ratio 350/380 nm (red trace). Black bars represent the length of the stimulus. (B) Application of high potassium for variable time periods (black bars). Inset shows the interdependence of the duration of calcium transients and the ratio change of ICAP. The data was fit with a linear fit.

We used different concentrations of KCl to create calcium transients with different amplitudes (Fig. 20 A). The application 10 mM KCl resulted in a very modest influx of calcium, around 50 nM into the cell. This apparently is not enough to significantly activate CREB since no response is seen in the CFP/YFP emission ratio (Fig. 20 A). Doubling the amount of KCl to 20 mM more than doubled the amount of calcium that entered the cell to 400 nM, which shows the non-linear relationship between the degree of membrane depolarization and calcium influx into the cell mediated by voltage gated calcium channels. With a short lag behind the calcium signal CREB got activated, reached a maximum exactly when the calcium signal went back to baseline and then, with a time constant that is slower than the activation, begins to decay (Fig. 20 A). These interdependent activation characteristics of calcium and CREB get even more pronounced at the optimal 50 mM of KCl, where the calcium concentration rises to 1 μ M and CREB is also activated with the characteristic delay. Interestingly, applying a superoptimal stimulus of 125 mM KCl did not result in a higher calcium influx and concurrently not in a higher CREB activation, rather both calcium response and CREB activation were smaller than with the 50 mM stimulus (Fig. 20 A). Not only the amplitude of the calcium transient is crucial to determine the strength of CREB activation but also the duration of the signal. Using iontophoretic

puffs of KCl with varying ejection times we generated calcium transients of defined length, between 30 sec and 5 min, and concurrently we measured CREB activation with ICAP (Fig. 20 B). It became evident, that the longer a calcium transient was, the greater was the activation of CREB (Fig. 20 B). Additionally, there seems to be a linear relationship between the duration of the calcium transient and the amount of CREB activation (Fig. 20 B, inset). Besides the amplitude and the duration of the signal the frequency of the transients over time, defined by the interstimulus interval, is a determinant of downstream processes. Employing microiontophoresis we tested three different temporal distributions of calcium transients and their effect on CREB activation (Fig. 21). The experimental design was to measure a baseline of five minutes before starting the stimulation. The overall length of the experiment was 30 minutes. When we spaced the calcium signals by 5 min we find a wave-like activation pattern of CREB. After each calcium influx event CREB phosphorylation started to increase shortly but immediately began to decrease again, however, not to baseline levels, rather to an elevated level. This results in an net increase of the activation of CREB. The period of the waves seems to be very close around 3 minutes for every CREB activation wave (Fig. 21 A).

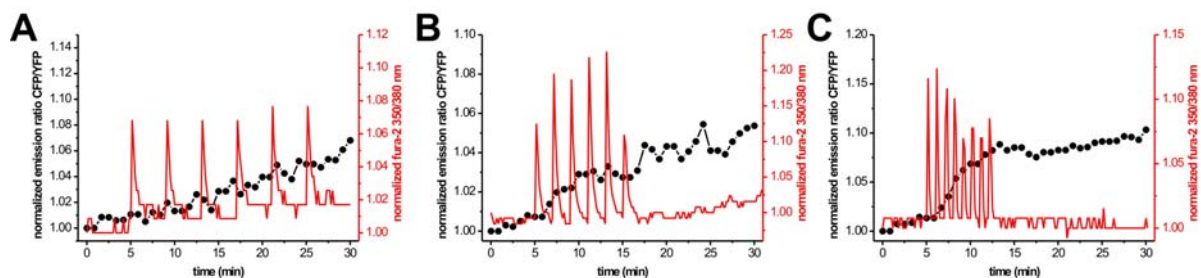


Figure 21: The influence of the interstimulus interval on CREB activation. (A - C) Time courses of CREB activation, measured with ICAP and plotted as the CFP/YFP emission ratio, and calcium, measured with fura-2 and plotted as the 350/380 nm ratio. The interstimulus interval was five minutes (A), two minutes (B) and one minute (C).

Reducing the interstimulus interval to two minutes caused the waves of CREB activation to melt together and to form a uniform rise of CREB phosphorylation over time (Fig. 21 B). Further shortening of the time between the stimuli to one minute, which was the minimal interstimulus interval feasible in our experimental setup, gave a short “burst” of calcium spikes, resulting in a steep rise in CREB activation that

saturated when the burst was over (Fig. 21 C). Unfortunately, it was in our hands impossible to keep the amplitude of the calcium transients constant, in spite of a constant ejection current of 1 nA in all experiments. Apparently, the shortening of the interstimulus interval lead to a summation of the activation of CREB over time. Comparing CREB activation after calcium transients spaced with 5 minutes and 1 minute in more detail it became evident that the activation of CREB after 1min spaced stimuli occurred faster than the wave-like activation in the 5 min spacing paradigm. From this follows that the integral beneath the CREB activation curve after 1min spaced stimuli should be greater than the integral beneath the 5 min spaced activation curve. Indeed, when we directly compare the two interstimulus interval dependent CREB activation curve integrals we find a significant difference (Fig. 22).

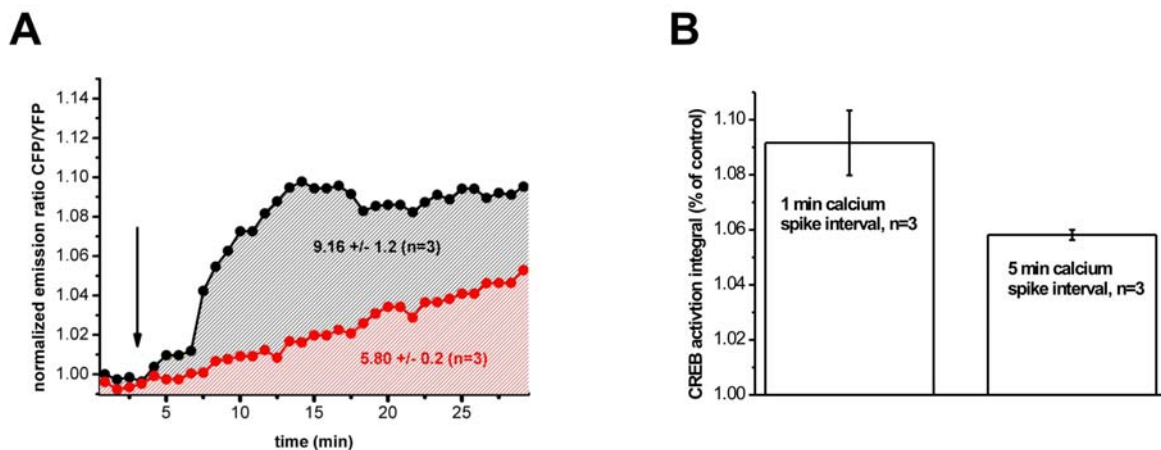


Figure 22: The influence of the interstimulus interval on the integral beneath the CREB activation curve as a measure for the net amount of total CREB activity. (A) Plotted are the integrals beneath the curves of CREB activation after one minute spaced calcium spikes (black) and five minute spaced calcium spikes (red). Arrows marks the time point where the stimulus paradigms started. (B) Quantification of the interstimulus interval dependent CREB activation curve integrals. Error bars indicate the standard error of the mean.

This interstimulus interval dependent CREB activation curve integral stands for the total amount of CREB molecules that are active per time. The shorter the interstimulus interval the greater the integral and thus also the greater the amount of putative CREB dependent transcription per time.

In the nervous system signal integration is not only dependent on the amplitude, duration and the frequency of the signal but also on the location of the initiation of the

signal. To investigate how different stimulus location affect CREB activation, we used microiontophoretic stimulation of single hippocampal neurons and successively moved the stimulation pipette from distal regions of the dendritic tree of the neuron to the nucleus. Unfortunately, it was not possible to image CREB activation and dendritic calcium transients simultaneously in a cell, because the calcium dye did not accumulate in the distal dendrites of ICAP transfected cells in the necessary concentration to allow for reliable measurement, as will be demonstrated later in the text (Fig. 25 A, B). That is why we demonstrated the feasibility of eliciting local calcium transients in dendrites of untransfected neurons that were just loaded with fura-2 (Fig. 23). We briefly puffed 50 mM KCl to the distal, dendritic region of a neuron and imaged a calcium transient that was initiated at the site of stimulation (Fig. 23 B) and propagated further through the dendrite (Fig. 23 C). The calcium transient did not reach the nucleus but faded away before reaching the soma (Fig 23 D). We confirmed that by defining and measuring in regions of interest in the dendrite at the site of initiation of the calcium transient and in the nucleus (Fig. 23 A). The elicited calcium transients give short increases of the 350/380 nm ratio of fura-2 in dendritic regions and only a bath application of KCl resulted in a global increase of the calcium concentration which included the nucleus of the neuron (Fig. 23 A). After that we transfected neurons with ICAP, loaded the cell with fura-2 and measured calcium and CREB in the nucleus. The first stimulus was set at the periphery of the neuron, as in Fig. 23, then we moved successively closer to the soma of the cell. In all three stimulus paradigms we measured calcium and CREB in the nucleus (Fig. 24). When we stimulated at a distal dendrite we could not detect an elevation of nuclear CREB nor could we find any CREB activation (Fig. 24 A). Half way to the soma, at a distance of approximately 80 – 100 μm , we could measure a slight activation of nuclear calcium, but no significant CREB activation in the indicated time period (Fig. 24 B). Stimulating the soma of the neuron directly resulted in a massive influx of calcium in the nucleus of the neuron and concurrently in a robust activation of CREB (Fig. 24 C).

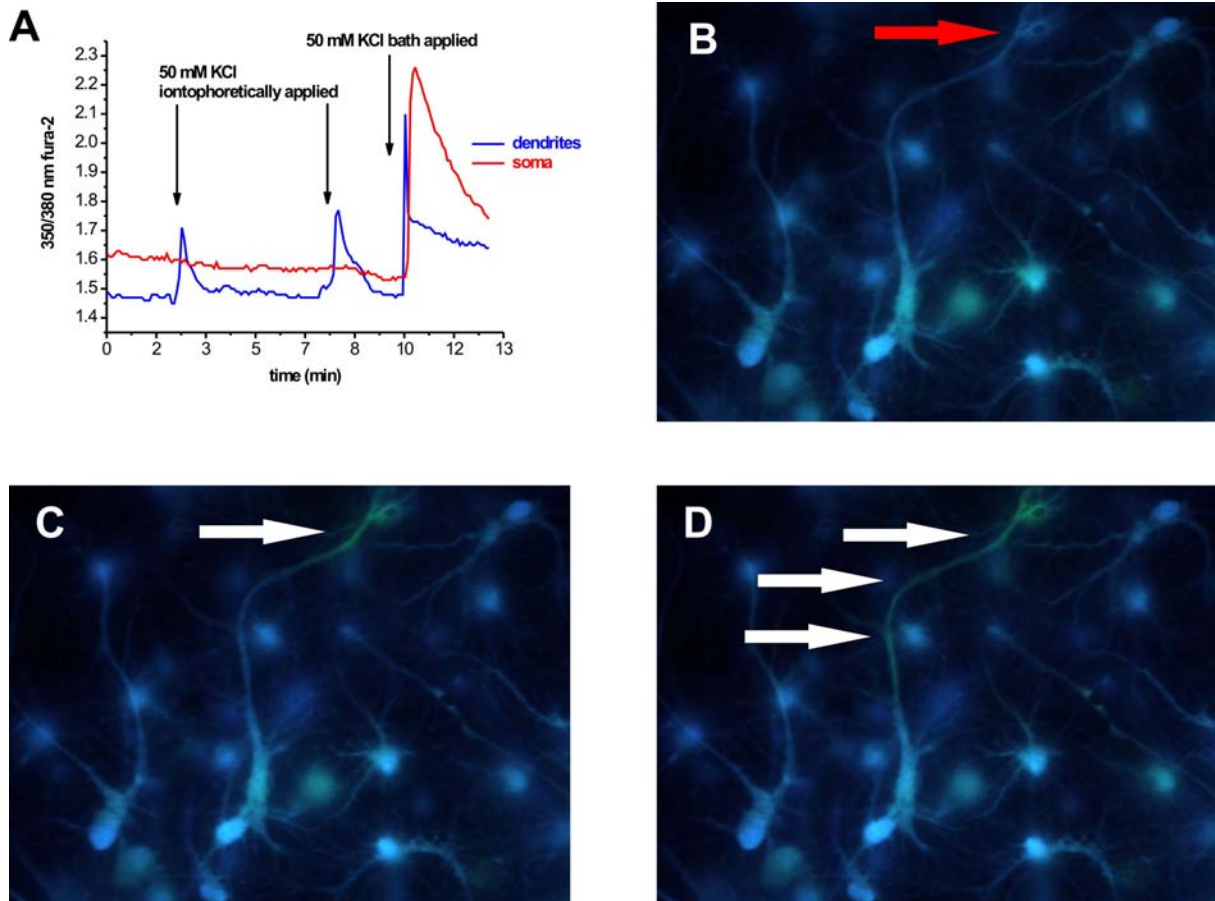


Figure 23: Measuring local calcium transients after microiontophoretic KCl application. (A) Time courses of the emission ratio 350/380 nm of fura-2 measured in regions of interest in the nucleus (red trace) and in the far dendrite (blue trace and red arrow in B). 50 mM of KCl was applied iontophoretically at the indicated time points (black arrows). (B - D) Hippocampal neurons loaded with fura-2. Red arrow indicates the point of stimulation. White arrows marks the calcium transients propagating through the dendrite.

An interesting phenomenon, that runs like a thread through the last Figures, is that CREB has an on-rate that is around 4 times faster than its off-rate after high potassium stimulation (Fig. 15 – 22). This seems to result in a summation of CREB activation due to the fact that after its maximal activation the decay of the phosphorylation is delayed because of the slow off-rate and CREB phosphorylation stays at an elevated level. In the following we set out to precisely assess the calcium dependent summation of CREB activation under defined experimental conditions. As in the previous experiments we transfected neurons with NLS-ICAP and loaded them simultaneously with fura-2 (Fig. 25 A, B). Then we stimulated the cells one, two and

three times with 50 mM KCl after having taken a five minute baseline, and measured ICAP and fura-2 for 30 minutes (Fig. 25 C-F).

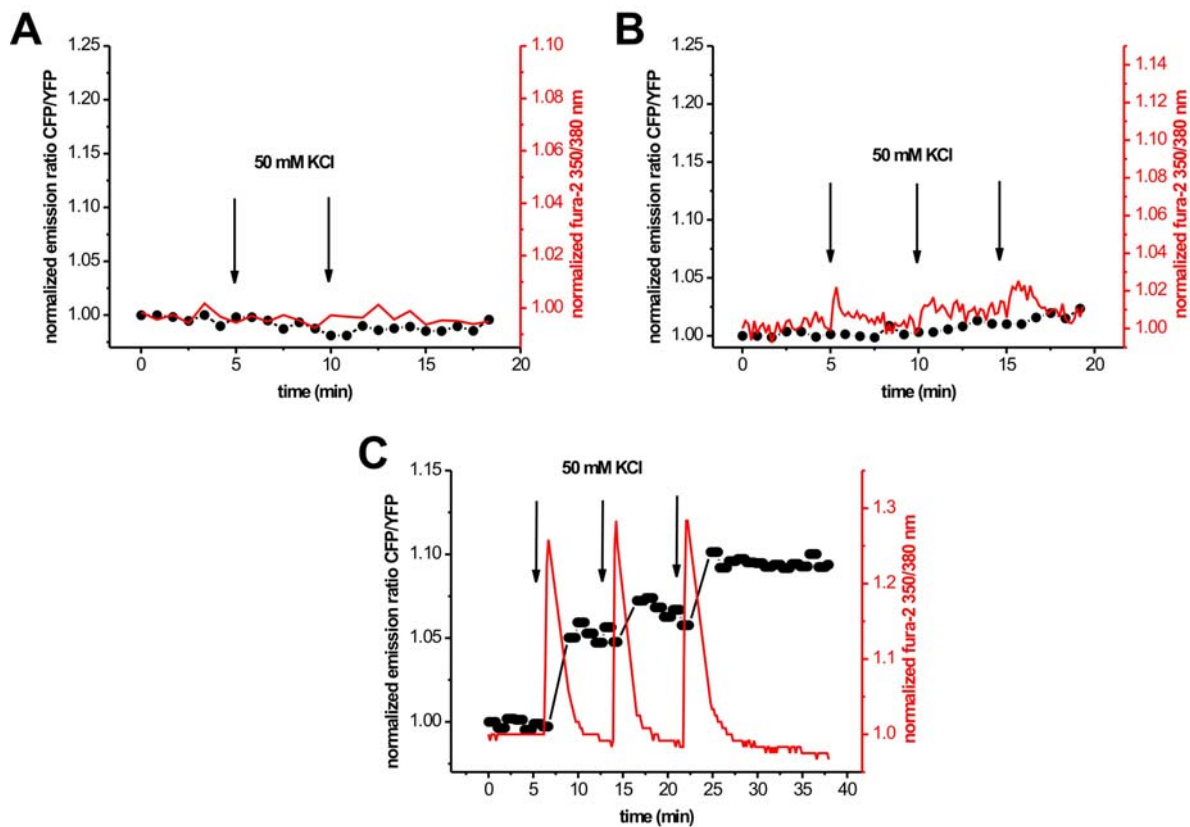


Figure 24: The distance of calcium events influences CREB activation. (A) The microiontophoresis pipette was located approximately 160 – 180 μm away from the soma at a far dendrite and 50 mM KCl was ejected at indicated time points (black arrows). (B) Here the distance was between 60 and 80 μm . In (C) the pipette directly stimulated the soma of the neuron.

In these experiments we stimulated the cells for 3 min with high potassium. This stimulation resulted in an immediate rise of the calcium concentration and a delayed rise in the CREB activity, whereby CREB activation lagged behind between 1 and 3 minutes (Fig. 25 A). The calcium concentration quickly returned to baseline levels, but CREB phosphorylation decayed in a slower manner and did often not even reach baseline levels but stayed at an elevated level (Fig. 25 A). On this plateau the following rise in CREB activity, after the next calcium transient, could build up, and reached ever higher activation states (Fig 25. B).

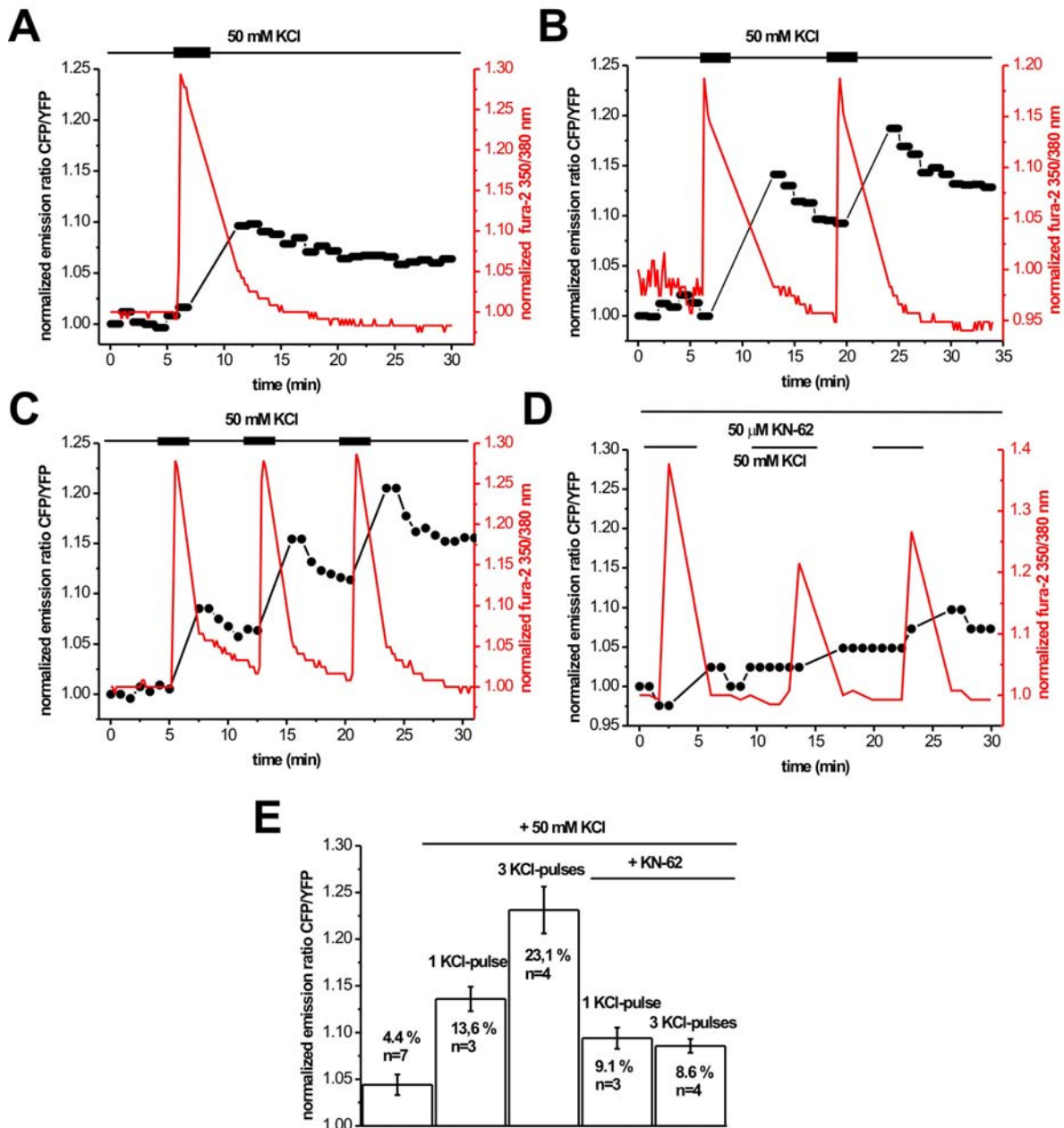


Figure 25: Calcium dependent summation of CREB activation. (A –C) Time courses of calcium measured as 350/380 nm emission ratio with fura-2 and CREB activation measured as CFP/YFP emission ratio with ICAP. Black bars represent the presence of KCl. (D) Time course of CREB activation and calcium with three stimulations in the presence of KN-62. (E) Quantification of all the results from A – C and a comparison of the stimulation paradigm in the presence and absence of KN-62. Error bars represent the standard error of the mean.

A third stimulation with high potassium built up on the plateau of the preceding two stimulations and in the end, after three stimuli, CREB activity was at a higher activation level than after one or two stimuli (Fig. 25 C, E). Since we showed in

Figure 14 that the fast onset of CREB activation is mediated by the CaMK IV, we speculated that CaMKIV is also an important player in the calcium dependent summation of CREB activation. We tested this hypothesis by adding the CaMKIV inhibitor KN-62 to the medium of neurons and stimulated these cells in the same way we did in Figure 25 A – C. CREB activation was not summed up as can be seen in Figure 25 D and E. Comparing CREB activation under the three KCl pulses paradigm with the CREB activation under the one KCl pulse paradigm in presence of KN-62 shows, that no significant difference between the two regimes was evident (Fig. 25 E). However, when we compared the CREB activation under the three KCl pulses paradigm in the presence and absence of KN-62 we found that CREB activation in the presence of KN-62 was reduced by about one third after 3 KCl pulses (Fig. 25 A,D,E). Interestingly, the maximal ratio change after one pulse KCl without KN-62 and one pulse KCl with KN-62 was not significantly different after 30 minutes (Fig. 25 E).

It has been shown, that serin 133 phosphorylation is necessary but not always sufficient to trigger CREB dependent transcription. Thus, when describing a phenomenon with ICAP it is crucial to demonstrate and also to emphasize its importance by showing that there is a direct influence on CREB dependent gene transcription, as well. This is the reason why we started to analyse CREB dependent transcription by using two different techniques. The first technique was to use a firefly – luciferase reporter construct, that was under the control of the evenskipped (EVX) promoter, which contains CRE - elements (Fig. 26 A) (Conkright et al., 2003). As a negative control we used the same vector, with the CRE – sequence mutated, where CREB cannot bind to the promoter any more. We subjected hippocampal neurons to the experimental paradigm we described in Figure 25 and afterwards measured luciferase activity in a fluorescence spectrophotometer (Fig. 26 B). We found that the luciferase activity was elevated after one pulse of KCl in comparison to no stimulation and that luciferase activity was even more elevated after three pulses of KCl (Fig. 26 B). In contrast, when we imaged neurons that were transfected with the mutant-CRE luciferase construct and stimulated three times with high potassium we saw a greatly reduced luciferase activity (Fig. 26 B).

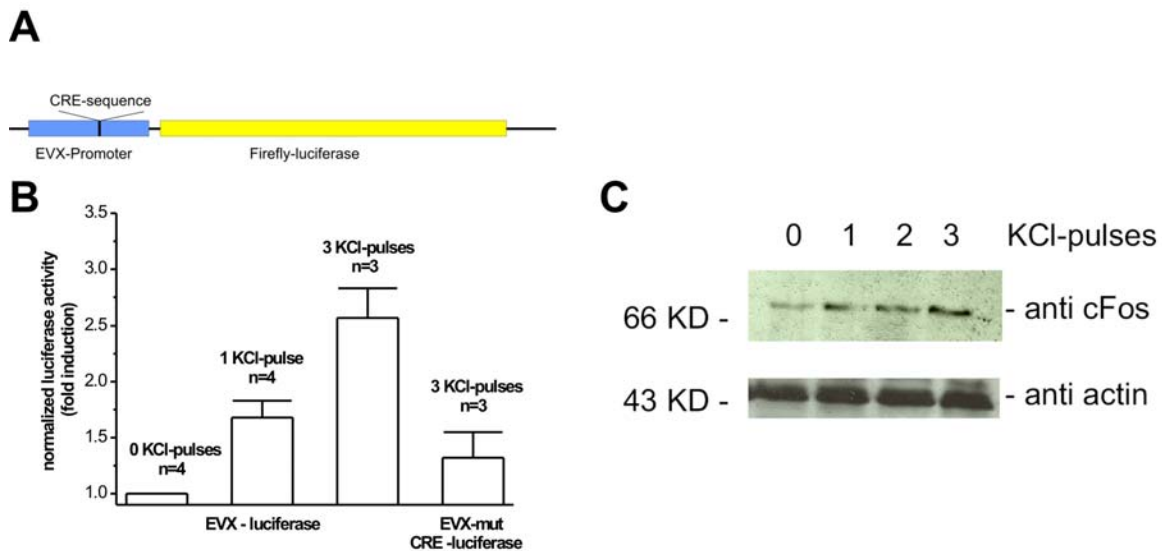


Figure 26: Analysing CREB dependent gene expression. (A) The firefly – luciferase construct we used in the experiment in (B). The evenskipped (EVX)- promoter contains a CRE-sequence and lies 5' to the firefly luciferase gene. (B) Normalized luciferase activity under the same experimental conditions as in Fig. 25 A-C. (C) Western blot analysis of hippocampal neurons stimulated in the indicated way. A anti-cFos antibody was used to probe for the expression level of the immediate early gene cFos at 67 KD. Anti-actin antibodies were used to assess the whole amount of protein in the neurons as a loading control.

In addition to monitoring CREB dependent gene expression with the firefly-luciferase, we used anti- cFos antibodies to probe for the expression level of the CREB regulated immediate early gene cFos. As in the previous experiments we stimulated primary hippocampal neurons with one, two or three pulses of high potassium then lysed the cells and subjected the lysate to western blot analysis using an antibody for cFos (Fig. 26 C). We find that cFos protein expression levels are increasing with the number of KCl pulses, whereas the amount of actin in the cells remains constant (Fig. 26 C).

CREB has been demonstrated to play a pivotal role in long term memory and long term synaptic plasticity, which is in accordance with the fact that CREB phosphorylation can be detected up to 12 hours after stimulation (Marie, H. et al., 2005; Liu, F. C. and Graybiel, A.M., 1996 and 1998). However, it remained unclear if, during the time CREB is active, it can integrate further signals. So we made use of the properties of our sensor and developed a long term imaging assay, where we monitored CREB activity over 2 hours. Two hours was the maximal measuring time

we achieved at 25°C, because after that the health status of the neurons deteriorated visibly. The experimental setup was to stimulate neurons, after having taken a five minute baseline, with high potassium, then wait for two hours and stimulate once again with high potassium to test if CREB can sum up the second stimulus after that time period. The first stimulus lead to massive influx of calcium into the nucleus of the neuron and, with a short delay, CREB activation (Fig. 27). After high potassium was removed calcium levels quickly returned to baseline levels. CREB activity, however, decreased with a slower time constant and during the two hours interstimulus time never reached baseline levels (Fig. 27).

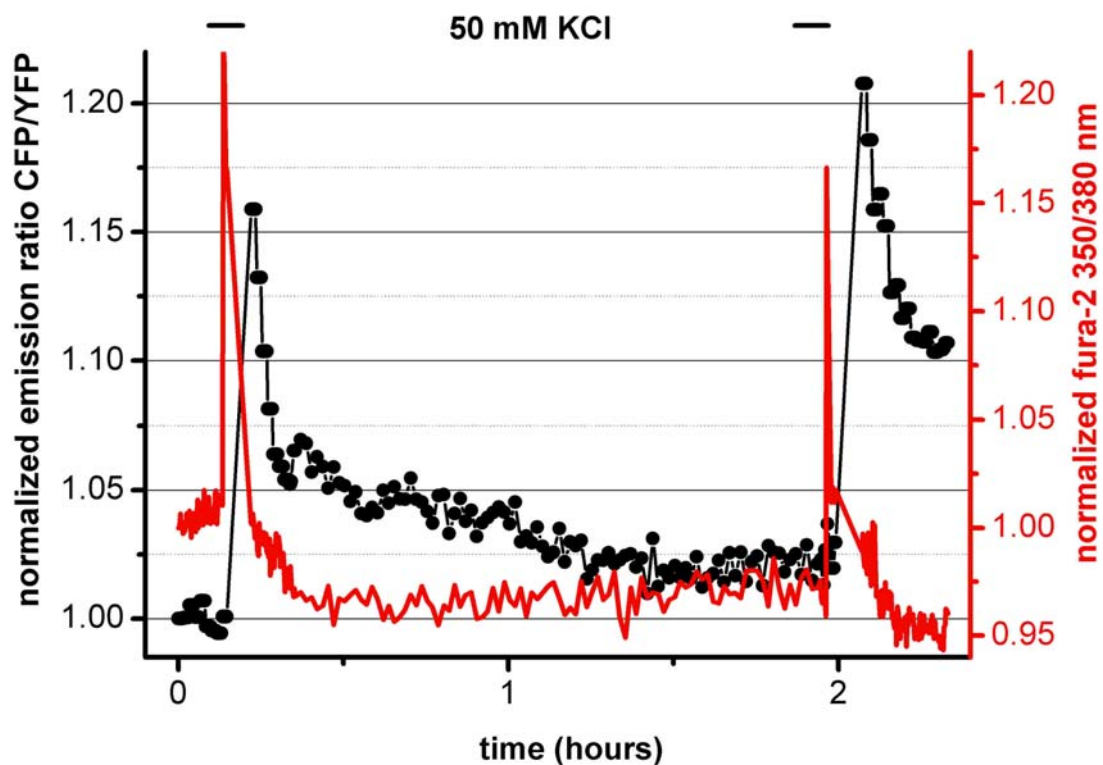


Figure 27: CREB can integrate stimuli that are separated by two hours. A single hippocampal neuron was stimulated with high potassium and after the stimulus was over, the emission ratio of both calcium (red trace) and CREB (black trace) was imaged for two hours. After two hours a second stimulus was applied.

Carefully scrutinizing the CREB deactivation curve, one can see that it seems as if two different time constants of decay occur (Fig. 27, black trace), a fast one immediately after the CREB activation maximum and a slower one. After two hours

we again stimulated the cell with high potassium. Due to the fact that CREB did not return to baseline levels, the second stimulus could build up on the plateau of the previous stimulus and thus sums up to a higher elevated level (Fig. 27).

4.4 Visualizing ATF-1, CREM and P300 activation

The transcription factor CREB is the most prominent member of a whole family of transcription factors. In the previous chapter the construction and characterization of ICAP as biosensor for CREB activation has been described. The indicator construct is shown in Figure 8. In the same Figure we can also see indicator constructs for ATF-1, CREM and P300. They are readily cloned by just exchanging the KID domain of CREB for the KIDs of ATF-1 or CREM and by replacing the KIX of CBP for the KIX of P300 (Fig. 8). It is interesting to speculate about the possible differences in the regulation of the respective CREB family members, but a functional test, so far has not been attempted. With our sensor constructs we now have the possibility to compare the activation kinetics and the stimulus response spectrum of the KIDs of the CREB family members in living cells and tissues. First, we characterized the new sensors in the cuvette. Therefore we expressed them in *E.coli*, purified the recombinant protein and measured the increase in the CFP/YFP emission ratio as in Figure 9. All three proteins display a pronounced increase of the emission ratio over time, when we stimulated the phosphorylation of the constructs with recombinant protein kinase A (PKA) (Fig. 28). The maximal ratio change after 60 minutes for the ATF-1 sensor was 40 % (Fig. 28 A), for the CREM sensor 25 % (Fig. 28 B) and for the P300 sensor 30 % (Fig. 28 C). To be sure that we measure a specific reaction in the cuvette, we performed control experiments, where we omitted the crucial components, PKA, ATP, serine 133, one after the other, from the reaction. All three sensors seem to be very specific in these terms, as none of them showed a significant ratio change over time under control conditions (Fig. 28 A-C). We did not mutate the serine 133 from the P300 construct, because the KID is, as in ICAP, the KID of CREB and for this we already tested the specificity extensively (Fig. 9, 10). It is interesting to see that the CREM sensor has apparently the slowest on-kinetic. After 30 minutes the ATF-1 construct has already a CFP/YFP emission ratio of almost 30% (which is equivalent to 75 % of the maximal activation), the P300 sensor

has a ratio of 22.5 % (= 72.3 % of maximal activation) and the CREM sensor is at a ratio of 12.5 % (= 54 % of the maximal activation (Fig. 28). The next step was to transfect primary hippocampal neurons with the constructs and characterize them in living cells.

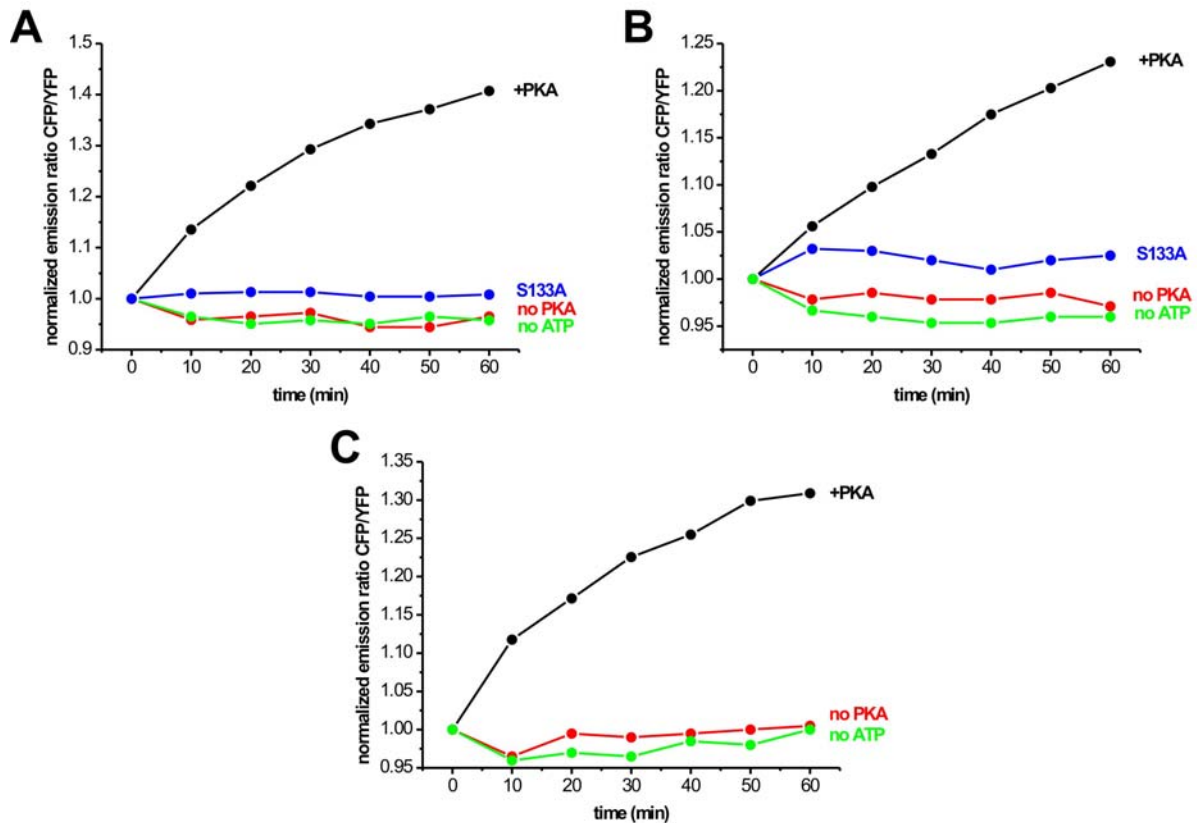


Figure 28: In vitro characterization of I-ATF-1, I-CREM and I-P300. (A-C) Time course of the emission ratio of I-ATF-1(A), I-CREM (B) and I-P300 (C) stimulated with recombinant PKA. The positive control is depicted in black. The blue line in (A) and (B) show representative traces of the emission ratio when the serine 133 is mutated to alanine. The red trace shows a time course when no PKA is present in the reaction mix. In green is shown the emission ratio time course when no ATP is present in the reaction mix. PKA is always added to the reaction at time point zero.

Therefore we subcloned all three of the sensors in pcDNA 3, a mammalian expression vector, and expressed the constructs in primary neurons. Then we stimulated the neurons by depolarizing them with high potassium and by activating their adenylyl cyclase by application of forskolin. Depolarizing neurons that were transfected with I-ATF-1 and measuring the CFP/YFP emission showed a fast increase in the emission ratio, which was with a time constant of 5.6 min not

significantly different to that of ICAP (Fig. 29 A). Activating in those cells the cAMP pathway and PKA resulted in robust I-ATF-1 activation that started immediately after application of forskolin and saturated after approximately 30 minutes (Fig. 29 A). The same experimental conditions were used to study the activation of I-CREM in hippocampal neurons. Application of high potassium to I-CREM transfected neurons resulted in a change in the emission ratio of the sensor with a delay of almost three minutes post stimulation (Fig. 29 B).

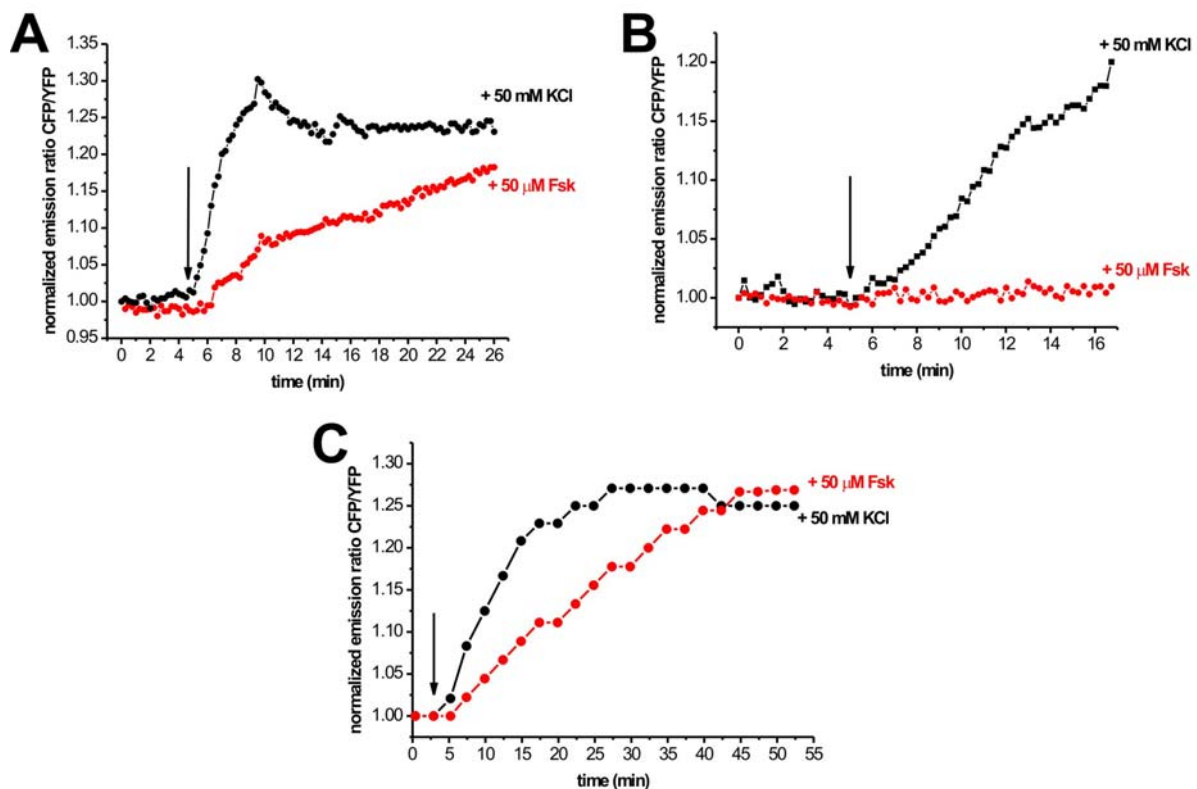


Figure 29: Characterisation of I-ATF-1, I-CREM and I-P300 in primary hippocampal neurons. (A-C) Time courses of I-ATF-1 (A), I-CREM (B) and I-P300 (C) activation as changes in the emission ratio CFP/YFP. Neurons were stimulated with high potassium (black trace) and forskolin (red trace). The black arrow indicates the time point of application.

In general, the reaction was slower in comparison to I-ATF-1 or ICAP activation. Remarkably, application of forskolin to I-CREM transfected cells did not result in a measureable change in the emission ratio over time (Fig. 29. B). Next, we transfected neurons with I-P300 and measured the kinetics of the recruitment of the KIX of P300 in comparison to the recruitment of the KIX of CBP. The depolarization mediated activation of the CREB-KID and the concurrent binding of the P300-KIX results in

strong increase of the CFP/YFP emission ratio that starts immediately after stimulation and saturates after 15 minutes (Fig. 29 C). The activation kinetics ($\tau = 8.1$ min) is slower than that of ICAP ($\tau = 3.2$ min) and comparable to that of I-ATF-1 ($\tau = 5.6$ min). Activating the cAMP-PKA pathway with forskolin also activated I-P300 in a robust manner, whereby the activation started 1-2 min after stimulation and saturated after approximately 40 minutes (Fig. 29 C).

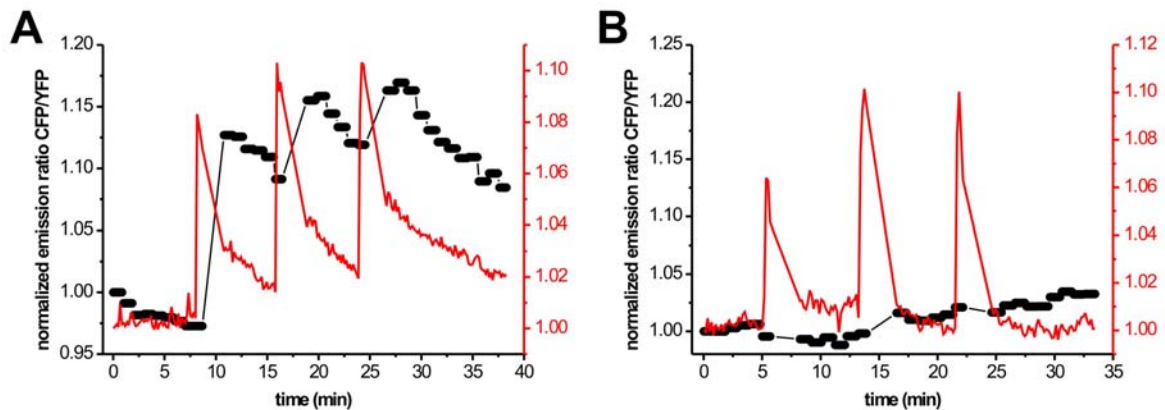


Figure 30: Calcium dependent summation of ATF-1 and CREM activation. (A, B) Time courses of calcium measured as 350/380 nm ratio with fura-2 (red traces) and I-ATF-1 (A) and CREM (B) activation as CFP/YFP ratio measured with I-ATF-1 (A) and I-CREM (B) (black traces, respectively). Three KCl pulses as indicated by black bars were applied to the cells.

In the next set of experiments we wanted to investigate the ability of ATF-1 and CREM to integrate calcium signals, and if this signal integration leads to a summation of the activation, and compare that to CREB. Our working hypothesis was that ATF-1 and, to a certain extent CREM, appear most of the time complementary to CREB and therefore should be able to compensate for the possible loss of CREB function, as demonstrated in previous studies (Balschun et al., 2003). Therefore we subjected primary neurons to the experimental paradigm we established in Figure 25 and measured ATF-1 and CREM activation with our biosensors I-ATF-1 and I-CREM. Stimulating neurons transfected with I-ATF-1 with high potassium resulted in a fast and robust increase of nuclear calcium, followed with a short 1-2 minutes delay by ATF-1 activation (Fig. 30 A). Calcium levels then decreased and ATF-1 activation quickly increased to a maximal activation of 12.5 %. After the maximum, ATF-1 activity began to slowly decrease until the the next stimulation. Due to the slow

decrease, the next incoming signal could build up on the previous and thus sum up the signal (Fig. 30 A). This paradigm was repeated three times and every time ATF-1 activity ended up on an elevated level, similar to CREB activity under the same conditions (compare Fig. 25 C and Fig. 30 A). We attempted the same stimulus paradigm on primary neurons transfected with I-CREM to investigate CREM activation. Interestingly, the three KCl pulses did not result in a significant ratio change of I-CREM, despite the presence of strong increases of calcium into the nucleus of the cells (Fig. 30 B). After the second KCl pulse there seems to be a small increase of CREM activity, but after three pulses of KCl the emission ratio of I-CREM is still not significantly higher than at the beginning of the measurement (Fig. 30 B).

5. Discussion

In this study we designed, constructed and characterized genetically encoded fluorescent biosensors for the activation of CREB family transcription factors. These indicators have been sketched to allow for visualization of CREB family transcription factor activation in live cells, tissue and transgenic animals on the one hand, and in different intracellular organelles, on the other hand. Current techniques to investigate CREB family transcription factor activation have certain drawbacks that either complicate their use in live cells or make it impossible at all. For example, biochemical and histological methods have been widely used in determining phosphorylation of CREB transcription factors in many different cell types. These assays often require grinding up large amounts of tissue and averaging activation over many different cell types within a tissue, while immunostainings are more difficult to quantify and at best only provide snapshots at given time points. A differentiation between nuclear and mitochondrial activation so far was difficult. All of these techniques were performed on dead cells and tissues, which allows conclusions on possible physiological events leading to CREB activation only to be made posthumously. Two attempts were made previously to image CREB activation in live cells. One employed intermolecular FRET between GFPs (Mayr, B.M., et al 2001) but due to small signals and the problem of co-transfecting two reporter constructs was not practical, while another approach used a highly sensitive β -lactamase-dependent reporter assay (Spotts, J.M., et al., 2002) which converts substrate in a non-reversible manner and cannot be targeted to subcellular organelles. Substrate loading into tissue to monitor CREB activation may be difficult. In the following pages I will discuss the properties of ICAP to demonstrate its advantages against the previous techniques.

5.1 The specificity and reliability of ICAP

ICAP is a unimolecular FRET-based biosensor that is specific for phosphorylation of the critical serine 133 and was tuned extensively to optimize phosphorylation-dependent increase in CFP/YFP emission ratio. Interestingly, by incorporating a circularly permuted acceptor protein we were able to construct the sensor in two

configurations with opposing response properties, either increasing or decreasing FRET due to phosphorylation. This unexpected behaviour demonstrates that it is possible to tune response properties of genetically encoded sensors in more ways than previously thought. In its overall architecture it is similar to other sensors of tyrosine kinase or PKA activity (Ting, A.Y. et al., 2001; Zhang, J. et al., 2001) but in contrast to these sensors preserves the promiscuous phosphorylation of the KID domain by the various CREB kinases. The specificity and reliability of the sensor has been demonstrated in several experiments (Fig. 9, 10). We hypothesized that for the ratio change to occur three things are crucial: protein kinase A, ATP and serine 133. In vitro we tested this hypothesis by control experiments, from which we excluded each one of these components and measured the CFP/YFP ratio. Indeed, all three ingredients together are absolutely necessary for the ratio change to occur (Fig. 9). So we concluded that PKA, in the presence of ATP as donor for inorganic phosphate, specifically phosphorylates serin 133. The specific phosphorylation was additionally proven by western blot analysis (Fig. 9). The same turned out to be true for the activation of ICAP in HeLa cells, where we also mutated the crucial serine 133 to alanine and blocked PKA by H-89 (Fig. 10).

But specificity and reliability are not the sole properties of the sensor that make it useful. Moreover, it is essential to show that the activation of the sensor corresponds well to the activation of the actual process we want to measure, endogenous CREB activation, and that the sensor does not perturb endogenous CREB signaling. Therefore we performed western blot analysis on ICAP transfected HeLa cells (Fig. 10). On this blot it was possible to directly compare endogenous CREB phosphorylation and ICAP phosphorylation, because of the different molecular weight of the two molecules. This experiment showed that the kinetics and the characteristics of the phosphorylation of both molecules are very similar (Fig. 10). In conclusion, it is valid to speak of CREB activation when measuring the CFP/YFP emission ratio increase of ICAP.

5.2 Studying CREB activation in mitochondria

Previously, it was not possible to easily and directly measure CREB activation in mitochondria. Having tried various mitochondrial localization signals fused to ICAP

for their ability to target ICAP to the mitochondrial matrix, we finally succeeded. Fusing the first 69 amino acids of the mitochondrial pre-sequence of the F_0/F_1 -ATPase of *neurospora crassa* to ICAP we achieved a mitochondrial targeting (Fig. 11). With mt-ICAP we set out to investigate how the cAMP pathway and the calcium pathway activate CREB in mitochondria. It was fascinating to see that calcium dependent CREB activation seemed to be faster and more pronounced than cAMP dependent CREB activation, reflected in the immediate response, the fast onset and the saturation after 15 minutes, when the cAMP mediated response has just reached its half maximal activation (Fig. 11 D). This could be because in contrast to cAMP, calcium directly enters mitochondria and there activates target proteins. The heterogeneity of the calcium dependent ICAP response, reflected in the error bars in Figure 11 F, prompted us to check, whether CREB activation in mitochondria is homogenous or heterogenous. In Figure 12 it is clearly visible, that the response is highly heterogenous, with the CREB in certain subsets of mitochondria responding faster to calcium than others. It has been demonstrated that calcium microdomains under endomembranes affect mitochondria in a sense that mitochondria that lie near to these calcium microdomains take up the calcium (for review see Alonso, M.T. et al., 2006). So it would be intriguing to hypothesize, that the calcium microdomains in subsets of mitochondria activate CREB there in a locally strictly regulated manner. This could have the far reaching effect, that downstream signaling events, like apoptosis or mitochondrial survival, could be directly influenced. Simultaneous calcium imaging and CREB activation, together with survival and apoptosis assays could shed light on these questions. In conclusion, we describe here the first technique for real-time measuring of CREB activation in mitochondria of living cells.

5.3 Reliable and reversible imaging of CREB activation in primary hippocampal neurons

Despite the fact that we put already a lot of effort in proving the reliability and specificity of ICAP, we performed additional control experiments in primary hippocampal neurons. Wu and colleagues from Richard Tsien's lab showed that two pathways with distinct kinetics converge on CREB, the fast CaMKIV pathway and the slower MAPK pathway. We could reproduce the experiments that were done in this

lab, distinguishing a fast CREB activation pathway that could be blocked by a CaMKIV blocker and a slow pathway that could be blocked by a MAPK inhibitor, and thereby further contribute to the trustworthiness of our approach (Fig. 14).

One of the best features of our sensor in comparison to the previous approaches is that ICAP can reversibly monitor CREB activation (Fig. 15). Wash out of the stimulus leads to a decrease in the CFP/YFP ratio, however, not down to baseline levels after high potassium stimulation. Here, again, we have to ask: is the response we see from our sensor an artefact of the sensor due to its intrinsic properties or does it reflect endogenous CREB activation. At least three lines of evidence point to the fact that our sensor specifically and reliably displays the activation of endogenous CREB and is not due to intrinsic properties of the sensor: The control experiments in Fig. 9, the western blot analysis in Fig. 10 and the experiments in Fig. 14. A fourth evidence is the observation, that after a short NMDA stimulation CREB activation decreases back to baseline levels. Consequently, we can rule out the possibility, that a back folding of the sensor into its unphosphorylated state is impossible. So it is most reasonable to explain the fact, that CREB activation stays at an elevated level after a 3 min high potassium stimulation, as a defined unbalance of the kinase-phosphatase equilibrium or is caused by a specific modification of the KID-KIX complex.

On the whole, we here present the first tool for real-time reversible and reliable measurements of CREB activation in the nucleus of living neurons.

5.3.1 CREB activation after GABAergic stimulation

It has been demonstrated that the action of GABA shifts from excitatory to inhibitory during early development of the nervous system (Stein and Nicoll, 2003). We asked if CREB is activated during the excitatory phase of GABA, if that putative activation stops with the developmental switch to inhibitory and how exactly the signaling to CREB activation would be. Our experiments showed, that CREB is activated by GABA early in development, but later, after 20 days in vivo the activation stops. Furthermore, we show that CREB activation can occur via GABA_A-receptors and GABA_B-receptors, by separately stimulating with muscimol (GABA_A-receptor agonist) and baclofen (GABA_B-receptor agonist) (Fig. 16). The developmental switch is explained by the up and down regulation of certain symporters that finally alter the

chloride potential of the cell. The younger the neurons are the more chloride is in the cell and the more prone are the cells to depolarization, because GABA_A-receptor activation in this case leads to a strong efflux of chloride and thus to an increase in net positive charge inside the cell. This changes in mature neurons, where the chloride concentration inside the cell is lower and GABA_A-receptor stimulation leads to an influx of chloride and a hyperpolarization of the cell. In this light, our observation that CREB activation after GABA_B-receptor stimulation with baclofen is also abolished after 20 days in vitro is very unexpected, because GABA_B-receptors are G-protein coupled receptors and work, as far as we know, independently from depolarization mediated effects. In accordance with this point of view we were not able to measure calcium transients in neurons after baclofen stimulation (Fig. 17 C). Nevertheless, blocking calcium dependent CaMKinases with KN-62, chelating all free calcium with BAPTA and inhibiting store operated calcium activation all block baclofen mediated CREB activation (Fig. 17 B, E). From this we concluded, that calcium somehow has to play a role in baclofen mediated CREB activation. One could speculate, that very fast calcium microdomains under the membrane or close to internal stores, that are not measureable by the techniques we used, are responsible for this calcium dependency. However, even if such calcium microdomains really occur and are responsible for baclofen mediated CREB activation, still the mechanism of the shut-off of this pathway after 20 days in vitro remains to be explained. There is plenty of room for wild speculations and testable hypothesis in this regard. I would like to mention just some of them. One possibility is, that via the GABA_A-receptor pathway a certain protein is expressed and after the developmental switch, this pathway is disrupted and the protein is not expressed any more. Such a protein could for example be a scaffolding protein, that compartementalizes a signaling domain which is necessary for the GABA_B-receptor mediated pathway to CREB. Alternatively, a regulatory protein for G-proteins could be down regulated, e.g. the regulator of G-protein signaling (RGS), or the expression and regulation of arrestin molecules could be altered. It will be interesting to solve this enigma, especially because baclofen is widely used as an anti epileptic drug and elucidating its exact mechanism would help in improving the positive effects and perhaps broaden its application spectrum.

5.3.2 Simultaneous measurement of calcium and CREB activation in microiontophoretically stimulated neurons

Doing research in cell biology often requires, as already touched on before, that signals are averaged over several cells or, when studying the crosstalk between two processes, the events are compared taking completely different cells. Take for example the analysis of calcium and CREB activation. A direct correlation of a calcium event in a single cell and its immediate effect on CREB phosphorylation in this same cell has not been feasible with current techniques. Making use of the appealing properties of ICAP we broadened our stimulation toolbox from bath application to single cell microiontophoresis. Thus, we can precisely time our stimuli and do real-time analysis of CREB activation in a single cell. Furthermore, when we load the neuron with the synthetic calcium dye fura-2, we can simultaneously measure calcium events in this neuron. These two refinements now allow us to directly and in real-time analyse the interdependence of the calcium concentration and CREB phosphorylation after precisely timed stimuli in single living cells (Fig. 18). In our first experiments we could see how CREB phosphorylation follows the elevation of calcium ions in the nucleus, with a delay of 1-3 minutes (Fig. 19). This lag of CREB activation could be due to the time it takes the CaMKinase pathway to get activated and to phosphorylate ICAP. These processes, however, are very fast and it is more likely that the calcium concentration first has to reach a certain threshold, which should be defined by the K_D of the involved calcium binding proteins, before the signaling pathways are activated. Certainly, our sensor is overexpressed in the nucleus of the neurons and therefore it should also take some time to have enough sensor molecules phosphorylated, before a visible signal comes out. Despite the lag of CREB activation, the speed is comparable to that of the calcium activation (Fig. 19, 25). Interestingly, the deactivation kinetics of CREB seems to be different for different stimuli. For example, after NMDA or glutamate application the deactivation of CREB is complete, until baseline levels, and occurs with a speed, that is comparable to that of the calcium signal (Fig. 19). The observation that the on-rate after calcium dependent stimuli, e.g. NMDA, glutamate and KCl, is almost the same for each of these agents, but that, in contrast, the off-rate is different for

NMDA/glutamate and KCl could hint to a high degree of regulation of this process. This discrepancy between the fast on-rate of CREB activation after membrane depolarization, that closely follows the rise of the calcium concentration, and the slower off-rate, that is decoupled from the fast decrease of the calcium concentration, is the main finding of this study and is a thread that leads through the rest of the text. This close interrelationship between calcium and CREB, measured simultaneously, has not been demonstrated before in single living cells.

5.3.3 Investigating the interrelationship of calcium and CREB activation in neurons

In the following experiments we investigated how the amplitude, the duration and the interstimulus interval between the nuclear calcium transients influenced CREB activation. The question we wanted to investigate was, if the strength of CREB activation is directly correlated to the strength of the calcium signal or if CREB is only activated when a certain threshold of calcium has been reached. We began by using different concentrations of KCl to create calcium signals of different amplitude. It was interesting to see, that the relationship between stimulus strength and calcium signal was not directly proportional. This could be because of the non-linearity of the membrane voltage-ion conductance relationship of the voltage gated calcium channel. More importantly, the strength of CREB activation seemed to directly follow the strength of the calcium transient, the strongest activation of CREB occurring at a intracellular calcium concentration of 1 μM (Fig. 20 A). The same was true, when we analysed the interrelationship between the duration of the calcium signal and the strength of CREB activation (Fig. 20 B). The longer the calcium transient, the stronger the emission ratio change of ICAP. There was no hint of a calcium signal duration threshold for CREB activation, since the correlation between the duration of the calcium elevation and CREB activation strength was best fit by a linear equation (Fig. 20 B, inset). Calcium transients can also vary in their frequency, in which they arrive at the cell. Interestingly, we found that the shorter the interstimulus interval is, the stronger the CREB activation becomes (Fig. 21). Stimulating every five minutes with high potassium, CREB activation increases and decreases, like a wave, following the calcium spikes (Fig. 21 A). Decreasing the interstimulus interval to two

or one minute leads to a summation of the CREB activation due to the fact, that the decrease in CREB activation has a much slower time constant than the activation (Fig. 15 A). Thus, after every calcium spike, CREB activation reaches a higher level, resulting in a temporal integration of the incoming signals (Fig. 21 B, C). The question that arises is, what exactly is the physiological effect of the summation of CREB activation. Of course, increasing the amount of activated CREB molecules after a stimulus very fast, should increase the amount of CREB dependent gene expression over the time period these molecules are active. We demonstrated this phenomenon by comparing the integrals beneath the CREB activation curves with five minute interstimulus interval and with one minute interstimulus interval (Fig. 22). Nevertheless, it remains to be shown, that the higher amount of CREB dependent gene expression after the summation of CREB activation really occurs. We assessed this question later in the text (see Fig. 26). Besides the amplitude, the duration and the frequency of the calcium signal, it is crucial to take the location of the stimulation into account. Unfortunately, we were not able to image dendritic calcium and CREB activation in the same cell, so we first showed, that we can elicit spatially confined calcium signals in dendrites (Fig. 23). When we stimulated neurons with high potassium at the distal dendrite, we could observe local increases of the calcium concentration. The calcium increase seemed to travel along the dendrite in the direction of the soma, but faded away approximately at half the distance to the soma. An elevation of nuclear calcium was not measurable (Fig. 23 A). In the next step we applied the same stimulus to a dendrite of a neuron and measured CREB activation and nuclear calcium (Fig. 24). We found that an increase of nuclear calcium is absolutely necessary for CREB activation. Dendritic local calcium signals do not trigger CREB activation in our experimental setup. This is interesting, because controversial ideas concerning nuclear calcium have been discussed (Deisseroth et al., 1998; Hardingham et al., 2001). Deisseroth and colleagues proposed a model where calcium ions activate calmodulin in the cytoplasm, which travels then to the nucleus, where it eventually activates CaMKinases. This process is independent of nuclear calcium. In contrast, Hardingham and colleagues found that nuclear calcium is solely responsible for CREB activation. Our results are clearly in favour for the nuclear calcium hypothesis.

Taken together we find that the on-rate of CREB activation is faster than the off-rate (Fig. 15 A) and that this slower off-rate enables CREB to temporally integrate stimuli

with a certain amplitude, duration and timing (Fig. 20, 21), if the calcium enters the nucleus (Fig. 24). To verify the relevance of this temporal summation of CREB activation, we had to show, that CREB dependent gene expression is affected, too. Therefore we developed a simple assay to quantify calcium dependent summation of CREB activation and CREB dependent gene expression (Fig. 25, 26). When we compared CREB activation and CREB dependent gene expression after one and three KCl pulses within half an hour, we find that after three pulses CREB activation and gene expression is significantly higher than after one pulse. Additionally, CREB dependent gene expression was investigated by two different experimental assays, by a CRE driven luciferase assay and by analysing CREB dependent cFos expression (Fig. 26). Both experiments clearly show that the calcium dependent summation of CREB activation is also reflected in CREB dependent gene expression.

CREB can stay activated up to 12 hours poststimulation as proposed by several studies (Marie, H. et al., 2005; Liu, F.C., and Graybiel, A.M., 1996 and 1998). Interestingly, the off-rate of CREB deactivation is slow enough to enable CREB to integrate stimuli, that are separated by time periods up to two hours. The relevance of this finding is unclear, but its tempting to speculate that certain learning tasks could allow long periods of time between two stimuli. Unfortunately, we could not measure for longer time periods, because the health of the cells declined after two hours, since we did not use a temperature chamber.

5.3.4 Visualizing CREB family transcription factors in living neurons

In style of ICAP we designed biosensors for the activation of ATF-1, CREM and the CBP homologue P300. It was important to take approximately the same lengths of the KIDs of ATF-1 and CREM, because we wanted to compare CREB activation with ATF-1 and CREM activation. If the lengths of the used fragments had been different, any inferences to differences in the activation of the three transcription factors would have been dubious. Of course, these sensors also had to go through the tests for specificity and reliability, in vitro (Fig. 28) and in living cells (Fig. 29). ATF-1 and P300 are ubiquitously expressed in all cells of the mammalian body, but CREM expression

localized to testis and certain parts of the neuroendocrine system (Foulkes et al., 1991 a,b). Nevertheless, CREM is upregulated in the absence of CREB and ATF-1 in CREB and ATF-1 knock-out mice, in cells, where it is not expressed under normal conditions and the knock-out is not impaired. (Balschun et al., 2003). It is important to state that, when comparing the sensors, we had to “normalize them, in a sense, that we find a stimulus that activates all four sensors in more or less the same way. This is necessary, because otherwise one cannot draw significant conclusions from the experiments. All four sensors were activated in vitro by purified protein kinase A and proved to be specific and reliable in control experiments (Fig. 28). However, in living neurons, I-CREM was the only sensor that responded completely different to high potassium and forskolin, than ICAP (Fig. 29, 30). The activation kinetics of I-ATF-1 and I-P300 were not significantly different after forskolin and high potassium stimulation stimulation from the activation kinetics of ICAP (Fig. 29, 30). So our results are in favour for the hypothesis that ATF-1 and P300 function are complementary to CREB and CBP function. This is not surprising because of the extensive sequence homology these molecules display in their KID and KIX regions, respectively (Fig. 2). On the other hand, P300 has been shown to have at least some functions that are distinct from CBP (Goodman and Smolik, 2000). This could be a cell type specific effect.

Unlike ATF-1 and P300, the activation kinetics of I-CREM were distinct from that of ICAP (Fig. 29, 30). The activation started with a delay of about 3-5 minutes and was slower than I-ATF-1 and ICAP and no summation could be seen when three KCl pulses were applied within half an hour. Furthermore, forskolin was not able to stimulate I-CREM activation. CREM, as well as ATF-1, shows some differences in its KID, e.g. at the position 106, which is analogous to position 122 in CREB, the glutamine of CREB has been replaced by histidine. These amino acid changes could alter the binding affinity of kinases, and thereby change the activation characteristics. All together, the results with I-CREM are interesting, because of the marked differences in the activation characteristics, but more experiments are necessary to demonstrate the reliability and significance of the obtained data. Then, these sensors could prove to be useful tools in various assays investigating differential activation of CREB family transcription factors in different cell types and tissues under different stimulus conditions.

5.4 Further outlook

In this study we designed, constructed, characterized and successfully applied genetically encoded fluorescent biosensors for the activation of CREB family transcription factors. We went from the level of measuring purified proteins in the cuvette to primary hippocampal neurons, where we investigated CREB activation together with calcium in single living cells. Surely, this work threw up more questions, than it answered. How exactly is CREB activated and regulated in mitochondria? Is mitochondrial CREB activation spatially dependent on calcium microdomains? Why is the on-rate of CREB activation faster than the off-rate? Why is this phenomenon dependent on the stimulus? Is the summation of CREB activation in the intact brain as important for memory formation as the spatial and temporal summation of synaptic potentials? What is the mechanism for the developmental switch in baclofen dependent CREB activation? Are these measurements from dissociated cell culture also relevant under more physiological conditions?

Eventually, our goal is to measure CREB activation under conditions that resemble as good as possible the conditions in an intact brain of a living and behaving animal. To meet that end it is first of all necessary to assess the properties of our biosensor in organotypic slice cultures and then in transgenic animals. We started out by building lentiviruses and semliki-forest-viruses that carry our sensor. Such viruses are very effective ways to deliver ICAP into the desired target cell and tissues. Lentiviruses belong to the retroviridae and integrate their DNA, after reverse transcription of their RNA, into the host genome. This opens new possibilities for making transgenic animals and infection of living animals. Semliki-forest-viruses are used to transiently transfect organotypic slices and also in the brains of living animals for short term measurements. Having these two viruses we can now begin to assess CREB activation in slice culture and even whole animals.

Another project we began is to make *drosophila melanogaster* transgenic for NLS-ICAP. The expression pattern in whole animals is shown in Fig. 32. The sensor construct is under the control of the elav driver, which leads to an expression in the nervous tissue. ICAP is expressed in the antenna lobes, in the whole brain and is also visible in motor neuron nodes innervating the wings (Fig. 32). The next steps will be to map the location of the sensor on the *drosophila* chromosomes. This is done by

an ingenious crossing of different fly lines that carry certain mutations and then look at the segregation pattern of the mutations in the back crossed offspring. As soon as we know the exact location of the insertion, we can selectively cross the brightest offspring to get optimal brightness of the expression of the sensor. A reasonable brightness of the sensor emission is crucial, because especially the signal to noise ratio is positively influenced by the brightness (Reiff, D. and personal observation).

NLS-ICAP x c155 65a

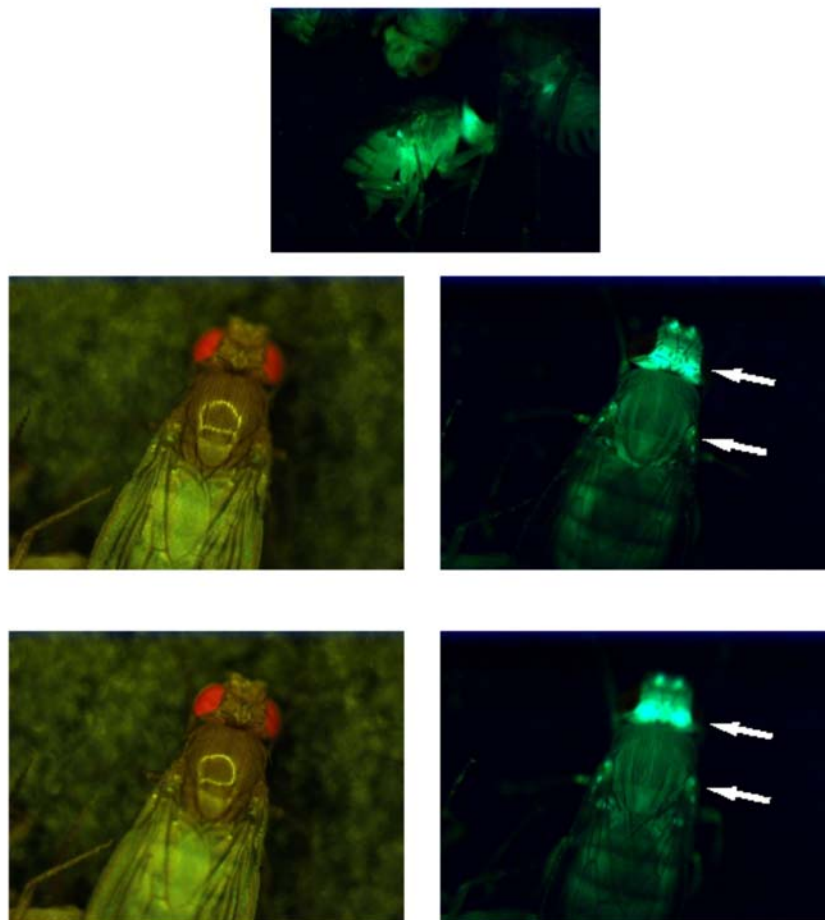


Figure 32: Expression of NLS-ICAP in transgenic *Drosophila*. Red eyed flies carrying ICAP were crossed with the driver line elav c155. In the upper picture a *Drosophila* is shown under fluorescent (Emission filter) light from the side. On the left are shown animals in bright light. On the right animals are shown in fluorescent light. White arrows mark the optical lobes in the brain and nerve nodes innervating the wings.

If ICAP was functional in vivo in transgenic drosophila, that would open up manifold avenues to investigate CREB activation in living animals. Established learning paradigms in concert with elaborate imaging machinery could allow for visualization of live CREB activation, e.g. in the mushroom body, in behaving animals.

6. References

Alonso MT, Villalobos C, Chamero P, Alvarez J, Garcia-Sancho J (2006) Calcium microdomains in mitochondria and nucleus. *Cell Calcium* 40: 513-525.

Ananthanarayanan B, Ni Q, Zhang J (2005) Signal propagation from membrane messengers to nuclear effectors revealed by reporters of phosphoinositide dynamics and Akt activity. *PNAS* 102: 15081-15086.

Baird GS, Zacharias DA, Tsien RY (1999) Circular permutation and receptor insertion within green fluorescent proteins. *PNAS* 96: 11241-11246.

Baker BJ, Lee H, Pieribone VA, Cohen LB, Isacoff EY, Knopfel T, Kosmidis EK Three fluorescent protein voltage sensors exhibit low plasma membrane expression in mammalian cells. *Journal of Neuroscience Methods* In Press, Corrected Proof.

Balschun D, Wolfer DP, Gass P, Mantamadiotis T, Welzl H, Schutz G, Frey JU, Lipp HP (2003) Does cAMP Response Element-Binding Protein Have a Pivotal Role in Hippocampal Synaptic Plasticity and Hippocampus-Dependent Memory? *J Neurosci* 23: 6304-6314.

Bevilaqua LRM, Cammarota M, Paratcha G, de Stein ML, Izquierdo I, Medina JH (1999) Experience-dependent increase in cAMP-responsive element binding protein in synaptic and nonsynaptic mitochondria of the rat hippocampus. *European Journal of Neuroscience* 11: 3753-3756.

Bitto H, Deisseroth K, Tsien RW (1996) CREB Phosphorylation and Dephosphorylation: A Ca²⁺- and Stimulus Duration-Dependent Switch for Hippocampal Gene Expression. *Cell* 87: 1203-1214.

Carlezon J, Duman RS, Nestler EJ (2005) The many faces of CREB. *Trends in Neurosciences* 28: 436-445.

Chrivia JC, Kwok RPS, Lamb N, Hagiwara M, Montminy MR, Goodman RH (1993) Phosphorylated CREB binds specifically to the nuclear protein CBP. *Nature* 365: 855-859.

Conkright MD, Canettieri G, Sreaton R, Guzman E, Miraglia L, Hogenesch JB, Montminy M (2003) TORCs: Transducers of Regulated CREB Activity. *Molecular Cell* 12: 413-423.

Conkright MD, Montminy M (2005) CREB: the unindicted cancer co-conspirator. *Trends in Cell Biology* 15: 457-459.

Deisseroth K, Heist EK, Tsien RW (1998) Translocation of calmodulin to the nucleus supports CREB phosphorylation in hippocampal neurons. *Nature* 392: 198-202.

Deisseroth K, Tsien RW (2002) Dynamic Multiphosphorylation Passwords for Activity-Dependent Gene Expression. *Neuron* 34: 179-182.

Deisseroth K, Mermelstein PG, Xia H, Tsien RW (2003) Signaling from synapse to nucleus: the logic behind the mechanisms. *Current Opinion in Neurobiology* 13: 354-365.

Duebel J, Haverkamp S, Schleich W, Feng G, Augustine GJ, Kuner T, Euler T (2006) Two-Photon Imaging Reveals Somatodendritic Chloride Gradient in Retinal ON-Type Bipolar Cells Expressing the Biosensor Clomeleon. *Neuron* 49: 81-94.

Fehr M, Frommer WB, Lalonde S (2002) From the Cover: Visualization of maltose uptake in living yeast cells by fluorescent nanosensors. *PNAS* 99: 9846-9851.

Fields RD, Eshete F, Stevens B, Itoh K (1997) Action Potential-Dependent Regulation of Gene Expression: Temporal Specificity in Ca²⁺, cAMP-Responsive Element Binding Proteins, and Mitogen-Activated Protein Kinase Signaling. *J Neurosci* 17: 7252-7266.

Fields RD, Lee PR, Cohen JE (2005) Temporal integration of intracellular Ca²⁺ signaling networks in regulating gene expression by action potentials. *Cell Calcium* 37: 433-442.

Finkbeiner S (2000) CREB Couples Neurotrophin Signals to Survival Messages. *Neuron* 25: 11-14.

Foulkes NS, Laoide BM, Schlotter F, Sassone-Corsi P (1991) Transcriptional Antagonist cAMP-Responsive Element Modulator (CREM) Down-Regulates c-fos cAMP-Induced Expression. *PNAS* 88: 5448-5452.

Foulkes NS, Borrelli E, Sassone-Corsi P (1991) CREM gene: Use of alternative DNA-binding domains generates multiple antagonists of cAMP-induced transcription. *Cell* 64: 739-749.

Foulkes NS, Mellstrom B, Benusiglio E, Sassone-Corsi P (1992) Developmental switch of CREM function during spermatogenesis: from antagonist to activator. *Nature* 355: 80-84.

Foulkes NS, Sassone-Corsi P (1992) More is better: Activators and repressors from the same gene. *Cell* 68: 411-414.

Gallegos LL, Kunkel MT, Newton AC (2006) Targeting Protein Kinase C Activity Reporter to Discrete Intracellular Regions Reveals Spatiotemporal Differences in Agonist-dependent Signaling. *J Biol Chem* 281: 30947-30956.

Ginty DD, Bonni A, Greenberg ME (1994) Nerve growth factor activates a Ras-dependent protein kinase that stimulates c-fos transcription via phosphorylation of CREB. *Cell* 77: 713-725.

Gonzalez GA, Yamamoto KK, Fischer WH, Karr D, Menzel P, Biggs III W, Vale WW, Montminy MR (1989) A cluster of phosphorylation sites on the cyclic AMP-regulated nuclear factor CREB predicted by its sequence. *Nature* 337: 749-752.

Goodman RH, Smolik S (2000) CBP/p300 in cell growth, transformation and development. *Genes and Development* 14: 1553-1577.

Griesbeck O, Baird GS, Campbell RE, Zacharias DA, Tsien RY (2001) Reducing the Environmental Sensitivity of Yellow Fluorescent Protein. MECHANISM AND APPLICATIONS. *J Biol Chem* 276: 29188-29194.

Griesbeck O (2004) Fluorescent proteins as sensors for cellular functions. *Current Opinion in Neurobiology* 14: 636-641.

Guerrero G, Isacoff EY (2001) Genetically encoded optical sensors of neuronal activity and cellular function. *Current Opinion in Neurobiology* 11: 601-607.

Hai TW, Liu F, Coukos WJ, Green MR (1989) Transcription factor ATF cDNA clones: an extensive family of leucine zipper proteins able to selectively form DNA-binding heterodimers [published erratum appears in *Genes Dev* 1990 Apr;4(4):682]. *Genes Dev* 3: 2083-2090.

Hardingham GE, Arnold FJL, Bading H (2001) Nuclear calcium signaling controls CREB-mediated gene expression triggered by synaptic activity. *Nat Neurosci* 4: 261-267.

Hardingham GE, Fukunaga Y, Bading H (2002) Extrasynaptic NMDARs oppose synaptic NMDARs by triggering CREB shut-off and cell death pathways. *Nat Neurosci* 5: 405-414.

Heim N, Griesbeck O (2004) Genetically Encoded Indicators of Cellular Calcium Dynamics Based on Troponin C and Green Fluorescent Protein. *J Biol Chem* 279: 14280-14286.

Heim N, Garaschuk O, Friedrich MW, Mank M, Milos RI, Kovalchuk Y, Konnerth A, Griesbeck O (2007) Improved calcium imaging in transgenic mice expressing a troponin C-based biosensor. *Nat Meth* advanced online publication.

Heim R, Tsien RY (1996) Engineering green fluorescent protein for improved brightness, longer wavelengths and fluorescence resonance energy transfer. *Current Biology* 6: 178-182.

Hoeffler JP, Meyer TE, Yun Y, Jameson JL, Habener JF (1988) Cyclic AMP-responsive DNA-binding protein: structure based on a cloned placental cDNA. *Science* 242: 1430-1433.

Hoffer BJ, Siggins GR, Bloom FE (1971) Studies on norepinephrine-containing afferents to Purkinje cells of rat cerebellum. II. Sensitivity of Purkinje cells to norepinephrine and related substances administered by microiontophoresis. *Brain Research* 25: 523-534.

Honda A, Adams SR, Sawyer CL, Lev-Ram V, Tsien RY, Dostmann WRG (2001) Spatiotemporal dynamics of guanosine 3',5'-cyclic monophosphate revealed by a genetically encoded, fluorescent indicator. *PNAS* 98: 2437-2442.

Hook SS, Means AR (2001) Ca²⁺/CaM-DEPENDENT KINASES: From Activation to Function. *Annual Review of Pharmacology and Toxicology* 41: 471-505.

Itoh RE, Kurokawa K, Ohba Y, Yoshizaki H, Mochizuki N, Matsuda M (2002) Activation of Rac and Cdc42 Video Imaged by Fluorescent Resonance Energy Transfer-Based Single-Molecule Probes in the Membrane of Living Cells. *Mol Cell Biol* 22: 6582-6591.

Kalab P, Pralle A, Isacoff EY, Heald R, Weis K (2006) Analysis of a RanGTP-regulated gradient in mitotic somatic cells. *Nature* 440: 697-701.

Kalab P, Weis K, Heald R (2002) Visualization of a Ran-GTP Gradient in Interphase and Mitotic *Xenopus* Egg Extracts. *Science* 295: 2452-2456.

Kuner T, Augustine GJ (2000) A Genetically Encoded Ratiometric Indicator for Chloride: Capturing Chloride Transients in Cultured Hippocampal Neurons. *Neuron* 27: 447-459.

Kunkel MT, Ni Q, Tsien RY, Zhang J, Newton AC (2005) Spatio-temporal Dynamics of Protein Kinase B/Akt Signaling Revealed by a Genetically Encoded Fluorescent Reporter. *J Biol Chem* 280: 5581-5587.

Kurokawa K, Mochizuki N, Ohba Y, Mizuno H, Miyawaki A, Matsuda M (2001) A Pair of Fluorescent Resonance Energy Transfer-based Probes for Tyrosine Phosphorylation of the CrkII Adaptor Protein in Vivo. *J Biol Chem* 276: 31305-31310.

Lee B, Butcher GQ, Hoyt KR, Impey S, Obrietan K (2005) Activity-Dependent Neuroprotection and cAMP Response Element-Binding Protein (CREB): Kinase Coupling, Stimulus Intensity, and Temporal Regulation of CREB Phosphorylation at Serine 133. *J Neurosci* 25: 1137-1148.

Lee J, Kim CH, Simon DK, Aminova LR, Andreyev AY, Kushnareva YE, Murphy AN, Lonze BE, Kim KS, Ginty DD, Ferrante RJ, Ryu H, Ratan RR (2005) Mitochondrial Cyclic AMP Response Element-binding Protein (CREB) Mediates Mitochondrial Gene Expression and Neuronal Survival. *J Biol Chem* 280: 40398-40401.

Liu FC, Graybiel AM (1996) Spatiotemporal Dynamics of CREB Phosphorylation: Transient versus Sustained Phosphorylation in the Developing Striatum. *Neuron* 17: 1133-1144.

Liu FC, Graybiel AM (1998) Region-dependent dynamics of cAMP response element-binding protein phosphorylation in the basal ganglia. *PNAS* 95: 4708-4713.

Lonze BE, Ginty DD (2002) Function and Regulation of CREB Family Transcription Factors in the Nervous System. *Neuron* 35: 605-623.

Mank M, Reiff DF, Heim N, Friedrich MW, Borst A, Griesbeck O (2005) A FRET-based calcium biosensor with fast signal kinetics and high fluorescence change. *Biophys J* biophysj.

Marie H, Morishita W, Yu X, Calakos N, Malenka RC (2005) Generation of Silent Synapses by Acute In Vivo Expression of CaMKIV and CREB. *Neuron* 45: 741-752.

Mayr BM, Canettieri G, Montminy MR (2001) Distinct effects of cAMP and mitogenic signals on CREB-binding protein recruitment impart specificity to target gene activation via CREB. *PNAS* 98: 10936-10941.

Miesenbock G, De Angelis DA, Rothman JE (1998) Visualizing secretion and synaptic transmission with pH-sensitive green fluorescent proteins. *Nature* 394: 192-195.

Miyawaki A, Llopis J, Heim R, McCaffery JM, Adams JA, Ikura M, Tsien RY (1997) Fluorescent indicators for Ca²⁺ based on green fluorescent proteins and calmodulin. *Nature* 388: 882-887.

Miyawaki A (2003) Fluorescence imaging of physiological activity in complex systems using GFP-based probes. *Current Opinion in Neurobiology* 13: 591-596.

Miyawaki A (2003) Visualization of the Spatial and Temporal Dynamics of Intracellular Signaling. *Developmental Cell* 4: 295-305.

Miyawaki A (2005) Innovations in the Imaging of Brain Functions using Fluorescent Proteins. *Neuron* 48: 189-199.

Mochizuki N, Yamashita S, Kurokawa K, Ohba Y, Nagai T, Miyawaki A, Matsuda M (2001) Spatio-temporal images of growth-factor-induced activation of Ras and Rap1. *Nature* 411: 1065-1068.

Nagai T, Sawano A, Park ES, Miyawaki A (2001) Circularly permuted green fluorescent proteins engineered to sense Ca²⁺. *PNAS* 98: 3197-3202.

Nagai T, Yamada S, Tominaga T, Ichikawa M, Miyawaki A (2004) Expanded dynamic range of fluorescent indicators for Ca²⁺ by circularly permuted yellow fluorescent proteins. *PNAS* 101: 10554-10559.

Nakai J, Ohkura M, Imoto K (2001) A high signal-to-noise Ca²⁺ probe composed of a single green fluorescent protein. *Nat Biotech* 19: 137-141.

Nikolaev VO, Bunemann M, Hein L, Hannawacker A, Lohse MJ (2004) Novel Single Chain cAMP Sensors for Receptor-induced Signal Propagation. *J Biol Chem* 279: 37215-37218.

Nikolaev VO, Gambaryan S, Engelhardt S, Walter U, Lohse MJ (2005) Real-time Monitoring of the PDE2 Activity of Live Cells: HORMONE-STIMULATED cAMP HYDROLYSIS IS FASTER THAN HORMONE-STIMULATED cAMP SYNTHESIS. *J Biol Chem* 280: 1716-1719.

Nikolaev VO, Gambaryan S, Lohse MJ (2006) Fluorescent sensors for rapid monitoring of intracellular cGMP. *Nat Meth* 3: 23-25.

Obrietan K, Gao XB, van den Pol AN (2002) Excitatory Actions of GABA Increase BDNF Expression via a MAPK-CREB-Dependent Mechanism---A Positive Feedback Circuit in Developing Neurons. *J Neurophysiol* 88: 1005-1015.

Okumoto S, Looger LL, Micheva KD, Reimer RJ, Smith SJ, Frommer WB (2005) Detection of glutamate release from neurons by genetically encoded surface-displayed FRET nanosensors. *PNAS* 102: 8740-8745.

Pertz O, Hahn KM (2004) Designing biosensors for Rho family proteins -- deciphering the dynamics of Rho family GTPase activation in living cells. *J Cell Sci* 117: 1313-1318.

Pertz O, Hodgson L, Klemke RL, Hahn KM (2006) Spatiotemporal dynamics of RhoA activity in migrating cells. *Nature* 440: 1069-1072.

Radhakrishnan I, Perez-Alvarado GC, Parker D, Dyson HJ, Montminy MR, Wright PE (1997) Solution Structure of the KIX Domain of CBP Bound to the Transactivation Domain of CREB: A Model for Activator:Coactivator Interactions. *Cell* 91: 741-752.

Richards JS (2001) New Signaling Pathways for Hormones and Cyclic Adenosine 3',5'-Monophosphate Action in Endocrine Cells. *Mol Endocrinol* 15: 209-218.

Rizzo MA, Springer GH, Granada B, Piston DW (2004) An improved cyan fluorescent protein variant useful for FRET. *Nat Biotech* 22: 445-449.

Ryu H, Lee J, Impey S, Ratan RR, Ferrante RJ (2005) Antioxidants modulate mitochondrial PKA and increase CREB binding to D-loop DNA of the mitochondrial genome in neurons. *PNAS* 102: 13915-13920.

Sambrook J, Russell D (2001) Gel electrophoresis of DNA pulsed-field agarose gel electrophoresis. In *Molecular Cloning: A Laboratory Manual* (Sambrook J, Russell D, eds), pp 5.1-5.86. Cold Spring Harbor: CSHL Press.

Sakai R, Repunte-Canonigo V, Raj CD, Knopfel T (2001) Design and characterization of a DNA-encoded, voltage-sensitive fluorescent protein. *European Journal of Neuroscience* 13: 2314-2318.

Sasaki K, Sato M, Umezawa Y (2003) Fluorescent Indicators for Akt/Protein Kinase B and Dynamics of Akt Activity Visualized in Living Cells. *J Biol Chem* 278: 30945-30951.

Schuh RA, Kristian T, Fiskum G (2005) Calcium-dependent dephosphorylation of brain mitochondrial calcium/cAMP response element binding protein (CREB). *Journal of Neurochemistry* 92: 388-394.

Shagin DA, Barsova EV, Yanushevich YG, Fradkov AF, Lukyanov KA, Labas YA, Semenova TN, Ugalde JA, Meyers A, Nunez JM, Widder EA, Lukyanov SA, Matz MV (2004) GFP-like Proteins as Ubiquitous Metazoan Superfamily: Evolution of Functional Features and Structural Complexity. *Mol Biol Evol* 21: 841-850.

Shaner NC, Campbell RE, Steinbach PA, Giepmans BNG, Palmer AE, Tsien RY (2004) Improved monomeric red, orange and yellow fluorescent proteins derived from *Discosoma* sp. red fluorescent protein. *Nat Biotech* 22: 1567-1572.

Shaywitz AJ, Greenberg ME (1999) CREB: A Stimulus-Induced Transcription Factor Activated by A Diverse Array of Extracellular Signals. *Annual Review of Biochemistry* 68: 821-861.

Siegel MS, Isacoff EY (1997) A Genetically Encoded Optical Probe of Membrane Voltage. *Neuron* 19: 735-741.

Spotts JM, Dolmetsch RE, Greenberg ME (2002) Time-lapse imaging of a dynamic phosphorylation-dependent protein-protein interaction in mammalian cells. *PNAS* 99: 15142-15147.

Stein V, Nicoll RA (2003) GABA Generates Excitement. *Neuron* 37: 375-378.

Stitt M (2002) Imaging of metabolites by using a fusion protein between a periplasmic binding protein and GFP derivatives: From a chimera to a view of reality. PNAS 99: 9614-9616.

Takao K, Okamoto KI, Nakagawa T, Neve RL, Nagai T, Miyawaki A, Hashikawa T, Kobayashi S, Hayashi Y (2005) Visualization of Synaptic Ca²⁺ /Calmodulin-Dependent Protein Kinase II Activity in Living Neurons. J Neurosci 25: 3107-3112.

Ting AY, Kain KH, Klemke RL, Tsien RY (2001) Genetically encoded fluorescent reporters of protein tyrosine kinase activities in living cells. PNAS 98: 15003-15008.

Tsien RY (1998) THE GREEN FLUORESCENT PROTEIN. Annual Review of Biochemistry 67: 509-544.

Villardaga JP, Bunemann M, Krasel C, Castro M, Lohse MJ (2003) Measurement of the millisecond activation switch of G protein-coupled receptors in living cells. Nat Biotech 21: 807-812.

Violin JD, Zhang J, Tsien RY, Newton AC (2003) A genetically encoded fluorescent reporter reveals oscillatory phosphorylation by protein kinase C. J Cell Biol 161: 899-909.

Wang Y, Botvinick EL, Zhao Y, Berns MW, Usami S, Tsien RY, Chien S (2005) Visualizing the mechanical activation of Src. Nature 434: 1040-1045.

Westernmann B, Neupert W (2000) Mitochondria-targeted green fluorescent proteins: convenient tools for the study of organelle biogenesis in *Saccharomyces cerevisiae*. Yeast 16: 1421-1427.

Wu GY, Deisseroth K, Tsien RW (2001) Activity-dependent CREB phosphorylation: Convergence of a fast, sensitive calmodulin kinase pathway and a slow, less sensitive mitogen-activated protein kinase pathway. PNAS 98: 2808-2813.

Wu GY, Deisseroth K, Tsien RW (2001) Spaced stimuli stabilize MAPK pathway activation and its effects on dendritic morphology. Nat Neurosci 4: 151-158.

Xing J, Ginty DD, Greenberg ME (1996) Coupling of the RAS-MAPK Pathway to Gene Activation by RSK2, a Growth Factor-Regulated CREB Kinase. *Science* 273: 959-963.

Zapata-Hommer O, Griesbeck O (2003) Efficiently folding and circularly permuted variants of the Sapphire mutant of GFP. *BMC Biotechnology* 3: 5.

Zhang J, Ma Y, Taylor SS, Tsien RY (2001) Genetically encoded reporters of protein kinase A activity reveal impact of substrate tethering. *PNAS* 98: 14997-15002.

Zhang J, Campbell RE, Ting AY, Tsien RY (2002) CREATING NEW FLUORESCENT PROBES FOR CELL BIOLOGY. *Nat Rev Mol Cell Biol* 3: 906-918.

Thanks and acknowledgements

First, I would like to thank Axel Borst, the big boss, for his precious advice and support. He used to cheered me up by showing me that it can always go worse: forcing me to read the soccer results and commentaries of “den Loewen”. All of his group deserve thanks for their helpfulness and cheerfulness, providing an excellent working atmosphere.

Very special thanks goes to my supervisor Oliver Griesbeck. Not the least because of the nice lab meetings, the evenings with “Weissbier” and conversation, but mainly for his unshakeable believe in this work and in me, and for the inspiration with countless ideas that lie at the heart of this study. Thanks also to the rest of the “Griesbeck-Group”, Anja, for technical assistance and not despairing, as the only women in a men’s world since Nicola left and Nicola herself, for providing us with the latest gossip. Having fun and making good science is not mutually exclusive, as Marco, “da Zipfaeh”, and Stephan, “Hiwianer”, showed to everyone who was not to busy making experiments.

Also, this work would not have been possible without the Chrisselion, the notorious burn-down-the-hut-extreme-garlic-onion-chilli noodles, the snowball target shooting and the numerous evening sessions.

I am also gracious to the P1 gang, that made working in hard science easier and more joyful.

Last but not least, I would like to say thanks to my family, my friends and my girlfriend for their lovely support and the possibility to recover from the daily struggle and to see that there is a live beyond science.

Curriculum Vitae

Surname: Friedrich
Name: Michael Werner
Date of birth: August 8th, 1978
Place of birth: Munich, Germany

Education:

since April 04: PhD thesis at the Max-Planck-Institute of Neurobiology, Martinsried, Germany under supervision of Dr. Oliver Griesbeck and Prof. Dr. Alexander Borst:
“ Visualizing CREB family transcription factor activation in live cells “.

August 03 - march 04: Diploma thesis at the Max-Planck-Institute of Neurobiology, Martinsried, Germany under supervision of Dr. Oliver Griesbeck and Prof. Dr. Alexander Borst:
“ Genetisch kodierte fluoreszierende Indikatoren für die Aktivierung von Transkriptionsfaktoren der CREB-Familie In lebenden Zellen”.

Oct 03: Practical course in patch clamp analysis of cultured HEK cells in the Lab of Dieter Wicher, Max-Plank-Institute of Chemical Ecology, Jena, Germany.

Sep. 02 – July 03: Internships at the Max-Planck-Institute of Neurobiology, Martinsried, Germany, in the labs of Prof. Dr. Rüdiger Klein and Dr. Oliver Griesbeck.

Nov. 99 – Aug. 03: Undergraduate studies in Biology at the University of Munich, Germany.

July 98: Graduation from High School: Louise – Schroeder – Gymnasium, Munich, Germany.

Publications:

Friedrich, M.W., Mank, M., Griesbeck, O. (2007) Visualizing CREB family transcription factor activation in live cells. Manuscript submitted.

Mank, M., **Friedrich, M.W.**, Griesbeck, O. Expressing And Imaging Troponin-based calcium sensors. (2007) Meth Mol Biol. Submitted.

Heim, N., Garaschuk, O., **Friedrich, M.W.**, Mank, M., Milos, R.I., Kovalchuk, Y., Holbro, N., Oerthner, T.G., Konnerth, A & Griesbeck, O. (2007) Improved calcium imaging in transgenic mice expressing a Troponin C-based FRET biosensor. Nat Meth advanced online publication.

Mank, M., Reiff, D.F., Heim, N., **Friedrich, M. W.**, Borst, A., Griesbeck, O. (2006) A FRET – based calcium biosensor with fast signal kinetics and high fluorescence change. *Biophys J* **90**: 1790-1796.

Friedrich, M.W., Heim, N., Griesbeck, O. Genetisch kodierte fluoreszierende Biosensoren. (2005) Bioforum **4**: 24-27.

Address:

Michael Friedrich
Cellular dynamics group
Max-Planck-Institute of Neurobiology
Am Klopferspitz 18
82152 Martinsried

Tel:+49-89-85783272
Fax: +49-89-8578 3252
friedrich@neuro.mpg.de
www.neuro.mpg.de

Private address:

Michael Friedrich
Georg-Habel-Strasse 47
81241 Muenchen

